JYVÄSKYLÄ STUDIES IN COMPUTING

5

Tapani Ristaniemi

Synchronization and Blind Signal Processing in CDMA Systems

UNIVERSITY OF JYVÄSKYLÄ

JYVÄSKYLÄ 2000

JYVÄSKYLÄ STUDIES IN COMPUTING 5

Tapani Ristaniemi

Synchronization and Blind Signal Processing in CDMA Systems

Esitetään Jyväskylän yliopiston informaatioteknologian tiedekunnan suostumuksella
julkisesti tarkastettavaksi yliopiston salissa (FYS 1)
heinäkuun 1. päivänä 2000 kello 12.

Academic dissertation to be publicly discussed, by permission of
the Faculty of Information Technology of the University of Jyväskylä,
in Auditorium (FYS 1), on July 1, 2000 at 12 o'clock noon.

UNIVERSITY OF JYVÄSKYLÄ

JYVÄSKYLÄ 2000

Synchronization and Blind Signal Processing in CDMA Systems

JYVÄSKYLÄ STUDIES IN COMPUTING 5

Tapani Ristaniemi

Synchronization and Blind Signal Processing in CDMA Systems

UNIVERSITY OF JYVÄSKYLÄ

JYVÄSKYLÄ 2000

Editors
Tommi Kärkkäinen
Department of Mathematical Information Technology, University of Jyväskylä
Pekka Olsbo and Marja-Leena Tynkkynen
Publishing Unit, University Library of Jyväskylä

URN:ISBN:978-951-39-9673-4
ISBN 978-951-39-9673-4 (PDF)
ISSN 1456-5390

Jyväskylän yliopisto, 2023

ISBN 951-39-0728-7
ISSN 1456-5390

Jyväskylä University Printing House, Jyväskylä and
ER-Paino Ky, Lievestuore 2000

ABSTRACT

Ristaniemi, Tapani
Sychronization and blind signal processing in CDMA systems
Jyväskylä: University of Jyväskylä, 2000, 112 p.
(Jyväskylä Studies in Computing,
ISSN 1456-5390;5)
ISBN 951-39-0728-7
Finnish summary
Diss.

In this thesis we consider signal processing in the Direct-Sequence (DS) Code Division Multiple Access (CDMA) systems. We pay special attention to the downlink (e.g. mobile phone) environment, where the knowledge of the system parameters as well as the signal processing capacity is limited, and where the near-far problem caused by dissimilar signal energies is difficult to mitigate. Given this setting, we propose algorithms for both synchronization, and symbol estimation.

Timing estimation of the propagation delay, also called synchronization, is a prerequisite task for conventional receivers. Once the delays are estimated, one can estimate the channel, possibly also the number of users in the system, and finally the symbols itself. We propose methods based on differential correlation, which can efficiently utilize the time correlation of the varying channel, unlike conventional approaches. Desired features like low computational complexity, and capability of suppressing strong interference are achieved. Competitiveness among existing methods are verified by numerical simulations.

For symbol estimation we consider the use of statistical technique called Independent Component Analysis (ICA). Blind multiuser detection is performed by separating the desired source signal blindly from the received signal. Term *blind* relates to the fact that the separation is performed based on the observations only. We propose ICA-based blind multiuser detectors, in which ICA is considered as an additional element attached to either conventional or MMSE-based detectors. The main benefit of using ICA in CDMA is that it offers a near-far resistant receiver which is not explicitly subject to code timing nor channel estimation errors, which both may limit the performance of conventional and other near-far resistant receivers. Also, the statistical independence of the source signals can be utilized.

Keywords: code division multiple access (CDMA), synchronization, differential correlations, blind multiuser detection, independent component analysis (ICA)

Author's Address Tapani Ristaniemi
Department of Mathematical Information Technology
University of Jyväskylä
P.O.Box 35, FIN-40351
Jyväskylä, Finland

E-mail: riesta@mit.jyu.fi

Supervisor Prof. Jyrki Joutsensalo
Department of Mathematical Information Technology
University of Jyväskylä

Reviewers Dr. Jarkko Vuori
Department of Electrical Engineering
Helsinki University of Technology

Dr. Risto Wichman
Nokia Research Center
Helsinki

Opponent Prof. Matti Latva-aho
Department of Electrical Engineering
University of Oulu

ACKNOWLEDGEMENTS

On this occasion, I wish to express my sincere gratitude to Prof. Pekka Neittaanmäki, who encouraged me to begin post-graduate studies in the first place, and offered excellent facilities for doing that in the COMAS Graduate School. I am deeply indebted to Prof. Jyrki Joutsensalo, who then introduced me into this exciting field of research, and offered a challenging working environment in his project "Blind Source Separation and Deconvolution in Telecommunication and Array Signal Processing". I wish to thank him for his valuable guidance during the entire course of this thesis, and for providing the most inspiring and fruitful co-operation. I am grateful to Dr. Jarkko Vuori (Helsinki University of Technology) and Dr. Risto Wichman (Nokia Research Center) for their careful review of the manuscript. Gary J. Littler deserves special thanks for helping to improve the linguistics of the thesis.

This work has been concluded in the Faculty of Information Technology at the University of Jyväskylä. For financial support I am grateful to the Department of Mathematical Information Technology at the University of Jyväskylä, the Academy of Finland, the Ellen and Artturi Nyyssönen Foundation, the Finnish Cultural Foundation, the Jenny and Antti Wihuri Foundation, and the Foundation for the Promotion of Technology.

Finally, warm thoughts to my wife Mervi, daughter Oona, and son Eetu for their never-ending support and ♡.

Jyväskylä, May 29, 2000 *Tapani Ristaniemi*

CONTENTS

1 INTRODUCTION

In this introductory chapter, the basic concepts in the area of the thesis are descriptively discussed.

1.1 Multiple access

In multiple access the question is about division of the common transmission medium among several users. This is an essential question particularly in wireless communication systems since the wireless is a broadcast medium. The goal in such a system design is, first of all, to make each user in the system able to communicate despite the fact the other users occupy the same resources, too, perhaps simultaneously. However, as the number of users in the system grows, the demand of using the common resources as efficiently as possible also arise. These requirements have given rise to the birth of a multitude of multiple access schemes.

Figure 1 illustrates the most common multiple access schemes [81]. In Frequency Division Multiple Access (FDMA) each user is given a frequency slot in which one and only one user is allowed to operate. Interference of other users is thus easily prevented by assigning slots that do not over-lap. An example of FDMA-based system is NMT (Nordic Mobile Telephone) [42] in Scandinavia.

In Time Division Multiple Access (TDMA) a similar idea is realized in the time domain, where each user is given a unique time period (or periods). One user can hence transmit and receive data only during its predetermined time interval while the others are silent at the same time. This scheme is implemented for example in GSM (Groupe Special Mobile), where a given frequency slot is divided into several users by the means of TDMA. A comprehensive chapter on the GSM system is found in [81].

The above schemes are based on disjoint division in frequency and time spaces, which are perhaps the most likely ideas to come first to mind. As distinct from both FDMA and TDMA, in Code Division Multiple Access (CDMA), each

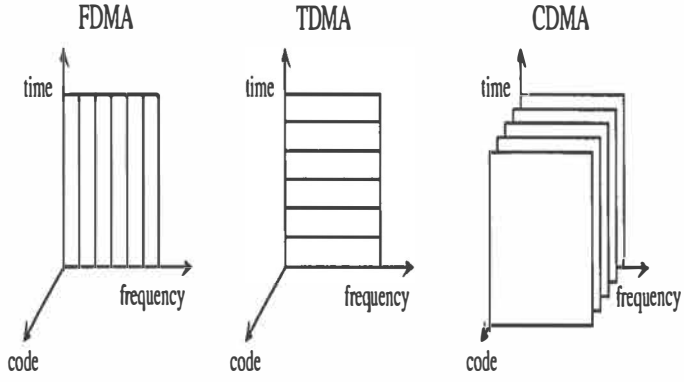

FIGURE 1 Multiple access schemes: FDMA,TDMA, and CDMA.

user occupies the same frequency band simultaneously. The users are now identified by so called codes, which are unique to each other. Roughly speaking, each user applies its unique code (this is an operation, which is explained later in detail) to its information signal before transmitting it through a common medium. In transmission the signals of different users gets mixed, because the same frequencies are used at the same time. 'Applying' this unique code, however, ensures that the transmitted signal of each user is resolvable from the mixture which is received by the receiver. The American IS-95 system [88] is based on CDMA, as well as evolving the European third generation system UMTS, which is based on the wideband CDMA (WCDMA) [60].

In its simplest form, the code is a sequence of ± 1's, also called a chip sequence, in which case we speak about Direct Sequence (DS) modulation [68], and call the access method as DS-CDMA. Other types of modulations exists, too, from which we mention Frequency Hopping (FH) [68]. In FH-CDMA, each user's code is a pattern of carrier frequencies that are used, hopping from one to another in predetermined order and time. Frequency hopping is used e.g. in the Bluetooth system [7], in which the hop rate of 1600 hops per second over 79 channels is used.

Since available frequencies are of limited resource, it should be used as efficiently as possible. In cellular systems, this brings out the question of frequency planning. Figure 2 depicts a cellular system, where each cell (illustrated as a hexagon) corresponds to a geographical area served by one base station. Inside each cell, say cell A, certain predetermined frequencies are used in the communication. In such a system, the only way to support more users is to allocate new cells, say, cell B. Now the critical question is: what frequencies can be used in that cell ? Due to the limited availability of the frequencies, it would be desirable to use the same frequencies as in another existing cell. This is the so called *frequency reuse*. In FDMA/TDMA based systems, the reuse pattern must be carefully designed to prevent different cells interfering with each other. More concretely, cells

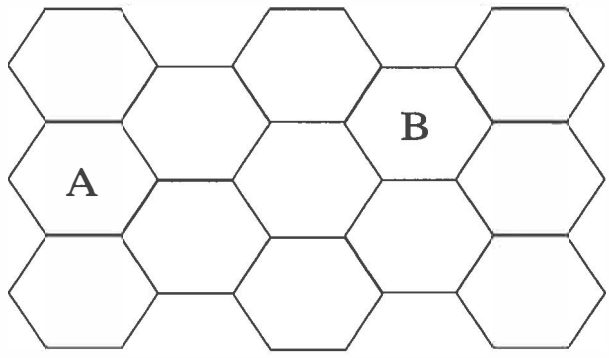

FIGURE 2 Cells in cellular communication system.

A and B should be far apart. This ensures that even though the signals from cell B are received in cell A, they are attenuated enough. In CDMA, as the same frequencies are used, no such design problems arise, but frequencies can be universally reused. This is usually regarded as the main advantage achieved by CDMA [103]. The real benefits of CDMA are hence seen at the system level, where an increased capacity is achieved [19].

1.2 Spread spectrum

CDMA is also called a commercial synonym of spread spectrum (SS) methods. In these methods, the key idea is to modulate the narrowband information signal using a wideband signal, independent of the data, called the spreading code. Since the code has a wider spectrum, in Figure 3 five times as wide, the modulation results in spreading the information signal in frequency domain, hence the name spread spectrum methods. For a more theoretical description, see e.g. [64].

Spread spectrum methods are initially developed to serve the needs which are familiar in a military context [64]. In such a context, one of the system's desired features is to have resistance against narrowband jamming. This is depicted in Figure 4. The desired narrowband signal (subfigure a) is spread (subfigure b) and transmitted, during which (subfigure c) the undesired narrowband signal (dotted) occupy the same frequencies. In the reception (subfigure d), the desired signal is *despread*, which results in a spreading of the interference by the same operation. Hence, the jammer's contribution in the demodulated signal, seen as the overlapping area (shaded), is minor, and can be decreased by using wider spectral spreading.

The above description also explains how the signals can be "hidden" by spectral spreading. This is because the despreading of the desired signal hap-

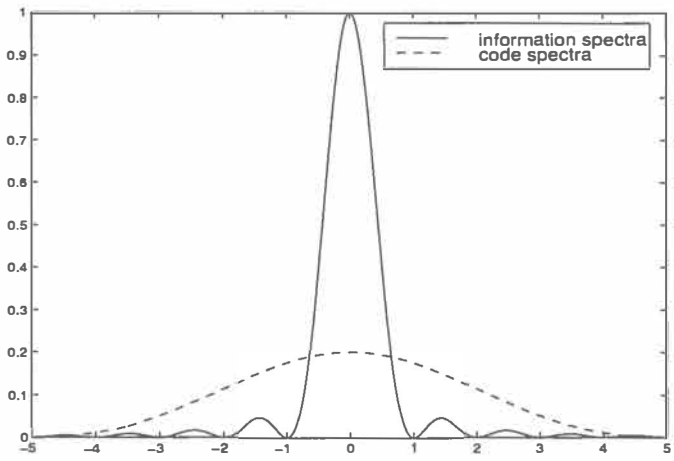

FIGURE 3 The frequency content of the information signal and the code.

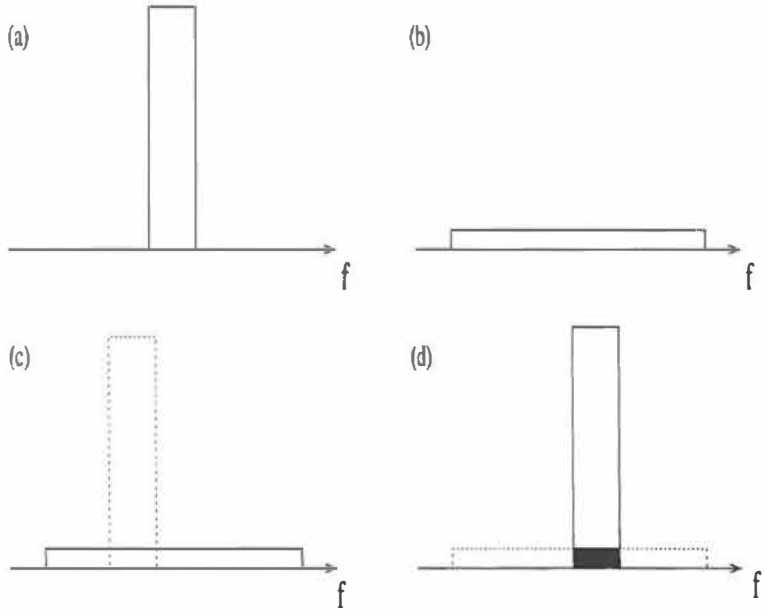

FIGURE 4 Desired user's spectrum (a), and spread spectrum (b). Narrowband interference occurs during transmission (c). Received (despread) spectrum (d).

pens only if a true spreading code is used in the reception. In addition, as the received signal is subject to transmission delay, the right timing of the code should be known. From a practical point of view, as the codes may be as long as $2^{42} - 1$ [81], eavesdropping is difficult. It is, however, possible due to the linear nature of the codes [64, 43]. Hence, the spread spectrum methods does not offer security in a strict sense, but encryption is still needed.

Multipath propagation means that the transmitted signal propagates through different routes called paths (or rays), which are all received by the receiver. These paths are due to reflections from solid surfaces or moving objects, and can be modeled as (among other kinds of) channel distortion. Urban multipath propagation is presented in Figure 5. The existence of different paths let the signal interfere with itself, which is known as inter-symbol interference (ISI)[1]. Spread spectrum methods can mitigate multipath interference [102]. In the case of direct sequence spreading, different paths usually correspond to different timings of the spreading code due to different path lengths. Therefore, when a certain path is demodulated in the receiver, only that path is despread while the other paths remain spread.

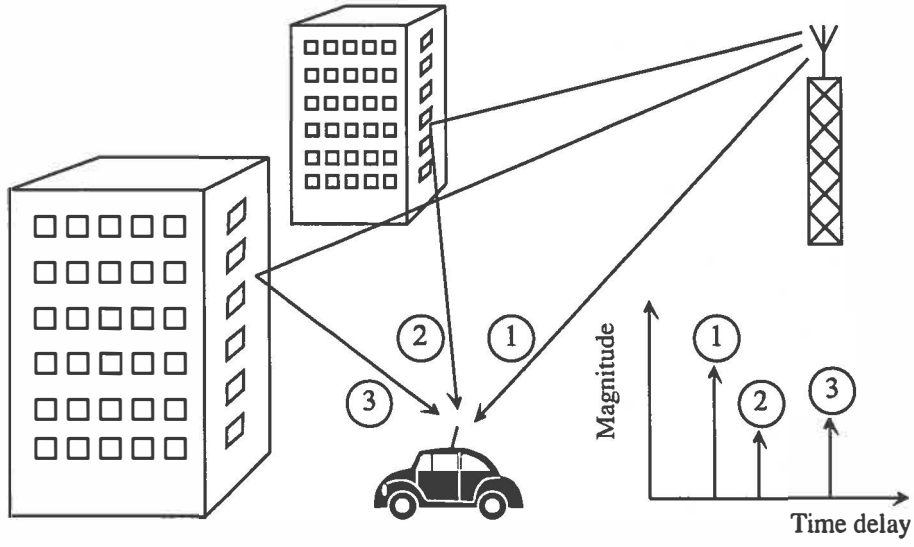

FIGURE 5 Urban multipath propagation.

[1] Usually ISI is understood as a case where the time difference of two paths is more than the duration of a symbol. Otherwise, the interference is called inter-path interference (IPI).

1.3 Problems in wireless access and CDMA

1.3.1 Power control

A wireless communication system usually suffers from a *near-far problem*, which means that a strong signal will interfere with the weak one if received simultaneously. This scenario can easily happen in the uplink (e.g. mobile to base) of a DS-CDMA system, where the mobiles are using the same frequency band, and are located at different distances from the base station. A solution for this is power control, whose purpose it is to guarantee (nearly) equal signal powers in the reception. As a consequence, no user will be completely wiped out by another user. In the uplink, there are two common power control principles: open and closed loop power control [60]. In the former case, a mobile measures the attenuation of the received signal, also called a *pathloss* or *distance attenuation* between the base and the mobile, and sets its signal power to respect the required performance criterion. Open loop power control is mainly to set the initial power of a mobile. However, as the attenuation is measured by the mobile from the downlink (e.g. base to mobile) communication, the short term channel conditions are different from those in the uplink if different frequencies are used. This is the case in the FDD mode (frequency division duplex), in which the uplink and downlink connections are separated in frequency. For this reason, a closed loop power control is needed to compensate fast channel variations. In the closed loop power control, the base station or mobile continuously measures the signal-to-interference ratio (SIR), and transmits back a power adjustment command.

In the downlink, the signals are sent simultaneously to each user, and thus the channel is the same for both. However, power control can still be used. The motivation now is to mitigate interferences from other sectors or cells, and thus to try to offer equal performance for any user regardless of their location. In cellular systems, slow downlink power control is used to improve the performance of a mobile in the cell boundary, where the interference from neighbouring cells gets stronger. In addition, if the mobile moves to another cell, the mobile must be switched to another base station. This is called *hard handover*. In *soft handover* the mobile in the cell boundary is connected to more than one base station simultaneously. So, by downlink power control each base station can now decrease their power.

For a more comprehensive reading about power control, and handover issues, see e.g. [60].

1.3.2 Multiple access interference

One of the most serious problems is Multiple Access Interference (MAI), which arises from the fact that the same frequency band is occupied simultaneously. MAI can be alleviated by increasing the length of the spreading code, but at fixed chip rate, this decreases the data rate. In addition, *near-far problem* arises when signals

from near and far are received at the same time. If the received powers from different users become too different, a stronger user will seriously interfere with the weaker ones, even if there is a small correlation between users. The near-far effect is not a problem in the FDMA and TDMA systems, as discussed earlier, since orthogonality between the users can be easily achieved in these systems.

Near-far problem in the base station can be mitigated by power control, as discussed earlier, or by multi-user detection (MUD), where the knowledge of one or several parameters, such as propagation delay, carrier phase, and received power level [98, 99, 45, 23, 17] are used. The problem in MUD is, however, that it is usually a complex solution because of the joint estimation of the parameters. Moreover, it requires several system parameters to be known or estimated, which is usually not possible in the downlink. In such a situation, however, *blind* MUD techniques can be used. This is considered in Chapter 4.

Even though power control is used, MUD can be used to improve the performance by suppressing MAI. Existing CDMA-based systems rely only on the power control (e.g. in IS-95, fast power control is used in the uplink), and use a conventional reception (, which neglects MAI). This guarantees a satisfactory performance due to the relatively long code sequence. However, the need for higher data rates with no bandwidth expansion may require to shorten the code length, and the MAI cannot be ignored anymore. In addition, downlink power control actually *cause* near-far problem for the downlink receiver. For these reasons, near-far resistant receivers are of great interest.

1.3.3 Fading channels

Fading is a problem in all wireless systems. It is caused, when the propagation channel in a mobile communication system distorts the transmitted signal. In wireless systems, the transmitted signal propagates through various paths. If there is an extremely short pulse, ideally an impulse, transmitted over a time-varying multipath channel, the received signal might appear as a train of pulses. When a transmitted signal travels over multiple propagation paths, time delay associated to each path is random. Thus, phases of the received multipath components are random. At times phases are adding destructively. When that occurs, the resultant received signal is very small or practically zero. The channel is then said to be in a fade. In Figure 6, the typical fading process is presented. The rapidity of amplitude variation, and accordingly the distance of two fades in time is affected by the speed of the mobile receiver/transmitter. Hence, distinctions of *slow* and *fast* fading are made, where the former is generally understood as a situation, where the channel remains constant during one symbol duration.

Fading is also classified as *flat* and *frequency selective* depends on whether the signal waveform is retained or not, respectively. The former happens [102] if the time delays of different paths are very similar. This is modeled as a single path -case. As the delays of different paths have more differences, which is modeled as a multipath-case, the signal waveform is scaled and reshaped. The term "fre-

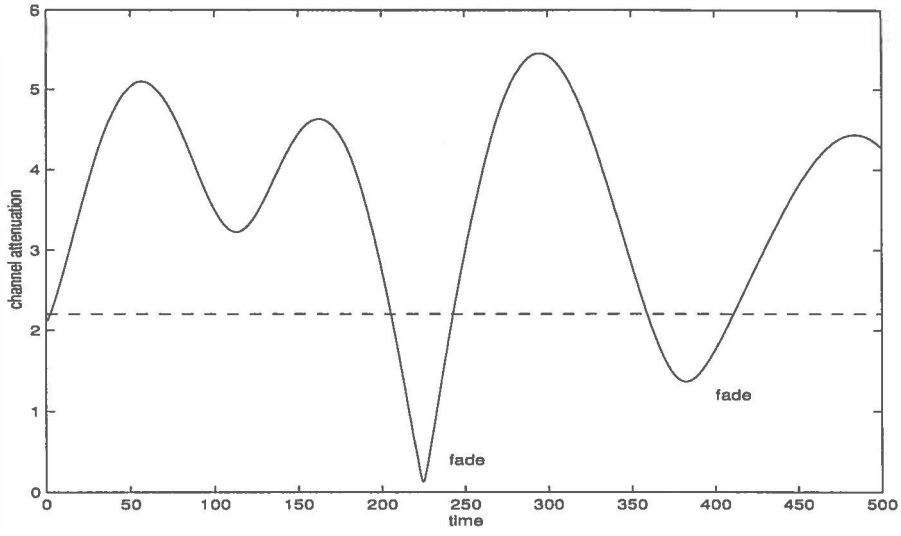

FIGURE 6 Typical fading process.

quency selective" arises from the observation that pulse reshaping is due to the different attenuation of different frequencies.

1.3.4 Synchronization

Accurate synchronization of the receiver carrier's frequency and phase, as well as chip timing, to that of a received signal is a prerequisite task before any demodulation can be performed. In CDMA, chip timing is acquired first. This requires the receiver to have a fairly good estimate for the carrier frequency only. No knowledge of the phase is needed yet [103]. Chip timing acquisition means rough estimation of the chip level timing, with a maximum acceptable error of half a chip duration. After this, conventional phase-lock loop (PLL) devices can be used for accurate phase estimation and for carrier frequency refinement. Finally, all the quantities can be tracked by PLL in non-stationary environments.

In this thesis, we consider more profoundly chip timing acquisition. Because it refers to the coarse synchronization of the received signal, it basically leads to a hypotheses testing problem. This means testing some possible chip timings whether some of them have correct values or not. The more candidates tested the more accurate the estimation will be. Figure 7 illustrates the problem. In this case, 31 delays are tested (horizontal axis) and they correspond to a certain value (vertical axis) which is related to its suitability for being a correct delay. In the figure, two paths seem to exist, corresponding to the 4^{th} and 8^{th} test delay, respectively. If the number of hypotheses were small, one could test all the hypotheses (in this case 31) in parallel manner, and choose the delays corresponding to the

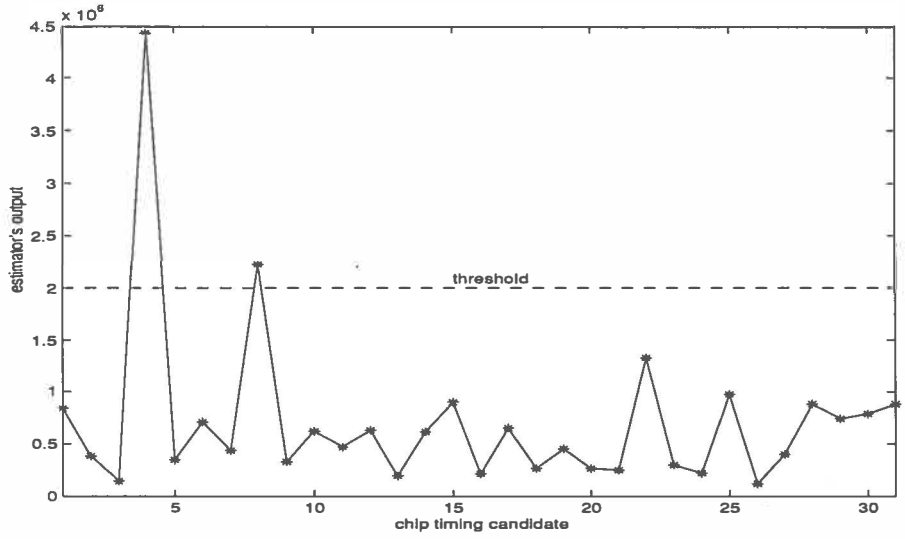

FIGURE 7 Delay spectrum for visualization of delay estimation procedure.

peaks of the delay spectra. However, this leads to a problem of how many peaks are chosen, since the number of paths is unknown. For example, the 22nd test delay in the figure could correspond to the third path, or it can be just a spurious peak. The problem is more concrete as the number of hypotheses grow, because then the delays are generally tested in a serial manner. This requires setting a certain threshold value. In serial operation, each incorrect hypothesis (contribution below threshold) is eliminated, before the next value is tested. The threshold setting hence becomes a problem, especially in highly loaded systems, where mutual interferences of different users may cause more spurious peaks. A good survey of the basic ideas of the existing serial and parallel acquisition schemes is given in e.g. [77].

The effect of inaccurate synchronization can be disastrous to conventional receivers [61]. The other part of the thesis proposes the use of Independent Component Analysis (ICA) to alleviate this problem. In ICA, no explicit synchronization is needed.

1.4 List of publications

For clarity and uniformity, the thesis is made as a monograph, although some of the results considered in this thesis have already been published at conferences, or submitted to international journal. One article is scheduled for publication as a chapter in a re-print book. The thesis contains also unpublished material.

In the publications below, the author was responsible for writing simulation programs and performing the experiments. In addition, whenever the author's name appears as the first one, he was responsible for writing the paper. Additional contributions are as follows: Publications 1,2,4,6, and 9 are almost completely author's own work. In Publication 7, the key idea of using whitened data in the differential correlations was invented together. The method for accurate estimation was due to the author, who also actively took part in writing. Patent pending 10 is based on the results of Publications 8, while 11 is based on Publication 9, and the content of section 4.3 of the thesis.

1. T. Ristaniemi and J. Joutsensalo, "Novel Scheme for Blind Symbol Separation in CDMA Downlink", *Proc. 32th Asilomar Conference on Signals, Systems, and Computers*, Monterey CA, USA, November 1998, pp. 1853-1857.
   https://doi.org/10.1109/ACSSC.1998.751644
2. T. Ristaniemi and J. Joutsensalo, "On the Performance of Blind Source Separation in CDMA Downlink", *Proc. International workshop on Independent Component Analysis and Signal Separation*, Aussois, France, January 1999, pp. 437-442.
3. J. Joutsensalo and T. Ristaniemi, "Single User Synchronization in Fading Channel", *Proc. IEEE 2nd Workshop on Signal Processing Advances in Wireless Communications*, Annapolis MD, USA, May 1999, pp. 133-137.
   https://doi.org/10.1109/SPAWC.1999.783037
4. T. Ristaniemi and J. Joutsensalo, "Accurate Differentially Coherent Code Acquisition in DS-CDMA with Fading Channel", *Proc. International Workshop On Mobile Communications*, Grete, Greece, June 24-26, 1999, pp. 341-347.
5. T. Ristaniemi, "Accurate Pilot Assisted PN Code Acquisition", *Proc. 50th IEEE Vehicular Technology Conference*, Amsterdam, The Netherlands, September 19-22, 1999, pp. 723-727.
   https://doi.org/10.1109/VETECF.1999.798424
6. T. Ristaniemi and J. Joutsensalo, "Independent Component Analysis with Code Information Utilization in DS-CDMA Signal Separation", *Proc. IEEE Global Telecommunications Conference*, Rio de Janeiro, Brazil, December 5-9, 1999, vol. 1a, pp. 320-324.
   https://doi.org/10.1109/GLOCOM.1999.831657
7. J. Joutsensalo and T. Ristaniemi, "Timing Acquisition in CDMA Systems", in P. Stavroulakis (ed.) , *Third Generation Mobile Systems*, Springer-Verlag, 2000, to appear.
8. T. Ristaniemi and J. Joutsensalo, "Code Timing Acquisition for DS-CDMA in Fading Channels by Differential Correlations", *IEEE Transactions on Communications*, revised and resubmitted.
   https://doi.org/10.1109/26.923813
9. T. Ristaniemi and J. Joutsensalo, "Advanced ICA-based Receivers for DS-CDMA Systems", *Proc. 11th IEEE International Symposium on Personal, Indoor, and Mobile Radio Communications*, London, U.K., September 18-21, 2000, to appear.
   https://doi.org/10.1109/PIMRC.2000.881433

10. J. Joutsensalo and T. Ristaniemi, "Synchronization by Correlation Method in Spread Spectrum System", patent pending, 1999.

11. J. Joutsensalo and T. Ristaniemi, "Receiver for Spread Spectrum Signal", patent pending, 2000.

1.5 Outline of the thesis

The rest of the thesis is organized as follows. In Chapter 2, we introduce the continuous-time asynchronous CDMA signal model, as well as its equivalent discrete-time model for the purpose of digital signal processing. Chapters 3 and 4 are devoted to chip timing acquisition and symbol demodulation, respectively. Some existing synchronization methods and receiver structures are reviewed and used later as reference methods. In Chapter 4 we also describe the statistical technique called Independent Component Analysis, which is proposed to be applied for symbol estimation. Finally, in Chapter 5 we summarize and draw conclusions of the thesis.

2 DIRECT SEQUENCE CDMA SYSTEM

In this chapter we introduce the system model and discuss the basic problems and goals. We start with the ideal single user DS-CDMA case to get a clear picture of the problem. Later, more general formulations are used.

2.1 Ideal reception

Suppose now that a user is going to start communication in the system. Before transmission, its information is spread by direct sequence modulation as follows:

$$y[i] = s[i]b[i]. \tag{1}$$

Here

- $b[i] \in \{-1, +1\}$ is a narrowband *bit* sequence having duration T, and
- $s[i] \in \{-1, +1\}$ is a wideband *chip* sequence having duration T_c.

Chip sequence is also called a spreading code or a *pseudo noise* (PN) sequence. In Figure 8, the operation is illustrated in time domain, where the bit and chip durations are $T = 5$ and $T_c = 1$, respectively. The amount of spreading in the frequency domain is determined by the ratio $C = T/T_c$, which is also called a *processing gain*. For the orthogonal synchronous DS-CDMA systems it also gives a theoretical upper limit for the amount of users that can be supported [102]. This is understandable from basic algebra, since from C-dimensional vector space one can find at most C orthogonal vectors.

PN sequences can be generated by a very simple shift register (see e.g. [102]). One special type of PN sequence is *m-sequence*, which obey many useful properties. These include [102]:

- the sequence has period $N = 2^n - 1$, where n may be even 42
- it has the following periodic autocorrelation function:

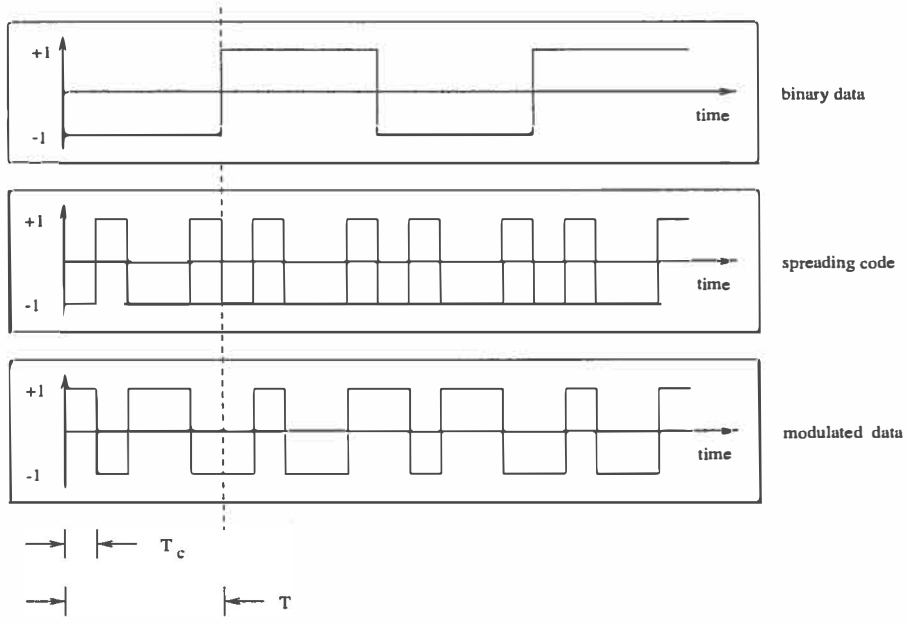

FIGURE 8 An example of the spreading operation: binary data symbols (top), PN sequence, and spread output process (bottom).

$$E(s[i]s[i+j]) = \begin{cases} 1 & \text{, when } j = 0, N, 2N, \ldots \\ -1/N & \text{, otherwise} \end{cases} \tag{2}$$

Hence, m-sequence has a very impulse-like autocorrelation. This means, that m-sequence is almost orthogonal to its any time-shifted replica of equal length.

Suppose the ideal case, so that the receiver would have the transmitted data buried in the interference. The data would thus have the simplified form

$$r[i] = s[i]b[i] + w[i], \tag{3}$$

where

- $s[i]b[i]$ is the *desired* signal, and
- $w[i]$ is the *interfering* signal.

The interfering signal consists for example of thermal noise, and the other users' signals. If the timing of the received signal is exactly known, the desired signal is got by performing the direct sequence modulation again. Formally,

$$\begin{aligned} o[i] &= s[i]r[i] \\ &= s[i](s[i]b[i] + w[i]) \\ &= b[i] + s[i]w[i], \end{aligned} \tag{4}$$

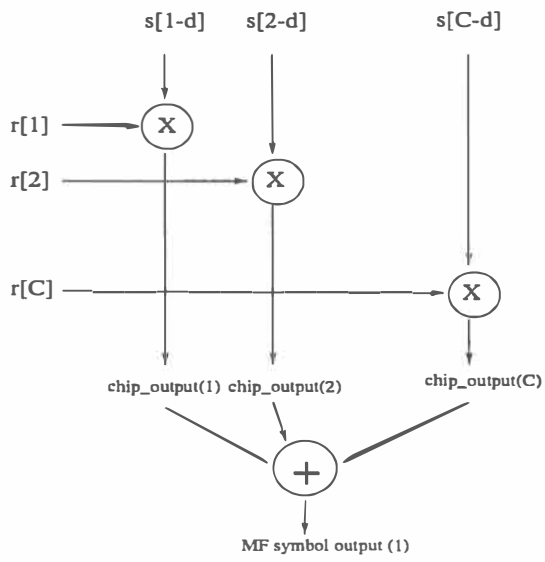

FIGURE 9 Ideal reception: d refers to the delay of the received data r.

where it is seen that the operation *despreads* the desired signal, while the interfering signal is *spread* by the same operation. Averaging over a symbol duration, one gets

$$\sum_{i=1}^{C} o[i] = Cb[i] + \sum_{i=1}^{C} s[i]w[i]. \tag{5}$$

If $s[i]$ is uncorrelated with $w[i]$, then the second term on the right hand side is roughly zero, and the symbol estimate is

$$\hat{b} = \text{sign}(\sum_{i=1}^{C} o[i]) \approx \text{sign}(Cb[i]). \tag{6}$$

This is a Matched Filter (MF) reception approach, illustrated in Figure 9, which is the Maximum Likelihood Method (MLM) if $w[i]$ is Gaussian white noise [102]. MLM means in other words that the probability of symbol estimation error is minimized given an observation $r[i]$.

2.2 DS-CDMA signal model

In this section we construct a discrete-time model of DS-CDMA system for the purposes of digital signal processing. The signal model studied in this thesis is a baseband model with a fading/non-fading single or multipath channel, and additive white gaussian noise. The channel model is depicted in Figure 10. Here

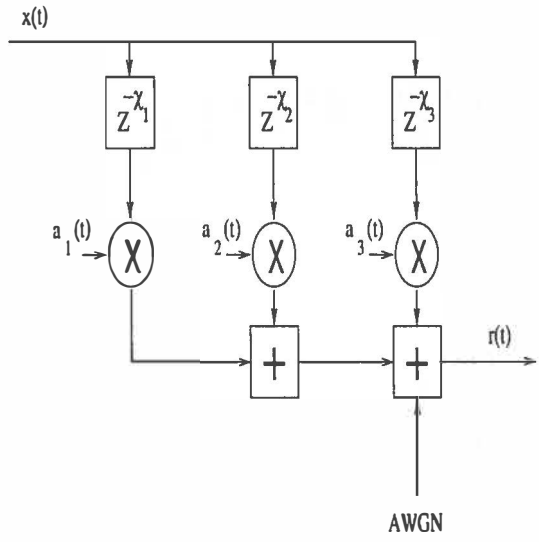

FIGURE 10 Channel model (with $L = 3$ paths): $x(t)$ is the data to be sent, z^{-d} stands for delaying by d chips, and $a_i(t)$ denotes path i attenuation at the time instant t.

the signal which is sent to (resp. by) user k is $x_k(t) = \sum_{m=1}^{M} b_{km} s_k(t - mT)$, which contains the information of M symbols b_{km}. $s_k(\cdot)$ is kth user's chip sequence i.e. the spreading code. It is supported only by the symbol duration T, and thus $s_k(t) \in \{-1, +1\}$, $t \in [0, T)$, $s_k(t) = 0$, $t \notin [0, T)$. We assume the channel is fixed during one symbol, i.e. $a_{kl}(t) = a_{klm}, t \in [mT, (m+1)T)$ in Figure 10. a_{klm} is called an attenuation factor of the lth path, which a complex number and may vary from symbol to symbol. The received signal hence has the form

$$r(t) = \sum_{m=1}^{M} \sum_{k=1}^{K} b_{km} \sum_{l=1}^{L} a_{klm} s_k(t - mT - \chi_{kl} T_c) + n(t), \tag{7}$$

where L is the number of resolvable paths, T_c is the chip duration, and $\chi_{kl} T_c$ is the delay of the user's k lth path, where $\chi_{kl} = d_{kl} + \delta_{kl}$ with d_{kl} integer and $\delta_{kl} \in [0, 1)$. The delay of each path is assumed to remain roughly constant during the interval of M symbols. $n(t)$ denotes noise, and the chip sequence length (i.e. processing gain) is $C = \frac{T}{T_c}$. From now on, we assume $T_c = 1$ for simplicity.

Since the chip sequence $s(\cdot)$ is now continuous by definition, it includes not only the binary chips $s_k[i]$, but also a chip waveform $p(t)$. More precisely,

$$s_k(t) = \sum_{i=0}^{C-1} s_k[i] p(t - iT_c), \tag{8}$$

where $p(t)$ is supported by $[0, T_c]$, only. In this thesis, rectangular waveforms are

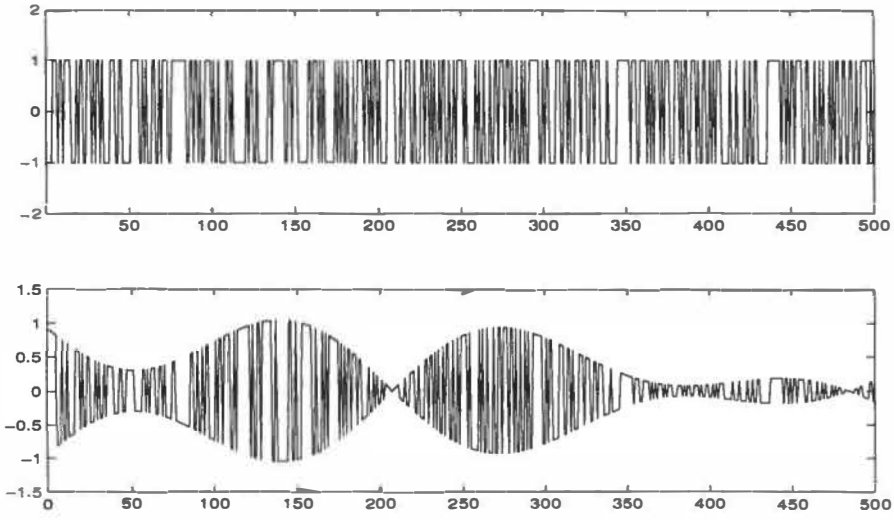

FIGURE 11 Single user's transmitted data (top), and its single path's contribution in the reception (bottom) according to the channel model.

assumed for each user, and hence

$$p(t) = \begin{cases} 1 & \text{, when } 0 \leq t \leq T_c \\ 0 & \text{, otherwise} \end{cases} \tag{9}$$

In distortionless transmission, the transmitted signal is only subject to scaling and delaying [10]. In our case, it would mean that

$$r_{\text{dist}}(t) = \sum_{m=1}^{M} \sum_{k=1}^{K} b_{km} a_k s(t - mT - \chi_k). \tag{10}$$

Hence, in addition to additive noise, the channel distortion in Eq. (7) can be characterized by multiple resolvable paths L and possibly time-varying path strengths a_{klm}. The modeled contribution of single user's single fading path in the reception is illustrated in Figure 11.

Continuous-to-discrete time conversion is realized by a chip-matched filter, which is a simple integrate-and-dump -device. In this thesis, chip-rate sampling is used, which means integrating over a chip duration T_c,

$$r[m] = \int_{mT_c - T_c + \tau}^{mT_c + \tau} p(t - (m-1)T_c - \tau) r(t) dt, \tag{11}$$

where the timing offset $0 \leq \tau \leq T_c$ is due to the fact that the receiver might not have an exact knowledge of chip edges. Sampling yields C-vectors

$$\mathbf{r}_m \stackrel{\text{def}}{=} [r[mC]\ r[mC+1]\ \cdots\ r[(m+1)C-1]]. \tag{12}$$

The sampled chip sequence of user k is denoted as

$$\mathbf{s}_k \stackrel{\text{def}}{=} [s_k[1]\ s_k[2]\ \cdots\ s_k[C]]. \tag{13}$$

Thus in each vector sample $\mathbf{r}_m$, information is collected from a time slot duration CT_c, that is, symbol duration. It is then said that the *processing window* is of length one symbol. It is hence possible that sampling is *symbol asynchronous*, i.e. the vector sample might contain samples of two successive symbols. As it is the spread data which is integrated, it means that the first element(s) in $\mathbf{r}_m$ correspond to the "late" part of the chip sequence $\mathbf{s}_k$,

$$\underline{\mathbf{s}}_{kl} = \underline{\mathbf{s}}_k(d_{kl}) \stackrel{\text{def}}{=} \left[\ s_k[C-d_{kl}+1]\ \ \cdots\ \ s_k[C]\ \ 0\ \ \cdots\ \ 0\ \right]^T, \tag{14}$$

while the rest correspond to the "early" part

$$\overline{\mathbf{s}}_{kl} = \overline{\mathbf{s}}_k(d_{kl}) \stackrel{\text{def}}{=} \left[\ 0\ \ \cdots\ \ 0\ \ s_k[1]\ \ \cdots\ \ s_k[C-d_{kl}]\ \right]^T. \tag{15}$$

In addition, sampling is usually *chip asynchronous*, which is related to τ in Eq. (11). Recall, that chip-syncronous sampling (with respect to user's k path l) would mean integration with $\tau = \delta_{kl}$. Thus, in chip-asynchronism we are interested in the effect of $r[m]$ having $\tau \in [\delta_{kl}, \delta_{kl} + T_c]$. But, as sampling is just integration, the chip sequences that are related to those two successive symbols (with respect to each path) are not exactly (14) nor (15), but their convex combinations [49]

$$\underline{\mathbf{c}}_{kl} = \underline{\mathbf{c}}_k(\chi_{kl}) \stackrel{\text{def}}{=} (1-\delta_{kl})\underline{\mathbf{s}}_k(d_{kl}) + \delta_{kl}\underline{\mathbf{s}}_k(d_{kl}+1) \tag{16}$$

$$\overline{\mathbf{c}}_{kl} = \overline{\mathbf{c}}_k(\chi_{kl}) \stackrel{\text{def}}{=} (1-\delta_{kl})\overline{\mathbf{s}}_k(d_{kl}) + \delta_{kl}\overline{\mathbf{s}}_k(d_{kl}+1). \tag{17}$$

Hence, the vector sample has a well-known form [4]

$$\mathbf{r}_m = \sum_{k=1}^{K}\sum_{l=1}^{L} a_{kl,m-1}b_{k,m-1}\underline{\mathbf{c}}_{kl} + a_{klm}b_{km}\overline{\mathbf{c}}_{kl} + \mathbf{n}_m, \tag{18}$$

where $\mathbf{n}_m$ denotes noise.

To get a more compact representation of the data (18), let us define a $C \times 2KL$ dimensional code matrix $\mathbf{G}$ as

$$\mathbf{G} = [\underline{\mathbf{c}}_{11}, \overline{\mathbf{c}}_{11}, \ldots, \underline{\mathbf{c}}_{1L}, \overline{\mathbf{c}}_{1L} \ldots, \underline{\mathbf{c}}_{KL}, \overline{\mathbf{c}}_{KL}], \tag{19}$$

and a 2×1 vector $\mathbf{z}_{klm}$,

$$\mathbf{z}_{klm} = [a_{l,m-1}b_{k,m-1}, a_{lm}b_{km}]^T. \tag{20}$$

Stacking all vectors $\mathbf{z}_{klm}$ into a $2KL$-vector $\mathbf{a}_m$,

$$\mathbf{a}_m = [\mathbf{z}_{11m}^T, \ldots, \mathbf{z}_{1Lm}^T, \ldots, \mathbf{z}_{KLm}^T]^T, \tag{21}$$

the sample vector (18) can be rewritten as

$$\mathbf{r}_m = \mathbf{G}\mathbf{a}_m + \mathbf{n}_m. \tag{22}$$

In this representation, $\mathbf{G}$ depends on the spreading codes, and paths via their number and delays, while $\mathbf{a}_m$ depends on the symbols, and paths via their number and strengths.

Notice that if the channel remains fixed during the observation, i.e. $a_{klm} = a_{kl}$ for all $m = 1, \ldots, M$, the datamodel can be further processed. Namely, each path is now just a scaled and delayed copy of the first path, say. Formally this means, that we can write

$$\mathbf{r}_m = \sum_{k=1}^{K} [b_{k,m-1} \sum_{l=1}^{L} a_{kl} \underline{\mathbf{c}}_{kl} + b_{km} \sum_{l=1}^{L} a_{kl} \overline{\mathbf{c}}_{kl}] + \mathbf{n}_m. \tag{23}$$

The datamodel (22) still holds, but the dimensions are reduced. The matrix $\mathbf{G}$ is now reduced in size to $C \times 2K$, $\mathbf{G} \stackrel{\text{def}}{=} [\mathbf{g}_1, \ldots, \mathbf{g}_{2K}]$, where

$$\mathbf{g}_{2k-1} = \sum_{l=1}^{L} a_{kl} \underline{\mathbf{c}}_{kl} \tag{24}$$

$$\mathbf{g}_{2k} = \sum_{l=1}^{L} a_{kl} \overline{\mathbf{c}}_{kl}, \tag{25}$$

and the vector $\mathbf{a}_m$ contains only the binary symbols,

$$\mathbf{a}_m = [b_{1,m-1}, b_{1m}, \ldots, b_{K,m-1}, b_{Km}]^T. \tag{26}$$

In the remaining part of the thesis, the former is used due to its more general form.

Remark: Notice that model (18) can be expressed also in another form frequently used in the literature. Namely, let us define new code vectors

$$\mathbf{c}_{kl}^{+} = \underline{\mathbf{c}}_{kl} + \overline{\mathbf{c}}_{kl} \tag{27}$$

$$\mathbf{c}_{kl}^{-} = \underline{\mathbf{c}}_{kl} - \overline{\mathbf{c}}_{kl}, \tag{28}$$

and joint symbol and channel terms

$$\psi_{klm}^{+} = (a_{kl,m-1} b_{k,m-1} + a_{klm} b_{km})/2 \tag{29}$$

$$\psi_{klm}^{-} = (a_{kl,m-1} b_{k,m-1} - a_{klm} b_{km})/2. \tag{30}$$

Then the data (18) can be rewritten as

$$\mathbf{r}_m = \sum_{k=1}^{K} \sum_{l=1}^{L} \psi_{klm}^{+} \mathbf{c}_{kl}^{+} + \psi_{klm}^{-} \mathbf{c}_{kl}^{-}. \tag{31}$$

□

The second order statistics of the data are gained from the autocorrelation matrix

$$\mathbf{R} = E\{\mathbf{r}_m \mathbf{r}_m^H\} = \mathbf{G}\mathbf{A}\mathbf{G}^T + \sigma^2 \mathbf{I}, \tag{32}$$

where $\mathbf{A} = E\{\mathbf{a}_m \mathbf{a}_m^H\}$, $\sigma^2 = E\{\mathbf{n}_m \mathbf{n}_m^H\}$ is the noise variance, and $\mathbf{I}$ is $2KL \times 2KL$ identity matrix. Some of the methods presented later will consider especially autocorrelation matrix with non-zero time lag, i.e

$$\mathbf{R}(\tau) = E\{\mathbf{r}_m \mathbf{r}_{m+\tau}^H\}, \tag{33}$$

which has a very fine property, provided τ is suitably chosen. To stress the non-zero time lag, we call $\mathbf{R}(\tau)$ a differential correlation matrix. In addition, $\mathbf{R}(0) \stackrel{\text{def}}{=} \mathbf{R}$.

Sometimes, the data is processed in larger window sizes than 1 symbol, just to ensure that at least one symbol falls entirely inside the window. Suppose the window size is $(D+1)$ symbols. Then we define the $(D+1)$-vector to be processed as

$$\tilde{\mathbf{r}}_m \stackrel{\text{def}}{=} [\mathbf{r}_m^T \cdots \mathbf{r}_{m+D}^T]^T. \tag{34}$$

3 CODE TIMING ACQUISITION

The final objective in the reception is to estimate the symbols that carry the information. Code timing acquisition, however, is often a prerequisite task for this. In the following we first review some of the benchmark methods for delay estimation, and continue with some new proposals. Numerical experiments are included at the end of the chapter.

3.1 Review of earlier work

3.1.1 Maximum likelihood method

The optimal estimates for all the unknown parameters in $\mathbf{r}_m$ can be obtained from the global maximum of the log-likelihood function [38]

$$J(\mathbf{r}_m) = \text{const.} - C\log(\sigma^2) - \frac{1}{\sigma^2}\|\mathbf{r}_m - \mathbf{G}\mathbf{a}_m\|^2, \tag{35}$$

where σ^2 is the noise variance. Hence, the delays ($\mathbf{G}$), as well as symbols and channel coefficients ($\mathbf{a}_m$) can be equally found by

$$[\hat{\mathbf{a}}_m, \hat{\mathbf{G}}]^T = \arg\min_{\hat{\mathbf{a}}_m, \hat{\mathbf{G}}} \|\mathbf{r}_m - \mathbf{G}\mathbf{a}_m\|^2. \tag{36}$$

In delay estimation we are interested only in $\mathbf{G}$, which is possible to estimate separately from the other parameters. Namely, the least-squares solution for $\mathbf{a}_m$ is $\hat{\mathbf{a}}_m = \mathbf{G}^+\mathbf{r}_m$, where $\mathbf{G}^+ \stackrel{\text{def}}{=} (\mathbf{G}^T\mathbf{G})^{-1}\mathbf{G}^T$ is the *pseudo-inverse* of $\mathbf{G}$. Substituting $\hat{\mathbf{a}}_m$ into (36) gives

$$\hat{\mathbf{G}} = \arg\min_{\hat{\mathbf{G}}} \|\mathbf{r}_m - \mathbf{G}\mathbf{G}^+\mathbf{r}_m\|^2. \tag{37}$$

Finally, the maximum likelihood solution for the timing is obtained from

$$\hat{\mathbf{G}} = \arg\max_{\mathbf{G}} \mathbf{r}_m^T\mathbf{G}\mathbf{G}^+\mathbf{r}_m. \tag{38}$$

Due to the joint-optimization nature of (38), it requires a multi-dimensional search over a given parameter space. Even if the estimation is performed by using a one chip increment for the test delay, one must test $(C(C-1)\cdots(C-L))^K$ different values.[2] Evaluation is therefore computationally too demanding if many users and paths exist. Moreover, it is impractical for the downlink receiver, where the codes of interfering users are not known. For these reasons (38) is not used in any numerical experiment in this thesis.

3.1.2 Matched filter

The simplest estimator is matched filter (MF) [68], which regards all the interference as noise. In contrast to (38) where the codes with different delays are tested, MF shifts the initial data and correlates it to the known code. The delays are then obtained from the data shifts which correspond to maximal correlations. Considering the data model (18), we can alternatively replace data shifting by code shifting, and process two successive data vectors. Formally,

$$\hat{\chi}_k = \arg\max_{\chi} \sum_{m=1}^{M} \frac{|\overline{\mathbf{c}}_k(\chi)^T \mathbf{r}_m + \underline{\mathbf{c}}_k(\chi)^T \mathbf{r}_{m+1}|}{\|\overline{\mathbf{c}}_k(\chi) + \underline{\mathbf{c}}_k(\chi)\|}. \tag{39}$$

Eq. (39) is known as a conventional non-coherent matched filter. It is non-coherent in the sense that different symbols are not in the same phase due to data modulation.

A common unmodulated pilot channel or dedicated pilot symbols, also called training symbols, can be used in the acquisition process. Pilot symbols are called a preamble, if they are located in the beginning of the data block. In case of "all ones" preamble, and provided that the path strengths vary slowly, we have $\psi^+_{klm} \approx a_{klm}$ and $\psi^-_{klm} \approx 0$, see Eqs. (29) and (30). Thus only $\mathbf{c}^+_{kl}$ is needed to apply to each $\mathbf{r}_m$ in the acquisition process. But the form of $\mathbf{c}^+_{kl}$ with test delay χ is exactly

$$\mathbf{c}_k(\chi) \stackrel{\text{def}}{=} \overline{\mathbf{c}}_k(\chi) + \underline{\mathbf{c}}_k(\chi), \tag{40}$$

and the resulting non-coherent MF is

$$\hat{\chi}_k = \arg\max_{\chi} \frac{|\mathbf{c}_k(\chi)^T \mathbf{R} \mathbf{c}_k(\chi)|}{\|\mathbf{c}_k(\chi)\|^2}, \tag{41}$$

Now also coherent detection can be used, giving an estimator [68]

$$\hat{\chi}_k = \arg\max_{\chi} \frac{|\mathbf{c}'_k(\chi)^T \mathbf{r}|}{\|\mathbf{c}'_k(\chi)\|}, \tag{42}$$

where $\mathbf{r}$ contains all the data in one vector, and $\mathbf{c}'_k(\chi)$ is an equal length vector

$$\mathbf{c}'_k(\chi) = [\mathbf{c}_k(\chi)^T, \ldots, \mathbf{c}_k(\chi)^T]^T. \tag{43}$$

[2] The first path needs C tests, but the second needs only $C-1$, since the one already found delay is not of interest any more. Accordingly, Lth path requires $C-L+1$ delay tests.

In AWGN channel, i.e. when the only channel distortion is the additive white gaussian noise, matched filter is the maximum likelihood method, if only one user occupies the system or the codes in a multiuser system are orthogonal [68, 102]. However, as orthogonality conditions are perturbed, e.g. by multiple paths with different delays, or by asynchronous access, MF becomes suboptimal. In the latter case, tolerable performance is still possible to achieve if the user's signal power levels in the reception are not too dissimilar.

3.1.3 Multiple Signal Classification (MUSIC)

Preceding methods are located in the very extremes in optimality vs. computationality axis. Subspace methods are therefore often introduced as suboptimal methods with tolerable computational cost. They rely on the low rank approximation of the data, which is possible to achieve in a short code system.

Denote λ_p and $\mathbf{u}_p$ the eigenvalues and -vectors of the autocorrelation matrix $\mathbf{R}$, respectively. The eigenvectors are orthonormal by definition. Then,

$$\mathbf{R} = \sum_{p=1}^{C} \lambda_p \mathbf{u}_p \mathbf{u}_p^H. \tag{44}$$

Suppose N is a positive integer ($N < C$), and make groupings

$$\mathbf{U}_s = [\mathbf{u}_1, \cdots, \mathbf{u}_N] \tag{45}$$

$$\mathbf{U}_n = [\mathbf{u}_{N+1}, \cdots, \mathbf{u}_C] \tag{46}$$

$$\mathbf{\Lambda}_s = \begin{bmatrix} \lambda_1 & & \\ & \ddots & \\ & & \lambda_N \end{bmatrix} \tag{47}$$

$$\mathbf{\Lambda}_n = \begin{bmatrix} \lambda_{N+1} & & \\ & \ddots & \\ & & \lambda_C \end{bmatrix}, \tag{48}$$

where the eigenvalues are in decreasing order. Due to Eq. (32), we have moreover

$$\lambda_p = \begin{cases} \mu_p + \sigma^2 & , \text{for } p = 1, \ldots, N \\ \sigma^2 & , \text{for } p = N+1, \ldots, C. \end{cases} \tag{49}$$

Hence,

$$\mathbf{R} = \mathbf{U}_s \mathbf{\Lambda}_s \mathbf{U}_s^H + \mathbf{U}_n \mathbf{\Lambda}_n \mathbf{U}_n^H \tag{50}$$

$$= \mathbf{U}_s \mathbf{\Lambda}_s \mathbf{U}_s^H + \sigma^2 \mathbf{I}. \tag{51}$$

The eigenvectors $\mathbf{u}_1, \ldots, \mathbf{u}_N$ hence span exactly the same space as the columns of $\mathbf{G}$. This space is called *signal subspace*, and its orthogonal complement is called *noise subspace*. Those subspaces are spanned by *signal* and *noise eigenvectors*, respectively.

MUSIC estimator was introduced in 1979 by Schmidt in direction-of-arrival (DOA) estimation [79, 80]. Recently, it has been successfully applied to the CDMA code timing estimation [82, 4]. In CDMA, the underlying observation is that the columns of the code matrix $\mathbf{G}$ are orthogonal to the noise eigenvectors. This is because,

$$\mathbf{R}\mathrm{u}_p = \sigma^2 \mathrm{u}_p \text{ , for } p = N+1, \ldots, C \tag{52}$$

$$\mathbf{R}\mathrm{u}_p = (\mathbf{G}\mathbf{A}\mathbf{G}^T + \sigma^2\mathbf{I})\mathrm{u}_p \text{ , for } p = 1, \ldots, C, \tag{53}$$

and subtraction immediately yields

$$\mathbf{G}\mathbf{A}\mathbf{G}^T \mathrm{u}_p = \mathbf{0} \text{ , for } p = N+1, \ldots, C. \tag{54}$$

If we denote $\mathbf{g}_{p'}$ the p'th column of $\mathbf{G}$, and $P \stackrel{\text{def}}{=} rank(\mathbf{G})$ we achieve an orthogonality condition

$$\mathbf{g}_{p'}^T \mathrm{u}_p = 0 \text{ , for any } p' = 1, \ldots, P \text{ , and } p = N+1, \ldots, C. \tag{55}$$

This immediately results in more general orthogonality condition

$$\mathbf{g}_{p'}^T \sum_{p=N+1}^{C} \alpha_p \mathbf{u}_p = 0 \text{ , } p' = 1, \ldots, P, \tag{56}$$

with scalar multiplicatives α_p. As a special case we thus have

$$\mathbf{g}_{p'}^T \mathbf{U}_n \mathbf{U}_n^H \mathbf{g}_{p'} = 0. \tag{57}$$

The MUSIC estimator now searches for the phase of the desired code that best satisfy the orthogonality condition (57). Formally, the noise subspace parameters $\mathbf{U}_n$ and $\mathbf{\Lambda}_n$ are first estimated from the sample autocorrelation matrix $\hat{\mathbf{R}} = \mathbf{X}\mathbf{X}^H/M$, and the delays are obtained from

$$\hat{\chi}_k = \arg\max_{\chi} \frac{1}{|\mathbf{c}_k(\chi)^T \hat{\mathbf{U}}_n \hat{\mathbf{U}}_n^H \mathbf{c}_k(\chi)|}. \tag{58}$$

Alternatively, signal eigenvectors can be used, giving an estimator

$$\hat{\chi}_k = \arg\max_{\chi} |\mathbf{c}_k(\chi)^T \hat{\mathbf{U}}_s \hat{\mathbf{U}}_s^H \mathbf{c}_k(\chi)|. \tag{59}$$

3.1.4 Minimum variance delay estimator

The Constrained Miminum Output Energy (CMOE) -method was introduced in [23] for interference suppression, but was also found to have good synchronization capability in [40, 41]. CMOE is a modification of the well known Capon's filter, which minimizes the output energy of the interfering sources while passing the desired source undistorted. The criterion with a processing window of $(D+1)$ symbols is

$$\arg\min_{\mathbf{c}} E\{|\mathbf{c}^H \tilde{\mathbf{r}}_m|^2\} \text{ , subject to } \mathbf{c}^H \tilde{\mathbf{c}}_{kl} = 1, \tag{60}$$

where

$$\tilde{\mathbf{c}}_{kl} = \tilde{\mathbf{c}}_k(\chi_{kl}) \stackrel{\text{def}}{=} (1-\delta_{kl})[\mathbf{0}_{d_{kl}}^T \; s_k \; \mathbf{0}_{DC-d_{kl}}^T]^T + \\ + \; \delta_{kl}[\mathbf{0}_{d_{kl}+1}^T \; s_k \; \mathbf{0}_{DC-d_{kl}-1}^T]^T. \tag{61}$$

This leads to a filter

$$\tilde{\mathbf{c}}^{\text{CMOE}} = \tilde{\mathbf{R}}^{-1}\tilde{\mathbf{c}}_{kl}, \tag{62}$$

where $\tilde{\mathbf{R}} = E\{\tilde{\mathbf{r}}_m\tilde{\mathbf{r}}_m^H\}$. In synchronization CMOE is applied as

$$\hat{\chi}_k = \arg\min_{\chi} \frac{|\tilde{\mathbf{c}}_k(\chi)^T\tilde{\mathbf{R}}^{-1}\tilde{\mathbf{c}}_k(\chi)|}{\|\tilde{\mathbf{c}}_k(\chi)\|^2}. \tag{63}$$

If the processing window is only one symbol, and the data modulation is on, the CMOE synchronization criterion is slightly different. Namely [40],

$$\hat{\chi}_k = \arg\min_{\chi} \frac{|\underline{\mathbf{c}}_k(\chi)^T\mathbf{R}^{-1}\underline{\mathbf{c}}_k(\chi) + \overline{\mathbf{c}}_k(\chi)^T\mathbf{R}^{-1}\overline{\mathbf{c}}_k(\chi)|}{\|\mathbf{c}_k(\chi)\|^2}. \tag{64}$$

3.1.5 Other methods

The preceding methods exploit only the known code information, and most of them can operate even without preambles. Efficient use of preamble was recently utilized in [112] and [5]. Both maximum likelihood -based algorithms modeled the training symbols as a desired signal and all the interference as colored non-Gaussian noise that is uncorrelated with the desired signal. The algorithm in [112] was found to be near-far resistant and can tolerate high system loading. In addition, the accuracy of the delay estimate was achieved by solving a second-order polynomial for each chip interval. A major limitation, however, is that the method cannot be extended to fading channels. This is mainly because of the need of long training period. This disadvantage was removed by the receiver diversity in [44], which allowed shorter training. The algorithm in [5] also has limitations with the extension to fading channels, and moreover looses its near-far resistance in highly loaded systems. The computational complexity of all those algorithms is also still quite high from the downlink signal processing point of view.

The most promising performance with low computation was found in [110], where the effects of interference were suppressed by correlating the matched filter output with a delayed version of it. The motivation for this *differential* correlation is, roughly speaking as follows: when only $+1$'s are sent to the desired user, its contribution in the received signal at the symbol level is only the fading process, whose time-correlatedness can be exploited. Basically the same idea was exploited also in [12], with the exception that the differential correlation was performed prior to matched filtering. This was due to the special shift-and-add -property of m-sequences, which makes the proposed algorithm sensitive to the choice of the spreading code.

Other quite recent papers on code acquisition include e.g. [15, 69, 20].

3.2 Delay estimation by differential correlations

Our goal is to compute the correlation matrix $\mathbf{R}(\tau)$ of the sampled data (23), where the time lag equals $\tau \neq 0$ symbols. In short, we call $\mathbf{R}(\tau)$ a differential- instead of autocorrelation matrix to stress the nonzero time lag. The proposed methods are based on the observation that $\mathbf{R}(\tau)$ contains timing information only of the desired user, which is first shown. Without loss of generality, let us assume that the user $k = 1$ is the desired one. The following assumptions are made:

#1. A constant preamble $b_{1m} = 1, m = 1, \ldots, M$ ("all ones") is available for the desired user.

#2. Symbols of interfering users are uncorrelated random binary variables of zero mean. Then $E\{b_{km}b_{k',m+\tau}\} = 0$, and $E\{b_{km}\} = 0$ for $k \neq 1$.

#3. Fading processes of each path are uncorrelated.Then $E\{a_{lm}a^*_{l'n}\} = 0$ for $l \neq l'$.

#4. Fading process of each path is stationary. Therefore, the correlation coefficient $\alpha_l(\tau) \stackrel{\text{def}}{=} \frac{E\{a_{lm}a^*_{ln}\}}{E\{|a_{lm}|\}E\{|a^*_{ln}|\}} = \frac{E\{a_{lm}a^*_{ln}\}}{\mu_l^2}$, where $\tau = m - n$, and $\mu_l = E\{|a_{lm}|\}$.

#5. Noise is a random zero mean variable, and independent with the data and fading. Then $E\{\mathbf{n}_m\mathbf{n}^H_{m+\tau}\} = \mathbf{0} = E\{\mathbf{n}_m\mathbf{a}^H_{m+\tau}\}$, where $\mathbf{n}_m$ and $\mathbf{a}_m$ are those of Eq. (22).

Notice that assumption (#1) can also be replaced by assuming that there exists a common unmodulated pilot channel. Notice also that assumptions (#3) and (#4) are equivalent to the common uncorrelated scatterer (US) model [68], and wide-sense stationary (WSS) model [63], respectively. It should be noted, however, that assumption (#3) is not necessary for the purposes of the paper, but it is made to achieve a simple and elegant representation of $\mathbf{R}(\tau)$. The case where (#3) do not apply is discussed in **Remark 1**.

According to Eq. (22), and assumption (#5), the differential correlation matrix now is

$$\begin{aligned}\mathbf{R}(\tau) \stackrel{\text{def}}{=} E\{\mathbf{r}_m\mathbf{r}^H_{m+\tau}\} &= E\{(\mathbf{G}\mathbf{a}_m + \mathbf{n}_m)(\mathbf{G}\mathbf{a}_{m+\tau} + \mathbf{n}_{m+\tau})^H\} \\ &= \mathbf{G}\mathbf{A}(\tau)\mathbf{G}^T, \end{aligned} \tag{65}$$

where the $2KL \times 2KL$ dimensional matrix $\mathbf{A}(\tau)$ is defined as

$$\mathbf{A}(\tau) \stackrel{\text{def}}{=} E\{\mathbf{a}_m\mathbf{a}^H_{m+\tau}\}. \tag{66}$$

According to Eq. (21), the matrix $\mathbf{A}(\tau)$ contains $(KL)^2$ submatrices of dimension 2×2. Denote these by $\mathbf{A}_{(kl),(k'l')}(\tau)$, i.e.

$$\mathbf{A}_{(kl),(k'l')}(\tau) \stackrel{\text{def}}{=} E\{\mathbf{z}_{klm}\mathbf{z}^H_{k'l',m+\tau}\}. \tag{67}$$

If we denote $[\cdot]_{ij}$ the (i,j) element of a matrix, we have from Eq. (20)

$$\begin{aligned}
\left[\mathbf{A}_{(kl),(k'l')}(\tau)\right]_{11} &= E\{a_{l,m-1}a^*_{l',m+\tau-1}b_{k,m-1}b_{k',m+\tau-1}\} && (68)\\
\left[\mathbf{A}_{(kl),(k'l')}(\tau)\right]_{12} &= E\{a_{l,m-1}a^*_{l',m+\tau}b_{k,m-1}b_{k',m+\tau}\} && (69)\\
\left[\mathbf{A}_{(kl),(k'l')}(\tau)\right]_{21} &= E\{a_{lm}a^*_{l',m+\tau-1}b_{km}b_{k',m+\tau-1}\} && (70)\\
\left[\mathbf{A}_{(kl),(k'l')}(\tau)\right]_{22} &= E\{a_{lm}a^*_{l',m+\tau}b_{km}b_{k',m+\tau}\} && (71)
\end{aligned}$$

Since fading and symbol processes are independent, we have moreover

$$\begin{aligned}
\left[\mathbf{A}_{(kl),(k'l')}(\tau)\right]_{11} &= E\{a_{l,m-1}a^*_{l',m+\tau-1}\}E\{b_{k,m-1}b_{k',m+\tau-1}\} && (72)\\
\left[\mathbf{A}_{(kl),(k'l')}(\tau)\right]_{12} &= E\{a_{l,m-1}a^*_{l',m+\tau}\}E\{b_{k,m-1}b_{k',m+\tau}\} && (73)\\
\left[\mathbf{A}_{(kl),(k'l')}(\tau)\right]_{21} &= E\{a_{lm}a^*_{l',m+\tau-1}\}E\{b_{km}b_{k',m+\tau-1}\} && (74)\\
\left[\mathbf{A}_{(kl),(k'l')}(\tau)\right]_{22} &= E\{a_{lm}a^*_{l',m+\tau}\}E\{b_{km}b_{k',m+\tau}\} && (75)
\end{aligned}$$

Next we show that almost all matrices $\mathbf{A}_{(kl),(k'l')}(\tau)$ are equal to $\mathbf{0}$, provided the time difference is equal to $\tau = 2,3,4,\ldots$ symbols. The reason why $\tau = 1$ is not a good choice for the time lag is discussed in **Remark 2**.

Case 1: $1 = k = k'$. Now all the symbols are equal to 1, and $\mathbf{A}_{(1l),(1l')}(\tau)$ depends only on the channel coefficients. With $l \neq l'$ we have $\mathbf{A}_{(1l),(1l')}(\tau) = \mathbf{0}$ due to the assumption (#3). On the other hand, with $l = l'$, we have due to the assumption (#4)

$$\mathbf{A}_{(1l),(1l)}(\tau) = \mu_l^2 \begin{bmatrix} \alpha_l(\tau) & \alpha_l(\tau+1) \\ \alpha_l(\tau-1) & \alpha_l(\tau) \end{bmatrix}. \qquad (76)$$

Case 2: $1 = k \neq k'$. Now $\mathbf{A}_{(1l),(k'l')}(\tau)$ depends on the channel coefficients and the symbols of user k'. Since these symbols are zero mean, $\mathbf{A}_{(1l),(k'l')}(\tau) = \mathbf{0}$ for all l, l'.

Case 3: $1 \neq k, k'$. In this case, we always have $\mathbf{A}_{(kl),(k'l')}(\tau) = \mathbf{0}$ due to the assumption (#2).

Hence, the matrix $\mathbf{A}(\tau)$ contains only L non-zero submatrices of 2×2, and they correspond to the situations where $k = k' = 1$ and $l = l'$. Due to the definition of Eq. (21), these submatrices are situated in the main diagonal of $\mathbf{A}(\tau)$. Therefore Eq. (65) reduces to

$$\mathbf{R}(\tau) = \mathbf{G} \left[\begin{array}{ccc|c} \mathbf{A}_{(11),(11)}(\tau) & & \mathbf{0} & \\ & \ddots & & \mathbf{0} \\ \mathbf{0} & & \mathbf{A}_{(1L),(1L)}(\tau) & \\ \hline & \mathbf{0} & & \mathbf{0} \end{array}\right] \mathbf{G}^T, \qquad (77)$$

from which we see that $\mathbf{R}(\tau)$ depends only on $2L$ first rows of the codematrix $\mathbf{G}$. Since these rows correspond to the desired user $k = 1$ only, see Eq. (19), the contribution of interference is suppressed from $\mathbf{R}(\tau)$. To express in detail the form of $\mathbf{R}(\tau)$, we make a mild assumption that $\alpha_l(\tau-1) \approx \alpha_l(\tau) \approx \alpha_l(\tau+1)$, and denote it $\bar{\alpha}_l(\tau)$. This means that the fading process has almost the same degree of

correlation whether the time difference is $\tau-1, \tau$ or $\tau+1$ symbols. Then, Eq.(76) reduces to $\mathbf{A}_{(1l),(1l)}(\tau)=\mu_l^2\bar{\alpha}_l(\tau)\mathbf{1}$, and consequently (see details in the Appendix 2)

$$\mathbf{R}(\tau)=\mathbf{G}\left[\begin{array}{ccc|c} \mu_1^2\bar{\alpha}_1(\tau)\mathbf{1} & & \mathbf{0} & \\ & \ddots & & \mathbf{0} \\ \mathbf{0} & & \mu_L^2\bar{\alpha}_L(\tau)\mathbf{1} & \\ \hline & \mathbf{0} & & \mathbf{0} \end{array}\right]\mathbf{G}^T=\sum_{l=1}^{L}\mu_l^2\bar{\alpha}_l(\tau)\mathbf{c}_{1l}\mathbf{c}_{1l}^T, \qquad (78)$$

where we recall that $\mathbf{c}_{1l}=\underline{\mathbf{c}}_{1l}+\overline{\mathbf{c}}_{1l}$ by definition (40). From the structure of $\mathbf{R}(\tau)$ we see explicitly that it contains the code and delay information of the desired user $k=1$ only.

Remark 1. The reason for assumption (#3) was to achieve a compact representation Eq. (78). However, to ensure that the differential correlation matrix $\mathbf{R}(\tau)$, with $\tau\geq 2$ symbols, contains *only* the desired user's information, assumption (#3) is not necessary. This is because the contribution of interfering users are got only via "Case 2" and "Case 3" above. However, in these cases the zero submatrices were *always* due to the uncorrelatedness and the zero-mean properties of the interfering user's symbols. Therefore, $\mathbf{R}(\tau)$ is free of contributions of interfering users even without assumption (#3), although the form of $\mathbf{R}(\tau)$ is a little bit different. This is because now in "Case 1", both subcases "$l=l'$", and "$l\neq l'$" cause non-zero submatrices. The case where assumption (#3) do not apply include e.g. fixed multipath channel. In that case, the paths are highly correlated.

Remark 2. It is important to notice, that the situation $\tau=1$ is not as desired as the case $\tau\geq 2$ symbols. The reason is as follows: due to symbol asynchronous sampling, the sample vectors $\mathbf{r}_m$ usually contain information about two successive symbols, see Eq. (18). Therefore, with the time lag $\tau=1$ symbol, two successive sample vectors also have some degree of correlation with respect to the interfering users. To see this in details, let $\tau=1$, and consider $\mathbf{A}_{(kl),(k'l')}(1)$,

$$\begin{aligned}
\left[\mathbf{A}_{(kl),(k'l')}(1)\right]_{11} &= E\{a_{l,m-1}a_{l'm}^*\}E\{b_{k,m-1}b_{k'm}\} && (79)\\
\left[\mathbf{A}_{(kl),(k'l')}(1)\right]_{12} &= E\{a_{l,m-1}a_{l',m+1}^*\}E\{b_{k,m-1}b_{k',m+1}\} && (80)\\
\left[\mathbf{A}_{(kl),(k'l')}(1)\right]_{21} &= E\{a_{lm}a_{l'm}^*\}E\{b_{km}b_{k'm}\} && (81)\\
\left[\mathbf{A}_{(kl),(k'l')}(1)\right]_{22} &= E\{a_{lm}a_{l',m+1}^*\}E\{b_{km}b_{k',m+1}\} && (82)
\end{aligned}$$

If now $1\neq k=k'$ with $l=l'$, which belongs to "Case 3" above, we would have a non-zero submatrix equal to

$$\mathbf{A}_{(kl),(kl)}(1)=\left[\begin{array}{cc} 0 & 0 \\ E\{|a_{lm}|^2\} & 0 \end{array}\right]. \qquad (83)$$

If $\mathbf{R}(1)$ is now rewritten in the form of Eq. (78), $\mathbf{R}(1)$ would clearly have a contribution which corresponds to the interfering user $k\neq 1$. For this reason, we only consider cases where $\tau\geq 2$ symbols.

Remark 3. It is worth mentioning that the differential correlation matrix $\mathbf{R}(\tau)$ with $\tau \geq 2$ contains two kinds of information about the channel: the average power of the paths, and the rapidity of their fading process. The latter is related to the correlation coefficient $\bar{\alpha}_l(\tau)$, which is closer to 0 (resp. 1) the faster (resp. slower) is the fading process.

3.2.1 MF-type approach

In practice $\mathbf{R}(\tau)$ is estimated by $\hat{\mathbf{R}}(\tau) = \frac{1}{M}\sum_{m=1}^{M} \mathbf{r}_m \mathbf{r}_{m+\tau}^H$. The simplest way to estimate the delay is to try and match the known code to the data as well as possible. I.e. to find the solution for

$$\hat{\chi} = \arg\max_{\chi} \frac{|\mathbf{c}_1(\chi)^T \hat{\mathbf{R}}(\tau)\mathbf{c}_1(\chi)|}{\|\mathbf{c}_1(\chi)\|^2}. \tag{84}$$

The delay estimator Eq. (84), which we label DC-MF (Differential Correlations based MF), was the main contribution of [32]. Notice that as "all ones" preamble is used, the conventional non-coherent MF (39) is exactly DC-MF with $\tau = 0$. It is also worth noticing that, since Eq. (84) equals

$$\hat{\chi} = \arg\max_{\chi} |\frac{1}{M}\sum_{m=1}^{M} \frac{\mathbf{c}_1(\chi)^T \mathbf{r}_m}{\|\mathbf{c}_1(\chi)\|} \frac{\mathbf{r}_{m+\tau}^H \mathbf{c}_1(\chi)}{\|\mathbf{c}_1(\chi)\|}|, \tag{85}$$

DC-MF includes, indeed, only MF operations. Moreover, it tells that DC-MF is applicable also in the system with aperiodic (long) codes, since only the MF outputs are needed. The estimator of form Eq. (85) would be the practical implementation of DC-MF, and is depicted in Figure 12.

3.2.2 MUSIC-type approach

In practice, the estimate $\hat{\mathbf{R}}(\tau)$ will always contain some contributions of interfering users and noise due to the finite length of the preamble. But if $\hat{\mathbf{R}}(\tau)$ would have exactly the form of Eq. (65), or equally Eq. (78), it could be rewritten by eigenvalue decomposition as

$$\mathbf{R}(\tau) = \mathbf{U}(\tau)\mathbf{\Lambda}\mathbf{U}(\tau)^H. \tag{86}$$

Here $\mathbf{\Lambda}$ is a diagonal matrix, whose diagonal elements are L non-zero eigenvalues of $\mathbf{R}(\tau)$, and $\mathbf{U}(\tau)$ is a $C \times L$ dimensional matrix, containing the related eigenvectors on its columns. But then MUSIC [80] could be used to estimate the delays. Due to finite number of samples, $\hat{\mathbf{R}}(\tau)$ will be in practice asymmetric, and it must be first symmetrized to achieve real eigenvalues and orthonormal eigenvectors. Therefore, we define symmetric $\hat{\mathbf{R}}_{\mathbf{sym}}(\tau) = \hat{\mathbf{R}}(\tau) + \hat{\mathbf{R}}(\tau)^H$, for which MUSIC is applied. More precisely, the delay estimation is performed as

$$\hat{\chi} = \arg\max_{\chi} \frac{\|\hat{\mathbf{U}}^H(\tau)\mathbf{c}_1(\chi)\|^2}{\|\mathbf{c}_1(\chi)\|^2}, \tag{87}$$

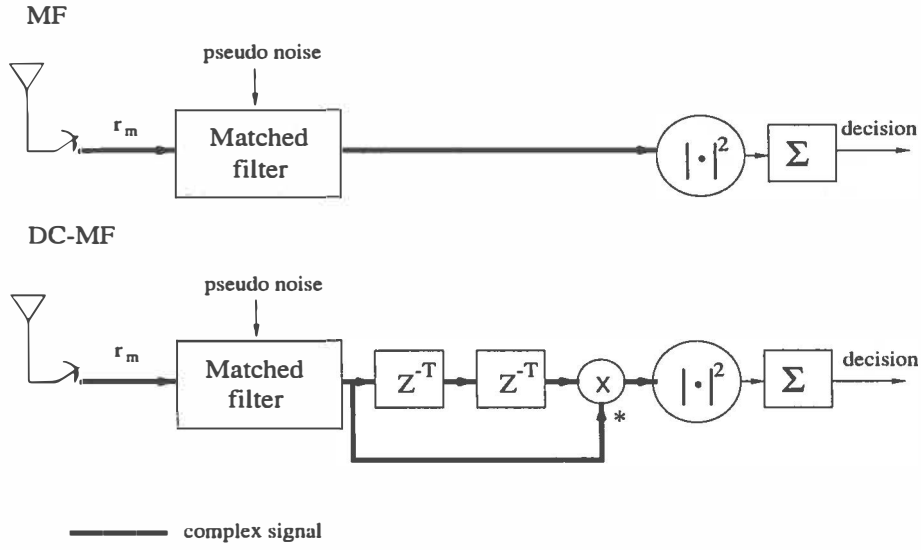

FIGURE 12 Conventional non-coherent MF (top) and DC-MF (bottom). The decision is performed by a threshold element, after cumulating the information from a predetermined number of data vectors. T is a symbol duration.

where $\hat{\mathbf{U}}(\tau)$ consists of L principal eigenvectors of $\hat{\mathbf{R}}_{\text{sym}}(\tau)$. We label this estimator as DC-MUSIC (Differential Correlations based MUSIC).

The difference between traditional MUSIC (59) and DC-MUSIC arise from the development of the autocorrelation matrix, whose principal eigenvectors are computed. In traditional MUSIC, a matrix $\mathbf{R} = \mathbf{R}(0)$ is computed, i.e. the time lag for the data is zero. As was seen earlier, $\mathbf{R}$ has a signal subspace of dimension $\min\{N, C\}$. Considering the data model (18), N can be as high as $N = 2KL$ due to multipath fading, and even in non-fading case N is still as large as $N = 2K$. In a highly loaded system, when $N > C$, $\hat{\mathbf{R}}(0)$ does not obey subspace structure anymore, and this causes the failure of MUSIC. In DC-MUSIC, on the other hand, the first thing to do is to filter the interference and noise out as much as possible by differential correlations, i.e. by estimating $\hat{\mathbf{R}}(\tau)$ instead of $\hat{\mathbf{R}}(0)$. In theory, $\mathbf{R}(\tau)$ is of rank L, which is a big enough rank reduction to make circumstances favorable for MUSIC. Equally important, the rank is reduced while still preserving the desired information. In practice, as the interference can not be suppressed totally due to a finite number of vector samples, L principal eigenvectors of symmetrized $\hat{\mathbf{R}}_{\text{sym}}(\tau)$ are estimated, after which MUSIC is applied.

3.2.3 Timing-offset estimation

Up to this point we have considered only the coarse delay estimation by fractional test delays, which is clearly enough to achieve an estimation error less than half of a chip duration. The accuracy of the estimate can then be achieved in the tracking mode. Of course, accuracy could also be achieved by using smaller step sizes for the test delays. However, differential correlations enable actual solving of the fractional part of the delay. Namely, we show in the following that in a frequency-flat fading channel it is enough to solve a system of two second-order polynomials for each chip interval.

Assume only one resolvable path exists. Suppose $d + \delta = d_1 + \delta_1$ is the propagation delay, so that the differential correlation matrix (78) becomes $\mathbf{R}(\tau) = \bar{\alpha}(\tau)\mathbf{c}_{11}\mathbf{c}_{11}^T$. Recall that $\mathbf{c}_{11} = \underline{\mathbf{c}}_{11} + \overline{\mathbf{c}}_{11}$ by Eq. (40). Analogously, we may define

$$\mathbf{s}_{11} = \mathbf{s}_1(d) \stackrel{\text{def}}{=} \underline{\mathbf{s}}_{11} + \overline{\mathbf{s}}_{11} \tag{88}$$

(see Eqs. (14) and (15)), which is thus just a d chips delayed replica of the desired code $\mathbf{s}_1$. Accordingly, we have $\mathbf{c}_{11} = (1-\delta)\mathbf{s}_1(d) + \delta\mathbf{s}_1(d+1)$. Suppose now that we use the test codes exactly $\mathbf{s}_1(d)$ and $\mathbf{s}_1(d+1)$. This is because the true delay lies between d and $d+1$. Considering the MF-type approach, we immediately have (see details in the Appendix 3)

$$|\mathbf{s}_1(d)^T\mathbf{R}(\tau)\mathbf{s}_1(d)| = |\bar{\alpha}(\tau)|[(1-\delta)\eta_0 + \delta\eta_1]^2 \tag{89}$$

$$|\mathbf{s}_1(d+1)^T\mathbf{R}(\tau)\mathbf{s}_1(d+1)| = |\bar{\alpha}(\tau)|[(1-\delta)\eta_1 + \delta\eta_0]^2, \tag{90}$$

where $\eta_i \stackrel{\text{def}}{=} \mathbf{s}_1(d)^T\mathbf{s}_1(d+i)$. Notice that these quantities are known, since they are (up to scaling) just values of the code autocorrelation function with time lag i chips. For example, for m-sequences $\eta_0 = C$, and $\eta_1 = -1$. Hence, only two unknowns, $|\bar{\alpha}(\tau)|$ and δ are included in Eqs. (89) and (90). The solutions for δ can be found (see details in the Appendix 4) to be equal to

$$\delta = \delta(d) = \frac{\eta_0 \mp P(d)\eta_1}{(\eta_0 - \eta_1)(1 \pm P(d))}, \tag{91}$$

where

$$P(d) = \sqrt{\frac{|\mathbf{s}_1(d)^T\mathbf{R}(\tau)\mathbf{s}_1(d)|}{|\mathbf{s}_1(d+1)^T\mathbf{R}(\tau)\mathbf{s}_1(d+1)|}}. \tag{92}$$

We can also rewrite Eq. (92) as

$$P(d) = \sqrt{\frac{|\frac{1}{M}\sum_{m=1}^{M}\mathbf{s}_1(d)^T\mathbf{r}_m\mathbf{r}_{m+\tau}^H\mathbf{s}_1(d)|}{|\frac{1}{M}\sum_{m=1}^{M}\mathbf{s}_1(d+1)^T\mathbf{r}_m\mathbf{r}_{m+\tau}^H\mathbf{s}_1(d+1)|}}, \tag{93}$$

which is more a suitable expression in the case of aperiodic codes. Eq. (91), which we label ADC-MF (Accurate DC-MF), is a closed form expression for the timing offset δ, for which we need only the information about the hypotheses d and $d+1$.

Also the MUSIC-type approach could be used. This is because $\mathbf{R}(\tau) = \bar{\alpha}(\tau)\mathbf{c}_{11}\mathbf{c}_{11}^T$ has only one non-zero eigenvalue, and the related eigenvector is $\mathbf{c}_{11}/\|\mathbf{c}_{11}\|$. Replacing $\mathbf{R}(\tau)$ by $\mathbf{U}(\tau)\mathbf{U}(\tau)^H = \mathbf{c}_{11}\mathbf{c}_{11}^T/\|\mathbf{c}_{11}\|^2$ is Eqs. (89) and (90), we would have

$$|\mathbf{s}_1(d)^T\mathbf{U}(\tau)\mathbf{U}(\tau)^H\mathbf{s}_1(d)| = \frac{1}{\|\mathbf{c}_{11}\|^2}[(1-\delta)\eta_0 + \delta\eta_1]^2 \quad (94)$$

$$|\mathbf{s}_1(d+1)^T\mathbf{U}(\tau)\mathbf{U}(\tau)^H\mathbf{s}_1(d+1)| = \frac{1}{\|\mathbf{c}_{11}\|^2}[(1-\delta)\eta_1 + \delta\eta_0]^2. \quad (95)$$

Since $\|\mathbf{c}_{11}\|$ is unknown, as being a function of δ, we end up with Eqs. (91) and (92). Naturarly, $\mathbf{R}(\tau)$ is replaced by $\mathbf{U}(\tau)\mathbf{U}(\tau)^H$ in Eq. (92). Analogously, we label this approach as ADC-MUSIC (Accurate DC-MUSIC), and summarize it together with ADC-MF in Table 1.

Remark 4. A slightly modyfied version of Eq. (91) could also be used in case of multipaths. This is because

$$\begin{aligned}\mathbf{R}(\tau) &= \sum_{l=1}^{L}\bar{\alpha}_l(\tau)\mathbf{c}_{1l}\mathbf{c}_{1l}^T, \text{ i.e. Eq. (78)} \\ &= \sum_{l=1}^{L}\bar{\alpha}_l(\tau)[(1-\delta_l)^2\mathbf{s}_1(d_l)\mathbf{s}_1(d_l)^T \\ &+ 2\delta_l(1-\delta_l)\mathbf{s}_1(d_l)\mathbf{s}_1(d_l+1)^T + \delta_l^2\mathbf{s}_1(d_l+1)\mathbf{s}_1(d_l+1)^T]. \quad (96)\end{aligned}$$

Letting now $d = d_1$, equations (89) and (90) would accordingly have more of a general forms

$$\begin{aligned}|\mathbf{s}_1(d_1)^T\mathbf{R}(\tau)\mathbf{s}_1(d_1)| &= |\bar{\alpha}_1(\tau)|[(1-\delta_1)\eta_0 + \delta\eta_1]^2 \\ &+ \sum_{l=2}^{L}\bar{\alpha}_l(\tau)[(1-\delta_l)\eta_{d_1-d_l} + \delta\eta_{d_1-d_l-1}]^2 \quad (97)\end{aligned}$$

$$\begin{aligned}|\mathbf{s}_1(d_1+1)^T\mathbf{R}(\tau)\mathbf{s}_1(d_1+1)| &= |\bar{\alpha}_1(\tau)|[(1-\delta)\eta_1 + \delta\eta_0]^2 \\ &+ \sum_{l=2}^{L}\bar{\alpha}_l(\tau)[(1-\delta_l)\eta_{d_1-d_l-1} + \delta\eta_{d_1-d_l}]^2. \quad (98)\end{aligned}$$

Assuming impulse-like code autocorrelation, i.e. $\eta_i \approx 0$ for $|i| \geq 1$, we would end up with (89) and (90), where in addition $\eta_1 \approx 0$. This would accordingly lead to an estimator

$$\hat{\delta} = \frac{1}{1 \pm P(d)}. \quad (99)$$

3.2.4 SVD approach

As the sampled CDMA signal has the linear form of Eq. (22), the subspace approach can be used for filtering additive noise out, and to improve the near-far resistance of DC-MF. More specifically, the data is first whitened e.g. by the

TABLE 1 Algorithms ADC-MF and ADC-MUSIC for timing offset estimation.

Denote Ω the set of delay candidates.

1. Estimate the differential correlation matrix with the time lag τ from available vector samples as $\hat{\mathbf{R}}(\tau) = \frac{1}{M}\sum_{m=1}^{M} \mathbf{r}_m \mathbf{r}_{m+\tau}^H$.
2. Let $\hat{\mathbf{U}}(\tau)$ contain L principal eigenvectors of $\hat{\mathbf{R}}(\tau) + \hat{\mathbf{R}}(\tau)^H$, where L is the number of paths to be acquired.
3. Set $\Omega = \{0, 1, \ldots, C\}$, i.e. multiples of a chip duration.
4. For each $d \in \Omega - \{C\}$ do:
   (a) Compute two candidates for fractional part of the delay, $\hat{\delta}(d)$, according to Eqs. (91) and (92). In the latter equation, replace
   - $\mathbf{R}(\tau)$ by $\hat{\mathbf{R}}(\tau)$ in case of ADC-MF,
   - $\mathbf{R}(\tau)$ by $\hat{\mathbf{U}}(\tau)\hat{\mathbf{U}}(\tau)^H$ in case of ADC-MUSIC

   (b) Insert $d + \hat{\delta}(d)$ to Ω, if $\hat{\delta}(d) \in (0, 1)$.
5. Obtain one delay estimate by choosing the strongest peak from the delay spectrum

$$\frac{|\mathbf{c}_1(\chi)^T \Theta \mathbf{c}_1(\chi)|}{\|\mathbf{c}_1(\chi)\|^2} \begin{cases} \Theta = \hat{\mathbf{R}}(\tau), \text{ ADC-MF} \\ \Theta = \hat{\mathbf{U}}(\tau)\hat{\mathbf{U}}(\tau)^H, \text{ ADC-MUSIC} \end{cases} \quad (100)$$

   where $\mathbf{c}_1(\chi)$ is of form Eq. (40), corresponding to delay $\chi \in \Omega$.
6. If other paths are acquired, too, choose such a next strongest peak of Eq. (100), which does not correspond to a delay closer than one chip to any already found delays.

means of Singular Value Decomposition (SVD). The SVD for the data matrix $\mathbf{X} \stackrel{\text{def}}{=} [\tilde{\mathbf{r}}_1 \cdots \tilde{\mathbf{r}}_M]$ gives

$$\mathbf{X} = \mathbf{U}\Sigma\mathbf{V}^H, \quad (101)$$

where $\mathbf{U}$ consists left orthonormal singular vectors, Σ consists singular values as its diagonal, and $\mathbf{V}$ consists right orthonormal singular vectors. Low-rank approximation of the data is then $\mathbf{U}_s\Sigma_s\mathbf{V}_s^H$, where the matrices correspond to the largest singular values. The dimensions of the matrices $\mathbf{U}_s$, Σ_s, and $\mathbf{V}_s^H$ are $(D+1)C \times (D+1)KL$, $(D+1)KL \times (D+1)KL$, and $(D+1)KL \times N$, respectively, where $D+1$ is the processing window size in symbols. By this choice the spanning property range($\mathbf{U}_s$) =range($\mathbf{G}$) holds, if no noise exists. The *whitened*

data is then defined as follows:

$$\mathbf{Y} \stackrel{\text{def}}{=} \mathbf{V}^H = \mathbf{\Sigma}_s^{-1}\mathbf{U}_s^H\mathbf{X}. \tag{102}$$

The differential correlation matrix $\mathbf{R}_w$ for whitened data then has the form

$$\begin{aligned} \mathbf{R}_w(\tau) &= \mathrm{E}\{\mathbf{y}_m\mathbf{y}_{m+\tau}^H\} && (103)\\ &= \mathbf{\Sigma}_s^{-1}\mathbf{U}_s^H\mathbf{R}(\tau)\mathbf{U}_s\mathbf{\Sigma}_s^{-1}. && (104) \end{aligned}$$

The delay estimates are finally obtained from the WDC-MF (Whitened DC-MF) estimator

$$\hat{\chi} = \arg\max_{\chi} \frac{|\mathbf{c}_1(\chi)^T\hat{\mathbf{U}}_s\hat{\mathbf{R}}_w(\tau)\hat{\mathbf{U}}_s^H\mathbf{c}_1(\chi)|}{\|\mathbf{c}_1(\chi)\|^2}. \tag{105}$$

If we use the theoretical form of the whitened matrix (104) and apply (78) and (105), we obtain the estimator

$$\mathbf{c}_1(\chi)^T\mathbf{U}_s\mathbf{R}_w(\tau)\mathbf{U}_s^H\mathbf{c}_1(\chi) = \sum_{l=1}^{L}\alpha_l|\mathbf{c}_1(\chi)^T\mathbf{U}_s\mathbf{\Sigma}_s^{-1}\mathbf{U}_s^H\mathbf{c}_{1l}|^2, \tag{106}$$

where the test code is tried to fit to the filtered low-rank data instead of the original data.

Figure 13 illustrates the gain achieved by WDC-MF in the near-far scenario. The figure plots a typical delay spectra of WDC-MF, and MUSIC when strong interference occurs. Two equal energy paths existed on the channel. Even though WDC-MF and MUSIC use the same subspace parameters, the use of known symbols and differential correlation enables the additional suppression of multiple access interference. In the delay spectrum of WDC-MF (upper subfigure) this is

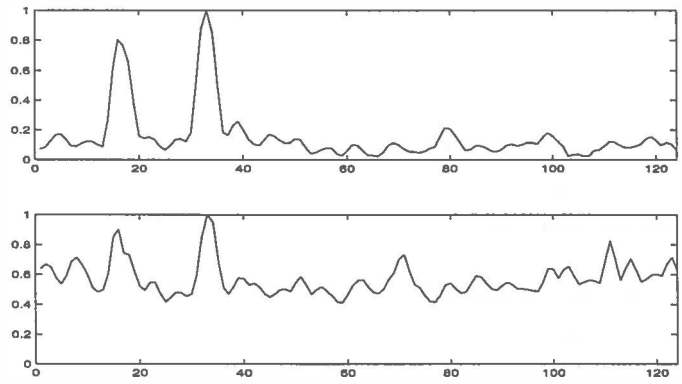

FIGURE 13 Typical delay spectra of WDC-MF (top), and MUSIC (bottom) in the presence of strong multiple access interference. The channel includes two equal energy paths.

seen as much smaller values around the peaks, which correspond to the correct delay candidates, compared to the corresponding values of the MUSIC delay spectrum (lower subfigure). Needless to say, it is possible to get a more reliable delay estimate with WDC-MF than MUSIC. This is assessed numerically in section 3.5.

3.3 Computational considerations

In this section we discuss the computational complexity of the proposed methods, expressed as the number of "multiply and add"-operations needed to test one delay candidate. We suppose here that the length of the data vector is C, the number of users is K, and that L uncorrelated paths exists on the channel.

First of all, the computational complexity of noncoherent MF is of order $O(C)$. This is because one MF output needs C summations. What is needed more by DC-MF, is the multiplication of two MF outputs. Hence, its computational complexity is the same $O(C)$. In ADC-MF the evaluation of $P(d)$ (Eq. (92)) requires dividing two successive DC-MF outputs, and square rooting, and the evaluation of $\delta(d)$ (Eq. (91)) needs 3 summations, and 2 multiplications. The total complexity is thus the same $O(C)$.

The other proposed methods are subspace methods in nature. The classical approach is either eigenvalue decomposition of the data autocorrelation matrix, or singular value decomposition of the data matrix. For computing the eigenvectors of a $C \times C$ dimensional matrix, several well-established $O(C^3)$ algorithms exists in the literature [22]. If only m eigenvectors are computed, their complexity reduces to $O(C^2 m)$. As a desire to lower the computational load, several recursive algorithms have also emerged (see [108], and references therein), which can reach a complexity of $O(Cm)$ per iteration.

In (A)DC-MUSIC, L eigenvectors should be estimated, which requires computation of order $O(C^2 L)$. From Eq. (87) we see, that testing a code with a delay candidate causes additional computation of order $O(CL)$, resulting in a total complexity of $O(C^2 L) + O(CL)$. Notice that since the eigenvectors are obtained from the *differential* correlation matrix, adaptive subspace tracking e.g. by PASTd do not directly apply. This is especially for further study.

The case is different with WDC-MF, which uses the eigenvectors of data autocorrelation matrix with zero time lag. Thus the complexity due to subspace tracking would be of order $O(CKL)$, since the subspace dimension (previously denoted as m) depends linearly on the number of users and paths. From Eq. (106) we see that testing a code requires the computation order $O(CKL) + O(K^2 L^2)$, which is also the final complexity.

3.4 Performance measures

In this thesis, we consider delay estimation only in a parallel manner. This is because the goal is to compare the performance of the methods without considering any threshold setting. Maximum selection was used to determine the delay, i.e. the strongest peak from the delay spectrum was selected. Traditional definition of acquisition is the case where any multipath component is found. In addition to this, we also use a more stringent criterion, which declares that the acquisition has happened when the strongest path has been found. The performance measure, probability of acquisition, is in both cases defined as

$$P_a = \frac{\#\text{ of acquisitions}}{\#\text{ of trials}}. \tag{107}$$

The other performance measure is mean acquisition time, which measures the average time spent in the acquisition process. This issue is profoundly considered in [65, 66]. The acquisition scheme is illustrated in Figure 14. A preamble of M symbols is sent, which is processed in the receiver's acquisition mode. In case of misacquisition, a request for the new preamble is sent, which takes a time of T_p symbols.

Suppose first that no failures occur in the acquisition process. Then the average time needed for acquisition is

$$\begin{aligned} t_1 &= P_a M + (1-P_a)P_a 2M + (1-P_a)^2 P_a 3M + \cdots && (108)\\ &= MP_a \sum_{i=1}^{\infty} i(1-P_a)^{i-1} && (109)\\ &= MP_a \frac{1}{P_a^2} && (110)\\ &= \frac{M}{P_a}. && (111) \end{aligned}$$

On the other hand, each misacquisition pays an additional price of T_p symbols.

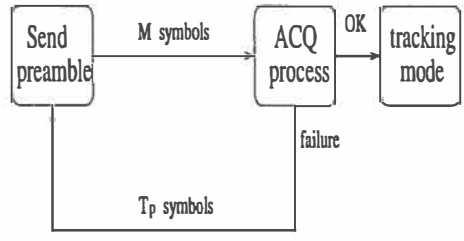

FIGURE 14 Code acquisition process.

This additional time is on average

$$t_2 = (1-P_a)P_aT_p + (1-P_a)^2P_a2T_p + (1-P_a)^3P_a3T_p\cdots \quad (112)$$

$$= T_pP_a\sum_{i=1}^{\infty} i(1-P_a)^i \quad (113)$$

$$= T_pP_a(1-P_a)\sum_{i=1}^{\infty} i(1-P_a)^{i-1} \quad (114)$$

$$= \frac{T_p(1-P_a)}{P_a}. \quad (115)$$

The mean acquisition time is thus

$$T_{ACQ} = t_1 + t_2 = \frac{M + T_p(1-P_a)}{P_a}. \quad (116)$$

The third performance measure is root-mean-square-error (RMSE). It measures the accuracy of the delay estimation according to

$$\text{RMSE} = \sqrt{\frac{1}{S}\sum_{i=1}^{S}(\hat{d}_i - d)^2}, \quad (117)$$

where d is the true delay, and S is the number of realizations. If the delay estimations are unbiased, the RMSE values can be directly compared to the Cramer-Rao bound (CRB). CRB is the lower bound for the variance of any unbiased estimator. The analytical forms of CRB's in different type of channels are derived e.g. in [61, 82, 112].

3.5 Numerical experiments

We compared the methods in the downlink environment with the Rayleigh fading channel. The data rate was assumed to be $f_d = 16$ kbit/s, carrier frequency $f_c = 1.8$ GHz, and mobile speed $v = 50$ km/h. This results in normalized Doppler shifts at most $\frac{v}{v_{\text{light}}} f_c/f_d = 5.21 \cdot 10^{-3}$. The typical fading process at the symbol level is seen in Figure 15.

The methods for delay estimation were: DC-MF (84), DC-MUSIC (87), ADC-MF and ADC-MUSIC (Table 1), WDC-MF (105), MUSIC (59), CMOE [40] , and conventional non-coherent and coherent MF [68]. Any parameters such as time-varying path strengths, and codes of the interfering users were not assumed to be known. Only the code of the desired user was known. In addition, a preamble $b_{1m} = 1$ was available for the desired user $k = 1$. Gold codes of length $C = 31$ were used. Signal-to-Noise Ratio (SNR) in the chip-matched filter output was always 10 dB. Both frequency-selective and -flat fading channel was considered. The number of users K was varied from $K = 5$ to $K = 25$. Therefore, the total

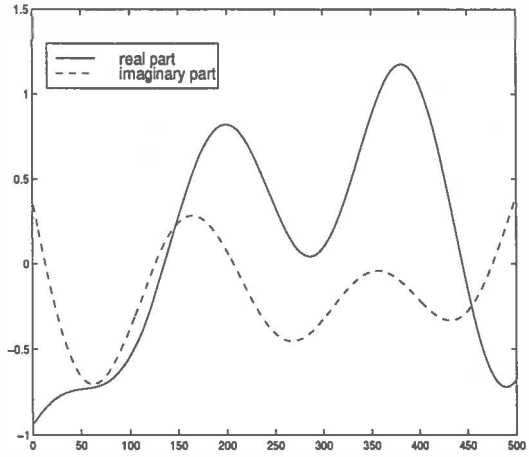

FIGURE 15 Typical fading process. The lines indicate the real and imaginary parts of the time-varying path attenuation factor for $M = 500$ symbols.

number of sources was $2KL = 6K = 30, \ldots 150$, while the maximum signal subspace dimension was $C = 31$. Therefore, highly loaded systems arise. We noticed that the performance of MUSIC became better by selecting the estimated signal subspace dimension $2K$ instead of $2KL$. This choice can be also justified by the fact that the number of users is known, while the number of paths is estimated. In one simulation, each parameter value was fixed, and the delays were estimated from the peaks of the delay spectrums. All the measured quantities are averaged over 1000 simulations.

Setup A: Two equal energy paths ($L = 2$)

In this experiment, the channel was Rayleigh fading with two equal energy paths, and all the users were assigned with equal powers. Maximum selection was used to find any multipath component. The probabilities of acquisition were measured as a function of the length of the preamble ($M = 30, \ldots, 500$), and the number of users ($K = 5, \ldots, 30$). From Figure 16 it is seen that conventional coherent MF seems to be the best when only a short preamble is available, although the difference is quite small compared to the methods based on differential correlations already with $M = 40$ symbols. Moreover, the setup is quite easy for conventional acquisition, since no strong interference exist. MUSIC predictably fails due to high system load. Also, both CMOE and the conventional non-coherent MF remains below 0.9 even with $M = 500$ symbols. Figures 17-21 shows the corresponding mean acquisition times as a function of the preamble length for each method. The penalty time T_p was set to $T_p = 500$ symbols. As can be predicted

from Figure 16, the conventional coherent MF together with the proposed methods clearly performs the best.

Figure 22 shows the performance with varying system loads, when the length of the preamble was $M = 200$. Nearly equal performance is seen when only a few users occupy the system, but the methods based on differential correlations were clearly the most tolerant against system loading. Quite remarkably, DC-MF reaches a probability of acquisition equal to 0.991 ± 0.001 with $K = 5, \ldots, 25$, and still 0.984 with $K = 30$.

Figure 23 shows the performance with different vehicle speeds, when the length of the preamble was $M = 200$. Conventional coherent MF predictably suffers from very fast vehicle speeds, since the fading process becomes too zero mean during the extended integration. The proposed methods, on the other hand, can exploit the time correlatedness of the fading process. The other remaining methods reached only a moderate level. Moreover, especially CMOE seems to suffer from low vehicle speeds, when the multipaths become more and more correlated.

In the remaining setups, we applied the more stringent definition to declare whether acquisition took place or not. Namely, the strongest multipath component should be found.

Setup B: Three unequal energy paths ($L = 3$)

In this setup, the channel was Rayleigh fading with $L = 3$ paths, whose relative difference in power was 5 dB. SNR was always set with respect to the strongest path.

In the first experiment we studied the effect of increasing the length of the preamble. The system included $K = 20$ users and the desired user had either equal (Figure 24) or a 5 dB weaker signal (Figure 25) than the others. Non-coherent MF failed in the near-far scenario, which was predictable, as well as MUSIC due to the high system load. The zero mean fading process also seemed to be too fast for the coherent MF, even though it was the most robust in this setting against MAI. CMOE performed better as more samples were available. This was because the estimation for the inverse of the autocorrelation matrix $\mathbf{R}(0)$ thus became more accurate. However, in the presence of MAI, see Figure 25, CMOE did not really manage to catch the strongest path first. The fact that the proposed methods are asymptotically invariant with respect to the interfering users and noise can be predicted from Figures 24 and 25, in which the probability of acquisition seems to tend to 1, whether the MAI is 0 or 5. In this experiment, $M = 500$ symbols were enough for them to achieve almost the same performance whether the interfering users were 5 dB stronger or not. The figures also tell the fact that the performance of the proposed methods depends essentially on the length of the preamble, because the goal is to "average interference out". For this reason, it is understandable that the methods fail if the preamble is too short. On the other hand, although coherent MF was the best among the others when the short preamble is used, its performance remained at a moderate level. In Figures 26 and 27, the mean acqui-

sition times in symbols are plotted. Due to reliable estimations, the acquisition time for the proposed methods was usually no more than the length of the preamble. As can be predicted from Figure 25, coherent MF was on average the fastest if only a short preamble was available. One can also notice, that DC-MF seemed to have better acquisition capability of the strongest path than DC-MUSIC. The reason for this is that the MF-type approach in general works well as the code autocorrelation function is impulse-like. To show the power of DC-MUSIC when the code autocorrelation is not that spiky, we assigned $K = 2$ users random codes of length $C = 7$ in $L = 3$ path Rayleigh fading channel. The paths had 5 dB differences in power. Figure 28 shows the average amount of acquired paths as a function of the preamble length. It is seen that DC-MUSIC found the most paths when the preamble length was greater than $M = 100$ symbols. Table 2 shows the case $M = 500$ in more detail. Namely, it tells the number of cases when each path was acquired. It is quite noticeable how frequently DC-MUSIC acquired also the weaker paths (-5 dB and -10 dB paths with probabilities 0.917 and 0.629, respectively) compared to the other methods, which had serious problems in acquiring even the second strongest path.

In the second experiment we studied the effect of system loading, i.e. when the number of users was increased. The system included $K = 5$ to $K = 25$ users with MAI equal to 0 dB. The length of the preamble was $M = 500$ symbols. Figure 29 shows the achieved probability of acquisition. Although the true model order (equal to $2KL$) was quite high, the model order underestimation (estimated as $2K$) helped MUSIC in the case of $K = 5$ users. This was not the case for the other system loads. Coherent MF performed almost the same regardless of the system load, although the performance level again was moderate. The difference of the other remaining methods (DC-MF,DC-MUSIC,CMOE, and MF) in this experiment was too small up to $K = 15$ users to draw conclusions. This was mainly because of the MAI-free case. On the other hand, especially in the case $K = 25$, which means quite a heavy system load, the proposed methods clearly performed the best. It is also seen that coherent MF, together with the proposed methods are the most robust against system loading. But among those only the proposed ones can exploit the time-correlatedness of the fading process, resulting in better performance level. Figure 30 tells the corresponding mean acquisition times. Assuming the bit rate of 16 kbit/s, these times for the case $K = 25$ would equal the following: DC-MF and DC-MUSIC 33 ms, coherent MF 44 ms, CMOE 52 ms, and non-coherent MF 54 ms. Thus, at least a 25% improvement would be gained by the proposed methods, compared to any reference ones.

Setup C: Different levels of IPI

In this experiment we studied the behavior of the methods when increasing the amount of inter-path interference (IPI). The IPI was generated by increasing the number of paths from $L = 2$ to $L = 10$. One of the paths was always 5 dB stronger, which was intended to be acquired. The system included $K = 20$ users, and

$M = 500$ symbols were used again as a preamble. MUSIC was no longer applied due to its obvious failure in highly loaded systems (see the Setup A). Hence, the only method which would need to know or estimate the number of paths L, is DC-MUSIC. Recall that DC-MUSIC computes L eigenvectors. In this experiment DC-MUSIC always assumed $L = 3$. Figure 31 shows that the proposed methods clearly resist IPI the best. Moreover, DC-MUSIC seems not to be that sensitive to the model order mismatch.

Setup D: Single-path channel ($L = 1$)

In the first experiment, we studied the achieved accuracy in a system with $K = 20$ users. Although MUSIC is a high-resolution method, it was not applied, again, due to its failure in this setting. The channel was frequency-flat fading, and ADC-MF and ADC-MUSIC were applied for the first time. The accuracy for all the other methods was achieved by using more delay candidates. More precisely, the increment for the delay candidate was always as small as $\frac{1}{100}$ chip. Recall that ADC-MF and ADC-MUSIC uses an increment equal to one chip, only. Figure 32 shows the achieved accuracies in RMSE. It can be stated that the high-resolution feature of MUSIC is now seen in the performance of ADC-MUSIC, which reached an RMSE of only $0.02 - 0.04$ chips, depending on the system load. CMOE seems also to yield quite accurate estimates, and performs better than ADC-MF, which reached RMSE of $0.04 - 0.08$ chips. However, it must be pointed out that there was no MAI in this experiment. Hence, it is expected that in the presence of MAI, the RMSE of CMOE as well as the coherent and non-coherent MF will degrade significantly, as it did in the first experiment.

The second experiment was dedicated for the comparison of the accuracy of ADC-MF and ADC-MUSIC to the Cramer-Rao lower bound (CRB). Although the estimators turned out to be approximately unbiased, the bias was estimated for each fixed parameter value. This was taken into account in the final RMSE calculation, giving an adequate measure for the CRB comparison. The system included $K = 5$ users, and the average SNR was 10 dB. The single-path time-invariant channel was assumed, and hence the data model coincided with that of [112], where the CRB was derived [pp. 88-89]. The RMSE curves are seen in Figure 33, from which we notice that neither methods attain the CRB. This was also the case in [82] with MUSIC. However, it must be pointed out that the preamble is not yet optimally utilized in ADC-MF nor in ADC-MUSIC. This is because the contribution of interference and noise was tried to suppress by estimating only one differential correlation matrix $\hat{\mathbf{R}}(\tau)$, with $\tau = 2$ in all the experiments. However, strong time correlations could take place with much larger time intervals. Thus, simple averaging over many $\hat{\mathbf{R}}(\tau)$'s, $\tau = 2, 3, \ldots$ would make even more interference suppression, and consequently offer better accuracy. This issue was treated in [34] for DC-MF, and in [74] for ADC-MF.

Setup E: Different levels of MAI

In this final setup we highlight the improvements in near-far resistance achieved by WDC-MF estimator. The system included $K = 5$ users in a equal energy $L = 2$ path Rayleigh fading channel. The observation interval of 2 symbols was used, and any multipath component was acquired.

In the first experiment, SNR was set to 10 dB, and MAI of 5 dB per interfering user was assumed. The length of the preamble was varied from $M = 50$ to $M = 500$ symbols. The results are seen in Figure 34. As seen earlier, DC-MF is inadequate with a small number of symbols, since the goal is to average out interference. When whitened instead of the original data are used in the differential correlation, i.e. the WDC-MF estimator is used, additional interference is suppressed even with short preambles. Recall that MUSIC and WDC-MF uses exactly the same signal subspace parameters. Thus the performance gain achieved by differential correlation is seen as the difference of these methods.

In the second experiment, the number of symbols was fixed to $M = 400$, and SNR of 10 dB was assumed. MAI per interfering user was varied from 0 to 20 dB. Figure 35 shows the achieved probabilities of acquisition. In this setup, DC-MF offered a better performance than the coherent MF up to MAI of 10 dB per interfering user. Naturally, the use of more symbols would improve the performance of DC-MF. On the other hand, WDC-MF could retain the MAI-free performance, as well as MUSIC. The influence of differential correlation is again seen from these two curves. The performance of all the methods except WDC-MF is quite moderate with MAI being greater than 10 dB per interfering user.

3.6 Summary

Code timing acquisition was considered in this chapter. It was shown that when a constant preamble, or an unmodulated pilot channel is available for the desired user, the receiver can efficiently filter out noise and interferers by differential correlations and suitably chosen time lags. Therefore, it is possible to estimate the desired user's delays even when a huge number of interferers exist. Three types of methods were proposed, labeled as (A)DC-MF, (A)DC-MUSIC, and WDC-MF, whose main characteristics, verified by numerical experiments, were as follows:

- most of them are computationally simple, containing only MF-operations (DC-MF) or at most computations of few, say $L = 3$, eigenvectors (DC-MUSIC). Only one of them (WDC-MF) needs the estimation of the whole signal subspace (like traditional MUSIC),
- they efficiently filter out interfering users and additive noise prior to actual delay estimation, regardless of the code non-orthogonalities,

- they can utilize the time correlation of the fading process, which is a major drawback for conventional acquisition if being zero mean,
- DC-MF succeeds well in acquiring the strongest path first in parallel search,
- DC-MUSIC is suitable especially for the acquisition of other, possibly less powerful paths,
- DC-MUSIC performs better than DC-MF when the processing gain C is small.
- an additional procedure can be attached to both methods, improving the estimation accuracy by a negligible increase in computation,
- WDC-MF can improve the near-far resistance of DC-MF and MUSIC, provided the signal subspace dimension does not exceed the dimension of the data vectors.

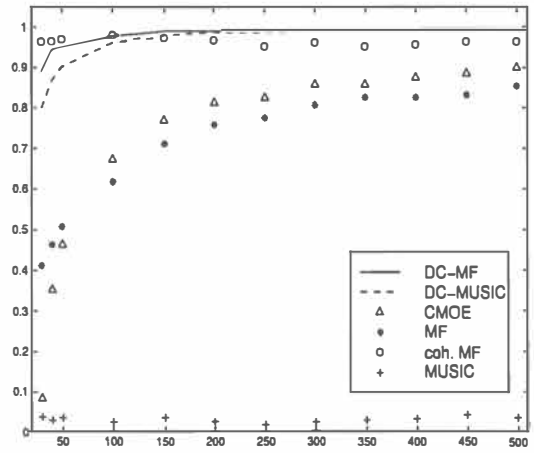

FIGURE 16 Probability of acquisition as a function of the length of the preamble in an equal energy two-path Rayleigh fading channel. The system includes $K = 20$ users with equal powers, and the average SNR is 10 dB.

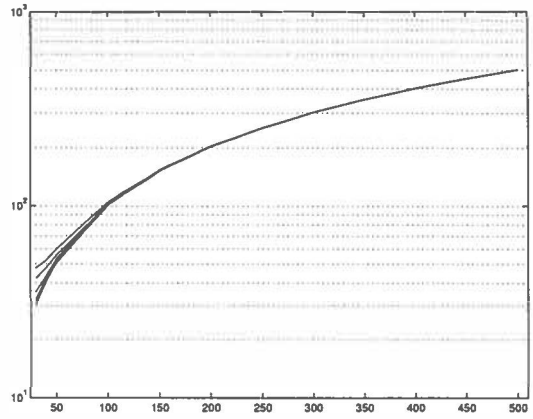

FIGURE 17 Mean acquisition times for the DC-MF delay acquisition as a function of the length of the preamble in an equal energy two-path Rayleigh fading channel. The system includes $K = 5$ (lowermost) to $K = 30$ (uppermost) users with equal powers, and the average SNR is 10 dB.

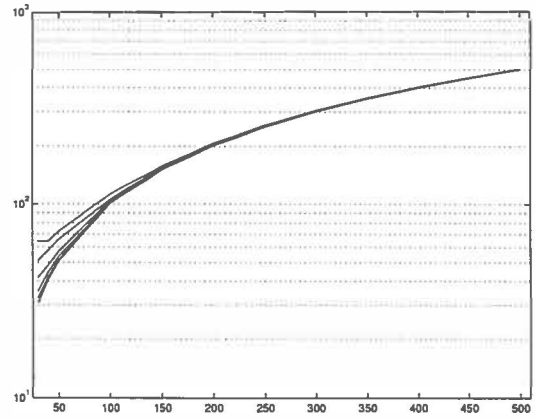

FIGURE 18 Mean acquisition times for the DC-MUSIC delay acquisition as a function of the length of the preamble in an equal energy two-path Rayleigh fading channel. The system includes $K = 5$ (lowermost) to $K = 30$ (uppermost) users with equal powers, and the average SNR is 10 dB.

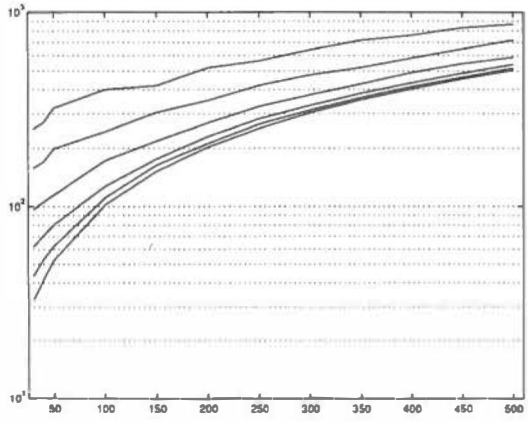

FIGURE 19 Mean acquisition times for the conventional non-coherent delay acquisition as a function of the length of the preamble in an equal energy two-path Rayleigh fading channel. The system includes $K = 5$ (lowermost) to $K = 30$ (uppermost) users with equal powers, and the average SNR is 10 dB.

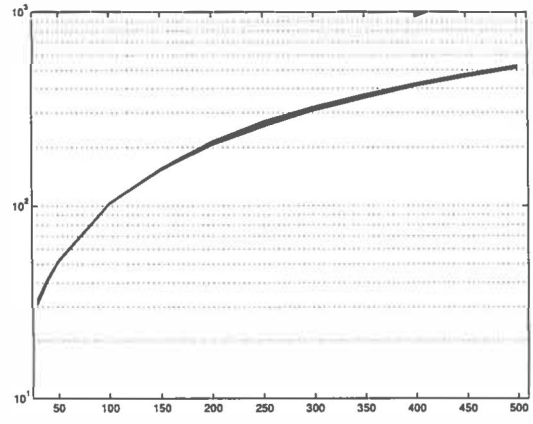

FIGURE 20 Mean acquisition times for the conventional coherent delay acquisition as a function of the length of the preamble in an equal energy two-path Rayleigh fading channel. The system includes $K = 5$ (lowermost) to $K = 30$ (uppermost) users with equal powers, and the average SNR is 10 dB.

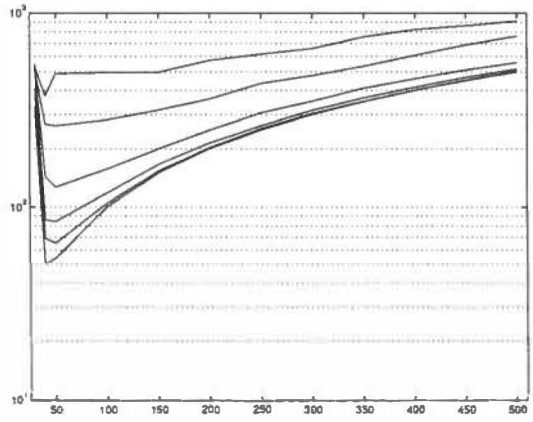

FIGURE 21 Mean acquisition times for CMOE delay acquisition as a function of the length of the preamble in an equal energy two-path Rayleigh fading channel. The system includes $K = 5$ (lowermost) to $K = 30$ (uppermost) users with equal powers, and the average SNR is 10 dB.

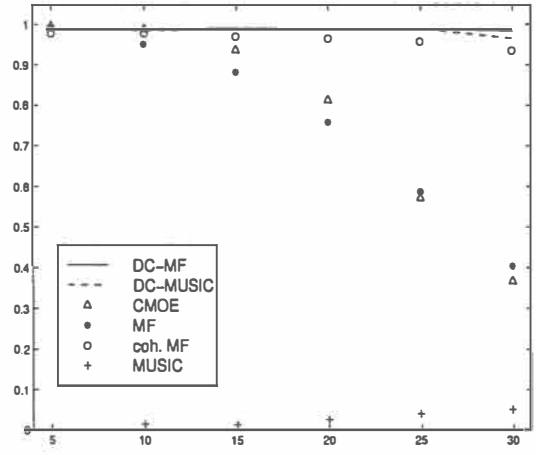

FIGURE 22 Probability of acquisition as a function of the number of users in an equal energy two-path Rayleigh fading channel. All the users have equal signal powers. The length of the preamble is $M = 200$, and the average SNR is 10 dB.

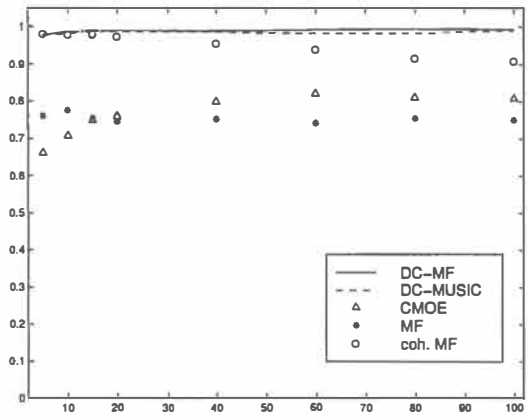

FIGURE 23 Probability of acquisition as a function of the vehicle speed (km/h) in an equal energy two-path Rayleigh fading channel. All the users have equal signal powers. The length of the preamble is $M = 200$ and the average SNR is 10 dB.

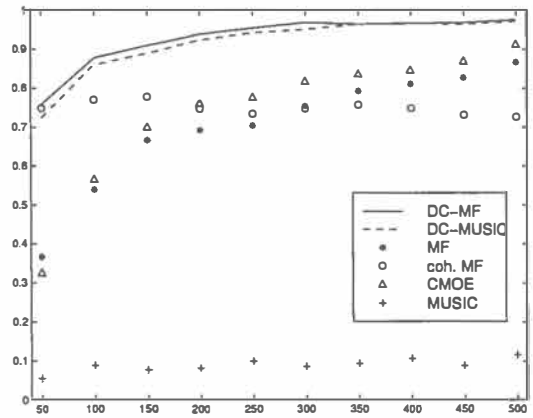

FIGURE 24 Probability of acquisition as a function of the length of the preamble in an unequal energy three-path Rayleigh fading channel. All the users have equal signal powers. The system includes $K = 20$ users, and the average SNR is 10 dB.

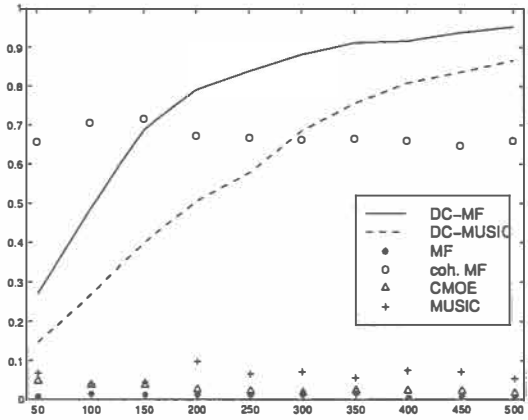

FIGURE 25 Probability of acquisition as a function of the length of the preamble in an unequal energy three-path Rayleigh fading channel. The interfering users are 5 dB stronger. The system includes $K = 20$ users, and the average SNR is 10 dB.

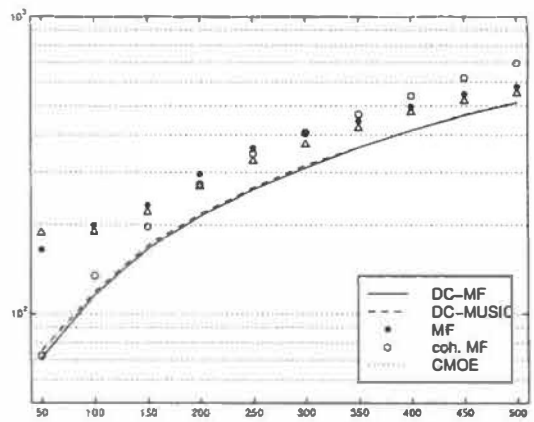

FIGURE 26 Mean acquisition time as a function of the length of the preamble in an unequal energy three-path Rayleigh fading channel. All the users have equal signal powers. The system includes $K = 20$ users, and the average SNR is 10 dB.

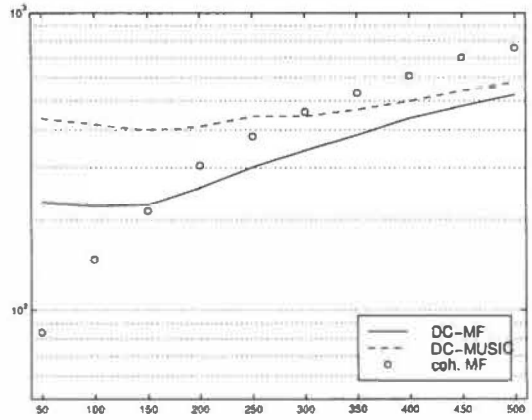

FIGURE 27 Mean acquisition time as a function of the length of the preamble in an unequal energy three-path Rayleigh fading channel. The interfering users are 5 dB stronger. The system includes $K = 20$ users, and the average SNR is 10 dB.

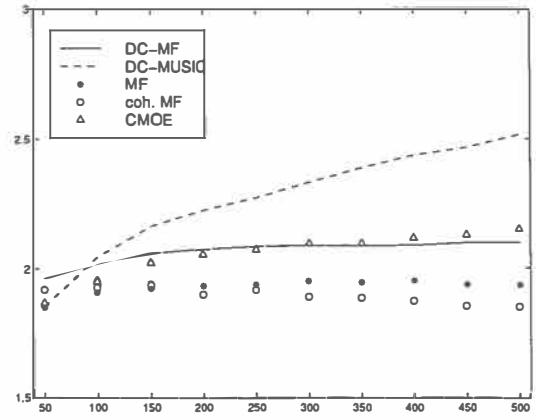

FIGURE 28 Relative number of acquired paths in an unequal energy three-path Rayleigh fading channel as a function of the length of the preamble M. The system includes $K = 2$ users, and the random codes are of length $C = 7$. The average SNR is 10 dB.

TABLE 2 Number of cases a certain path is acquired in a $K = 2$ user's system with random codes of length $C = 7$. The length of the preamble is $M = 500$, and the average SNR is 10 dB. The fractional parts δ_i, $i = 1, 2, 3$ are uniformly distributed over $(0, 1)$.

path power delay (chips)	1^{st} 0 dB $1 + \delta_1$	2^{nd} -5 dB $3 + \delta_2$	3^{rd} -10 dB $5 + \delta_3$	
	#/1000	#/1000	#/1000	Σ/3000
DC-MUSIC	969	917	629	2515
DC-MF	975	710	414	2099
MF	958	620	357	1935
coh. MF	878	570	404	1851
CMOE	953	765	433	2151

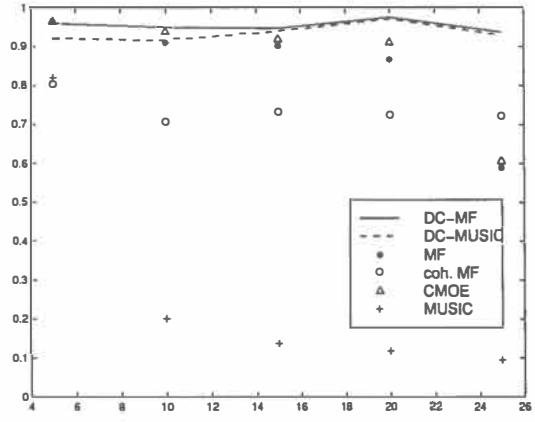

FIGURE 29 Probability of acquisition as a function of number of users in an unequal energy three-path Rayleigh fading channel. The length of the preamble is $M = 500$, and the average SNR is 10 dB.

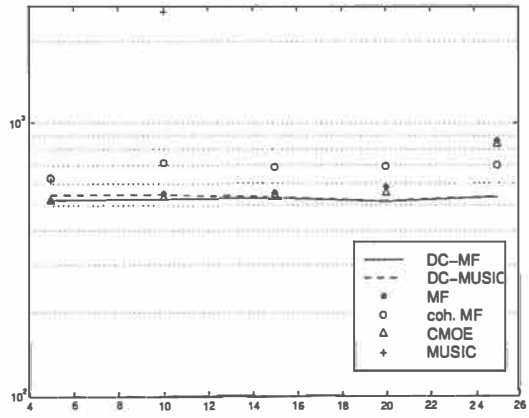

FIGURE 30 Mean acquisition time (symbols) as a function of number of users in an unequal energy three-path Rayleigh fading channel. The length of the preamble is $M = 500$, and the average SNR is 10 dB.

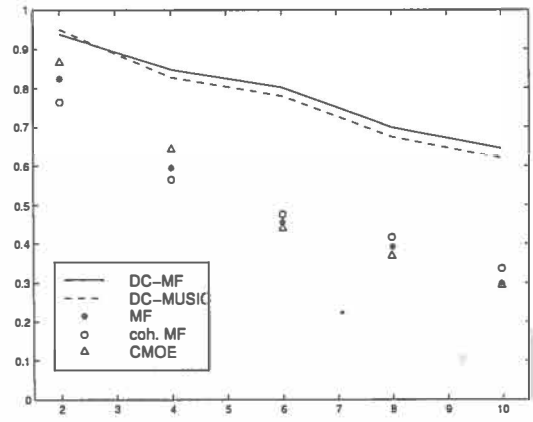

FIGURE 31 Probability of acquisition as a function of the number of paths. The system includes $K = 20$ users, and the length of the preamble is $M = 500$. Among $L = 2, \ldots, 10$ paths, the desired one is always 5 dB stronger. The average SNR is 10 dB.

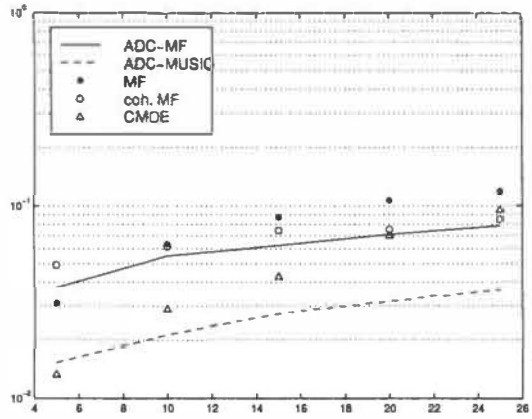

FIGURE 32 RMSE (chips) as a function of the number of users in a single-path Rayleigh fading channel with the average SNR of 10 dB. The length of the preamble is $M = 500$.

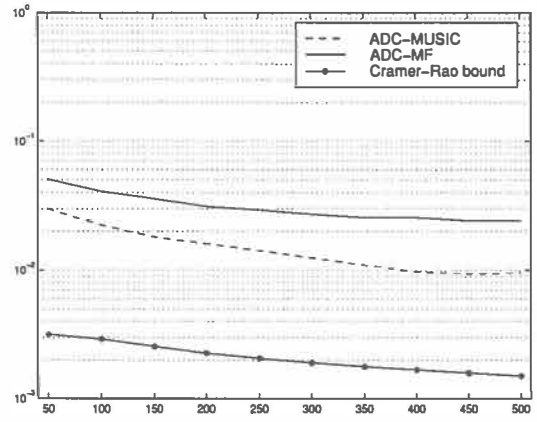

FIGURE 33 RMSE as a function of the length of the preamble in a single-path time-invariant channel with the average SNR of 10 dB. The system includes $K = 5$ users.

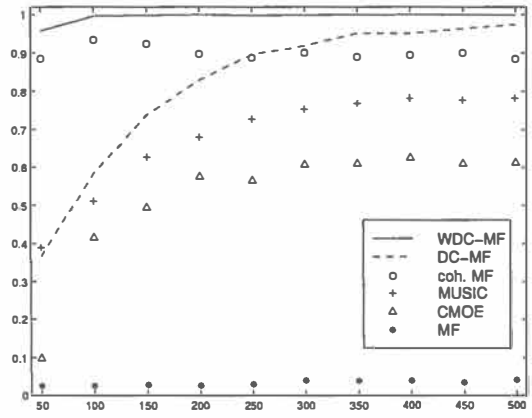

FIGURE 34 Probability of acquisition as a function of the length of the preamble. The system includes $K = 5$ users with MAI of 5 dB per interfering user in a $L = 2$ path Rayleigh fading channel. The average SNR is 10 dB.

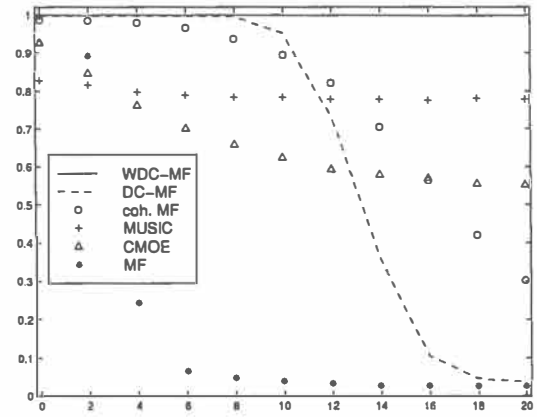

FIGURE 35 Probability of acquisition as a function MAI per interfering user. The system includes $K = 5$ users in a $L = 2$ path Rayleigh fading channel. The average SNR is 10 dB and the length of the preamble is $M = 400$.

4 SYMBOL DEMODULATION

In the reception, the final objective is to estimate the data symbols which carry the information. This is also called detection. In the following we first review some of the benchmark methods. We then discuss a statistical technique called *independent component analysis* (ICA), and consider applying the means of it to the problem at hand. Numerical experiments are included at the end of the chapter.

4.1 Review of earlier work

4.1.1 Single user detection

The traditional way to estimate the symbols is to handle the interference as additional noise, and thus ignore the structure of multiaccess interference. This is single user detection (SUD), which traditionally leads to matched filtering (MF) [68]. If only one path exists, MF estimates the symbols according to

$$\hat{b}_{km} = \text{sign}(\hat{a}^*_{km}(\overline{\mathbf{c}}_k(\hat{\chi})^T \mathbf{r}_m + \underline{\mathbf{c}}_k(\hat{\chi})^T \mathbf{r}_{m+1})), \tag{118}$$

or equivalently

$$\hat{b}_{km} = \text{sign}(\hat{a}^*_{km} \tilde{\mathbf{c}}_k^T(\hat{\chi}) \tilde{\mathbf{r}}_m), \tag{119}$$

where $\hat{a}_{km}$ is the estimate for path gain during mth symbol, and $\hat{\chi}$ is the estimated path delay [3]. In case of multipath propagation, it is possible to enhance the overall signal-to-noise ratio (SNR) by utilizing time-diversity. This is because all paths are not likely to be in a fade simultaneously. RAKE receiver [67] is commonly used to combine the signal energy of multipath components. RAKE estimates according to

$$\hat{b}_{km} = \text{sign}(\sum_{l=1}^{L} \hat{a}^*_{klm}(\overline{\mathbf{c}}_k(\hat{\chi}_l)^T \mathbf{r}_m + \underline{\mathbf{c}}_k(\hat{\chi}_l)^T \mathbf{r}_{m+1})), \tag{120}$$

[3] Notice that for BPSK symbols the sign is taken only from the real part. In case of QPSK symbols, the sign is taken from both real and imaginary parts.

or equivalently

$$\hat{b}_{km} = \text{sign}(\sum_{l=1}^{L} \hat{a}_{klm}^{*} \tilde{\mathbf{c}}_k(\hat{\chi}_l)^T \tilde{\mathbf{r}}_m). \quad (121)$$

4.1.2 Multiuser detection

In multiuser detection (MUD) the question is about demodulation of the particular user by attempting to exploit the structure of multiaccess interference [102, 49]. Multiuser receivers have been an attractive field of research only for some twenty years, mainly because of the strong belief of the essential optimality of conventional single user detection (cf. [101]). Tutorial reviews about the subject can be found e.g. in [100, 54].

The optimum strategy, maximum likelihood method, as described in previous chapters, leads to a joint estimation of *each* user's parameters, and has thus an exhausting complexity.[4] A significant computational gain was introduced by Verdú [98], who took into account the inherent structure of interference. The resulting maximum-likelihood sequence detector (MLSD) consists of a bank of matched filters followed by a Viterbi-algorithm. Verdú's invention meant that the interference of multiple access and the near-far effect can be mitigated, although not by a conventional single user receiver. For this reason his work has been widely regarded as a spark to the development of lower complexity near-far resistant multiuser receivers (e.g. [93, 94, 45, 17]).

In this thesis, however, we will not use optimal MUD as a reference due to two limitations:

- it is computationally still quite complex, and
- it is not applicable in downlink environments, which is the scenario in this thesis.

The second limitation is due to the fact that the method should know e.g. the codes of interfering users, which is not the case in the downlink receiver.

4.1.3 Blind multiuser detection

To ease the computational load of the maximum likelihood method, blind multiuser detection can be considered instead. In blind MUD, no knowledge of interference parameters are needed, but still the structure of MAI is exploited in the demodulation of a particular user. Hence, the term "blind". In blind MUD the goal is to learn the structure of MAI to be able to suppress it. Learning is possible in short code systems, since the MAI seen by the desired user's symbols is statistically identical, provided the channel varies relatively slowly [49].

[4] Quite recently, connection of optimal MUD to a minimum capacity cut problem was also found [92, 76].

Perhaps the most intuitive way to demodulate a particular user's symbol in the presence of multiaccess interference is to first try to eliminate all the interference. This is the idea behind decorrelation which is also called zero-forcing. A decorrelating detector (DD) tries to totally suppress the interference while preserving some energy of the desired user, such that the only interference left is background noise.

First suppose a synchronous system with a single path channel. The data (18) has thus the form

$$\mathbf{r}_m = a_{km} b_{km} \mathbf{s}_k + \mathbf{G}' \mathbf{a}'_m + \mathbf{n}_m, \tag{122}$$

where the $C \times K - 1$ matrix $\mathbf{G}'$ contains all the columns of $\mathbf{G}$ except $\mathbf{s}_k$, and $K - 1$ vector $\mathbf{a}'_m$ contains all the elements of $\mathbf{a}_m$ except $a_{km} b_{km}$. Hence, $\mathbf{s}_k$ represents the desired user. If the signal of the desired user is to be demodulated, then all the columns of $\mathbf{G}'$ span the interference subspace. A matched filter is a detector which is a scalar multiple of $\mathbf{s}_k$ (Figure 36, left subfigure). If $\mathbf{s}_k$ has a non-zero projection in the interference subspace, as is the case in the figure, the demodulated signal has a contribution from the interferers. A decorrelating detector, however, use detector $\mathbf{c}^{DD}$, which is orthogonal to the interference subspace. Hence, it totally eliminates the multiaccess interference, but at the same time the detector has a nonzero projection in the desired direction $\mathbf{s}_k$ (right subfigure). Formally, a decorrelating detector is a solution to

$$\arg\min_{\mathbf{c}} E\{|\mathbf{c}^H \mathbf{G} \mathbf{a}_m|^2\}, \text{ subject to } \mathbf{c}^H \mathbf{s}_k = 1. \tag{123}$$

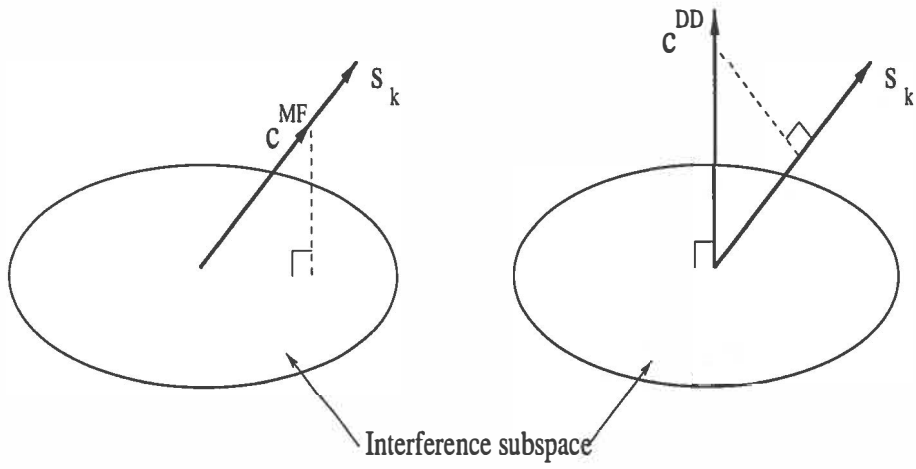

FIGURE 36 Geometric visualizations: Desired signal corresponds to $\mathbf{s}_k$, and matched filter $\mathbf{c}^{\mathrm{MF}}$ (left) is aligned with it. Decorrelating detector $\mathbf{c}^{\mathrm{DD}}$ (right) is perpendicular to the interference.

For the purpose of downlink signal processing, the use of subspace DD is more relevant. It has the form [105]

$$\mathbf{c}^{\mathrm{DD}} = \frac{1}{\mathbf{s}_k^T \mathbf{U}_s (\mathbf{\Lambda}_s - \sigma^2 \mathbf{I})^{-1} \mathbf{U}_s^H \mathbf{s}_k} \mathbf{U}_s (\mathbf{\Lambda}_s - \sigma^2 \mathbf{I})^{-1} \mathbf{U}_s^H \mathbf{s}_k, \tag{124}$$

where σ^2 is the estimated noise variance. The dimensions of the signal subspace parameters $\mathbf{U}_s$ and $\mathbf{\Lambda}_s$ are $C \times K$ and $K \times K$, respectively. The mth symbol is then estimated as

$$\hat{b}_{km} = \mathrm{sign}(\hat{a}_{km}^* (\hat{\mathbf{c}}^{\mathrm{DD}})^H \mathbf{r}_m). \tag{125}$$

It is well known, that although a decorrelating detector totally eliminates multiaccess interference, the price to pay is decreased SNR in the soft desicion, i.e. just before sign-decision in (125) [102]. This is understandable also from Figure 36. Notice, that the direction of $\mathbf{s}_k$ is from where all the desired user's energy is captured. On the other hand, the same amount of noise energy is (on average) captured by both detectors, since noise exists equally in any direction. Hence, the decorrelating detector captures less signal energy as MF but the captured noise energy remain the same.

To overcome this noise enhancement, a common approach in the estimation theory, the minimum mean-square error (MMSE) criterion can be considered instead. The objective is to find a detector, whose job it is to estimate a symbol from noisy observations which gives the best fit to the actual symbol. Formally, we want the solution to be

$$\arg\min_{\mathbf{c}} E\{|b_{km} - \mathbf{c}^H \mathbf{r}_m|^2\}, \text{ subject to } \mathbf{c}^H \mathbf{s}_k = 1. \tag{126}$$

This leads to detector, whose subspace version is [105]

$$\mathbf{c}^{\mathrm{MMSE}} = \frac{1}{\mathbf{s}_k^T \mathbf{U}_s \mathbf{\Lambda}_s^{-1} \mathbf{U}_s^H \mathbf{s}_k} \mathbf{U}_s \mathbf{\Lambda}_s^{-1} \mathbf{U}_s^H \mathbf{s}_k. \tag{127}$$

Notice that the two detectors above become identical as background noise tends to zero. Both can also be viewed as matched filters, which only operate in signal subspace. To see this, recall that both detectors estimate symbols as

$$\hat{b}_{1m} = \mathrm{sign}(\alpha (\mathbf{T}\mathbf{r}_m)^H (\mathbf{T}\mathbf{s}_k)), \tag{128}$$

where α is a scalar, and, in MMSE case, $\mathbf{T} = \mathbf{\Lambda}_s^{-1/2} \mathbf{U}_s^H$. Hence, both the data and the code are first projected to signal subspace which is followed by matched filtering.

In case of multipaths, the processing window must be enlarged. With window size of $D+1$ symbols, the subspace DD and MMSE detectors, respectively, would accordingly have the forms [104]

$$\tilde{\mathbf{c}}^{\mathrm{DD}} = \sum_{l=1}^{L} \frac{1}{\tilde{\mathbf{c}}_{kl}^T \tilde{\mathbf{U}}_s (\tilde{\mathbf{\Lambda}}_s - \sigma^2 \mathbf{I})^{-1} \tilde{\mathbf{U}}_s^H \tilde{\mathbf{c}}_{kl}} \tilde{\mathbf{U}}_s (\tilde{\mathbf{\Lambda}}_s - \sigma^2 \mathbf{I})^{-1} \tilde{\mathbf{U}}_s^H \tilde{\mathbf{c}}_{kl} \tag{129}$$

$$\tilde{\mathbf{c}}^{\mathrm{MMSE}} = \sum_{l=1}^{L} \frac{1}{\tilde{\mathbf{c}}_{kl}^T \tilde{\mathbf{U}}_s \tilde{\mathbf{\Lambda}}_s^{-1} \tilde{\mathbf{U}}_s^H \tilde{\mathbf{c}}_{kl}} \tilde{\mathbf{U}}_s \tilde{\mathbf{\Lambda}}_s^{-1} \tilde{\mathbf{U}}_s^H \tilde{\mathbf{c}}_{kl}. \tag{130}$$

Now, the dimensions of $\tilde{\mathbf{U}}_s$ and $\tilde{\mathbf{\Lambda}}_s$ are $(D+1)C \times (D+2)K$ and $(D+2)K \times (D+2)K$, respectively.

4.1.4 Other blind methods

The MMSE detector just considered is actually a subspace counterpart of CMOE discussed in section (3.1.4). Recall that the CMOE filter for interference suppression is

$$\tilde{\mathbf{c}}^{\mathrm{CMOE}} = \tilde{\mathbf{R}}^{-1}\tilde{\mathbf{c}}_{kl}. \tag{131}$$

From Eq. (50) we have

$$\begin{aligned} \tilde{\mathbf{R}}^{-1} &= \tilde{\mathbf{U}}_s\tilde{\mathbf{\Lambda}}_s^{-1}\tilde{\mathbf{U}}_s^H + \tilde{\mathbf{U}}_n\tilde{\mathbf{\Lambda}}_n^{-1}\tilde{\mathbf{U}}_n^H & (132)\\ &= \tilde{\mathbf{U}}_s\tilde{\mathbf{\Lambda}}_s^{-1}\tilde{\mathbf{U}}_s^H + \sigma^{-2}\mathbf{I}, & (133) \end{aligned}$$

where the first equation follows from the fact that the column vectors of $\tilde{\mathbf{U}}_s$ are orthogonal to those of $\tilde{\mathbf{U}}_n$. Subspace MMSE (up to scaling) now uses only the signal subspace conterpart of $\tilde{\mathbf{R}}^{-1}$, see Eq. (127). In [105], subspace implementations were also noticed to offer better robustness against signature waveform mismatch. Adaptive implementation of the blind MMSE method was considered, also, where adaptivity was achieved by a proposed on-line channel estimation procedure, and signal subspace tracking by PASTd (Projection Approximation Subspace Tracking with deflation) [108, 109]. This resulted in computational savings compared to existing batch mode channel estimators, e.g. the SVD-based method in [4]. Joint multiuser detection and channel estimation was considered in [106], where Kalman filtering was used.

For all these methods, the desired user's timing was assumed to be known. This is not the case in practice but the receiver must perform both timing acquisition and symbol demodulation. Moreover, timing should be estimated accurately to avoid performance loss [61].

Joint timing acquisition and symbol demodulation was addressed in [49], where MUSIC [79, 4, 82] was used for timing acquisition with extended observation interval. In [47], only CMOE criterion was used for both timing acquisition and symbol demodulation. In [62] MUSIC was also used, but symbol demodulation was based on the MMSE criterion. Extension to the multipath scenario was considered in [91, 104].

Timing estimation could also be performed with training symbols[5]. In [49] timing was implicitly estimated by M_p training symbols by assigning

$$\sum_{l=1}^{L}\tilde{\mathbf{c}}_{kl} = \frac{1}{M_p}\sum_{m=1}^{M_p} b_{km}\tilde{\mathbf{r}}_m. \tag{134}$$

[5] Sometimes training based algorithms are not regarded as *blind* but *semi-blind* algorithms. However, the interference parameters are still assumed to be unknown.

Adaptive MMSE-based interference suppression was considered in [46, 52], where training symbols and coarse timing of the desired user was needed. After training, a decision directed mode was used. Improved MMSE detection in case of chip timing estimation mismatch was considered in [11]. In [48] the need of coarse timing was avoided, and training symbols were used for initial timing acquisition, as well as in [112]. In [23] the need for sending new training symbols was relaxed in case of failure in the decision directed mode by using blind mechanisms. An improvement of robustness to asynchronous MAI with D-BPSK modulated signals is found in [18]. Bounds for the average near-far resistance of MMSE receivers were derived in [50] with random (short) codes.

A major hurdle which arises in fading channels is that standard adaptation mechanisms such as Least Mean Squares (LMS) and Recursive Least Squares (RLS) adaptation [68] does not work in fast fading channels [49]. The behavior of the MMSE receiver in frequency flat-fading channel was considered in [3]. It was shown that the MMSE detector works poorer when the Rician parameter is smaller. For the Rayleigh channel (Rician parameter equal to zero) MMSE failed. The main reason for this is that the adaptation looses phase lock during deep fades, because incorrect symbol estimates are fed back. The failure was also the bigger the faster is the fading. This is because the adaptive algorithm is then only able to track the mean values of the fading process. Linear MMSE receivers in frequency selective fading channels were considered in [40], in which adequate training for the LMS was provided by the conventional RAKE receiver.

An interesting class of single user receivers are chip-equalizers, which are considered e.g. in [24, 39] (and references therein). In these receivers, the channel is equalized prior to despreading. This is reasonable when orthogonal spreading codes are used, since then the multiple access interference is essentially caused by multipath propagation. Therefore, equalization can be used for MAI suppression, which restores the orthogonality of the users.

In the most challenging approach no training symbols are used and even the known code information is not utilized. Only the model order is assumed, and that the signals are digitally modulated at a given symbol rate. The former assumption could be relaxed by using known estimation procedures like Akaike Information Criteria (AIC) or Minimum Description Length (MDL) [107]. Given this setting, the symbol demodulation is possible by utilizing the constant modulus (CM) property of the signals.

The constant modulus -criteria seeks a filter which yields a symbol whose modulus is as close as possible to some given constant value. These constant modulus algorithms (CMA) were originally introduced in [21, 89] in ISI suppression. Linearly constrained and multistage CMA were considered in [51, 90], respectively, in order to avoid convergence to the undesired CMA solution. Analytical constant modulus algorithms were considered in [95, 96, 97]. What really makes CMA algorithms interesting is their close relationship to MMSE [16, 111, 29]. More precisely, the local minima of the CMA contrast function corresponds

to the MMSE solutions. This observation hence means that CMA may in practice outperform MMSE. This is because the performance of the MMSE estimation is always subject to timing and/or channel estimation inaccuracy, unlike CMA. Constant modulus algorithms can also be regarded to belong to a much wider class of algorithms based on independent component analysis (ICA), for which CMA can act as an objective function [8]. Algorithms of this type include e.g. [72, 73]. ICA is emphasized later in section 4.2

One could utilize alternatively a finite alphabet (FA) property, which is more general than the CM criteria. This was addressed in [83, 84, 85] in the separation of multiple co-channel digital signals using antenna array. More profound handling of these methods is found in [86, 87]. These algorithms are block algorithms in nature, and are based on an alternating maximum likelihood minimizations procedure. A subspace counterpart was presented in [30], which resulted in noticeable computational savings by avoiding matrix inversions.

4.2 Independent component analysis

In this section we consider a signal processing technique called *independent component analysis* (ICA), and justify its suitability to the demodulation of DS-CDMA signals.

4.2.1 Preliminaries

In ICA [36, 13] (see also a survey [27]) the question is about expressing a set of random variables as a mixture of component variables which are statistically independent, or as independent as possible. One of the main applications of ICA is the blind source separation (BSS) [36], while the others include e.g. feature extraction, and blind deconvolution. Recently, ICA has attracted a lot of interest both in statistical signal processing and neural network communities [9]. Several good algorithms utilizing higher-order statistics either directly or indirectly via suitable nonlinearities are now available for solving the basic linear ICA/BSS problem (see e.g. [1, 55]).

The main reason for the growing interest in ICA is that the independant assumption is both powerful and realistic in many practical situations, making it possible to find meaningful source signals or independent components from the data to be analyzed in a completely blind manner. Blind separation of a source is a problem which easily arises also in the wireless communication scenario, since it may involve a multitude of sources and sensors (e.g. antenna elements or microphones), with the objective to recover individual signals. Often very little is known about source signals, or about how they are mixed, which makes the separation process *blind*.

We now describe in mathematical terms linear the ICA scenario, which is also illustrated in Figure 37. Suppose n scalar random variables, $x_1, \ldots, x_n$, are

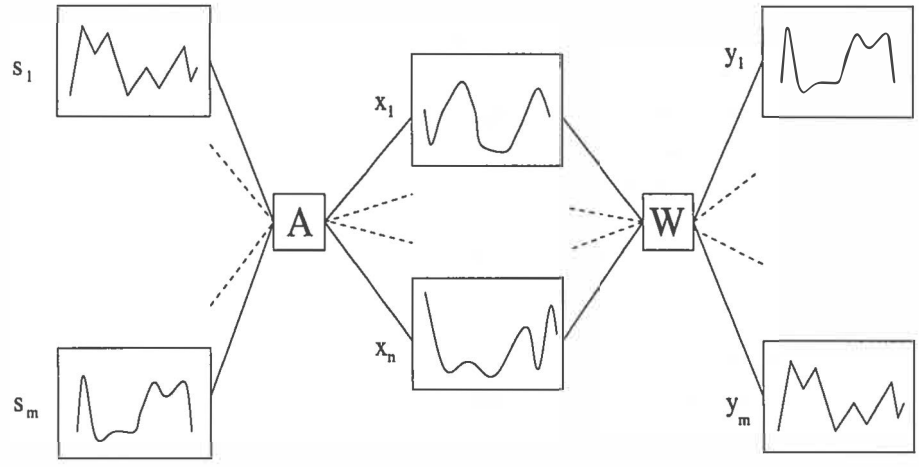

FIGURE 37 Linear ICA scenario: m sources are mixed ($\mathbf{A}$) and n mixtures are observed. Separation ($\mathbf{W}$) gives the estimate for the set of original sources.

observed (e.g. in n antenna elements). Each observed variable is assumed to be a linear mixture of component variables (i.e. sources) $s_1, \ldots, s_m$, which are assumed to be statistically independent. Hence the name independent component (IC). IC's are also assumed to be zero mean, and non-Gaussian, but otherwise unknown. Stacking scalar variables[6] into vectors $\mathbf{x}$ and $\mathbf{s}$, $\mathbf{x} = [x_1, \ldots, x_n]^T$, $\mathbf{s} = [s_1, \ldots, s_m]^T$, we gain a compact relation

$$\mathbf{x} = \mathbf{A}\mathbf{s}, \tag{135}$$

where $\mathbf{A}$ is $n \times m$ full rank matrix, which determines the linear mixing. $\mathbf{A}$ is thus usually called a mixing matrix. The goal in ICA is to estimate the independent component variables $\hat{s}_1, \ldots, \hat{s}_m$ given only (possibly noisy) observations $x_1, \ldots, x_n$. More precisely, one should estimate $n \times m$ matrix $\mathbf{W}$, such that the separated variables

$$\mathbf{y} = \mathbf{W}^T\mathbf{x} \tag{136}$$

are as independent as possible. The columns of $\mathbf{W}$ are also called ICA basis vectors. Now, hopefully, each estimate corresponds to some individual variable, i.e.,

$$\hat{\mathbf{s}} = \mathbf{T}\mathbf{y}, \tag{137}$$

where $\mathbf{T}$ is a permutation matrix.

The estimated independent components $\hat{s}_i$, however, contain some indeterminacies. To see this, rewrite the ith mixture as $x_i = \mathbf{a}_i\mathbf{s}$, where $\mathbf{a}_i$ is a row of $\mathbf{A}$. But naturally, also $x_i = (\sigma\mathbf{a}_i)(\frac{1}{\sigma}\mathbf{s})$, where σ is non-zero real scalar. This means that ICA cannot determine the sign nor the amplitude of the sources.

[6] The variables are real valued for now.

The statistical independence of $\hat{s}$'s is measured by some contrast functions, which are objective functions for source separation. The classical contrast is kurtosis, since its local extrema have a direct connection to independent components [14]. The others include e.g. constant modulus and information theoretic contrasts like entropy and mutual information [13, 8].

4.2.2 Principal vs. independent components

ICA is a useful extension of standard *principal component analysis* (PCA) [13], whose goal is to estimate largest variances in the observed data. The directions of those variances are identified by *principal components*. Formally, the principal components $\mathbf{u}_i^T\mathbf{x}$ of $\mathbf{x}$, $i = 1, \ldots, l$, $(l < n)$, are defined by the unit-norm eigenvectors $\mathbf{u}_i$ of the data covariance matrix $\mathbf{R} = \mathrm{E}\{\mathbf{x}\mathbf{x}^T\}$, corresponding to l largest eigenvalues. Vectors $\mathbf{u}_1, \ldots, \mathbf{u}_l$ are hence also called principal eigenvectors or PCA basis vectors, and could equally be defined as solutions of

$$\max E\{(\mathbf{u}_i^T\mathbf{x})^2\}, \text{ subject to } \mathbf{u}_k^T\mathbf{u}_i = \begin{cases} 1, & i = k \\ 0, & i > k \end{cases} . \tag{138}$$

Here the constraint forces each $\mathbf{u}_i$ to have unit norm, and to be orthogonal to all other $\mathbf{u}_k$'s. Since PCA extracts the largest variances, the subspace spanned by principal eigenvectors contains most of the initial data. It can be shown (see e.g. [37]), that PCA actually arises as an optimal solution from minimum data representation error -problem (as well as other problems [37]). In other words, if $\hat{\mathbf{x}}$ is the representation of the data, the error $\mathrm{E}\{\|\mathbf{x} - \hat{\mathbf{x}}\|^2\}$ is minimized by

$$\hat{\mathbf{x}} = \sum_{i=1}^{l} (\mathbf{x}^T\mathbf{u}_i)\mathbf{u}_i. \tag{139}$$

Since PCA is based on second order statistics, the representation (139) might not be the most meaningful for non-Gaussian data, since higher order statistics are neglected. This is depicted above. Here, the mixtures of two binary signals s_1 and s_2 are observed by three sensors. The noisy observations are

$$\mathbf{x} = \begin{bmatrix} x_1 \\ x_2 \\ x_3 \end{bmatrix} = \begin{bmatrix} 1 & 1 \\ -1 & 1 \\ -1 & -1 \end{bmatrix} \begin{bmatrix} s_1 \\ s_2 \end{bmatrix} + \mathbf{n}, \tag{140}$$

which is plotted in Figure 38. The dotted lines indicate the directions of the two largest variances. In Figure 39, the data is viewed along these directions, and the third direction is seen to have only a minor variance. Based on that observation, the data is projected into PCA subspace. In Figure 40, the 2D data representation is seen (left subfigure), as well as the extracted principal components (right subfigure). It is seen that this data representation is clearly not the best, having source separation in mind, since the principal components seems still to be mixtures of binary signals. PCA is then followed by ICA, which search out another

basis $\mathbf{w}_1, \ldots, \mathbf{w}_l$ for the data, and represent the data as

$$\hat{\mathbf{x}} = \sum_{i=1}^{l} (\mathbf{x}^T \mathbf{w}_i) \mathbf{w}_i. \tag{141}$$

The results are seen in Figure 41. In this particular example, the ICA basis vectors are found by merely rotating the PCA basis vectors (left subfigure). Resulting independent components (right subfigure) seems to be fairly good estimates of binary signals, and the effect of noise can be finally reduced by a threshold element.

4.2.3 Fast fixed-point algorithm for ICA

One of the benchmark ICA algorithms has been reported quite recently [25] - FastICA. In this algorithm, a neural network learning rule is transformed into a very simple fixed-point iteration, which has cubic convergence, and does not depend on any user-defined parameters.

The observed data $\mathbf{x}_{\text{obs}}$ is first whitened, which can be performed e.g. by PCA as follows:

$$\mathbf{x} \stackrel{\text{def}}{=} \Lambda_s^{-1/2} \mathbf{U}_s^T \mathbf{x}_{\text{obs}}. \tag{142}$$

Here $\mathbf{U}_s$ corresponds to the principal eigenvectors of the data correlation matrix $E\{\mathbf{x}_{\text{obs}} \mathbf{x}_{\text{obs}}^T\}$, and the diagonal matrix Λ_s contains the related eigenvalues on its diagonal. FastICA now performs as follows:

1. Take a random initial vector $\mathbf{w}(0)$ of norm 1, and let $t = 1$.
2. Let $\mathbf{w}(t) = \mathrm{E}\{\mathbf{x}(\mathbf{w}(t-1)^T \mathbf{x})^3\} - 3\mathbf{w}(t-1)$.
3. Divide $\mathbf{w}(t)$ by its norm.
4. If $|\mathbf{w}(t)^T \mathbf{w}(t-1)|$ is not close enough to 1, let $t = t + 1$, and go back to step 2. Otherwise, output the vector $\mathbf{w}(t)$.

In step 2, the expectation can be estimated by using a large sample of $\mathbf{x}$ vectors. This algorithm estimates one ICA basis vector $\mathbf{w}$, and hence an independent component $\mathbf{w}^T \mathbf{x}$. If more components are estimated, then in the beginning of step 2, an additional projection operation in performed during the first few iterations:

2a. Let $\mathbf{w}(t) = \mathbf{w}(t) - \bar{\mathbf{W}} \bar{\mathbf{W}}^T \mathbf{w}(t)$.

Here $\bar{\mathbf{W}}$ contains all previously found ICA basis vectors in its columns.

4.2.4 ICA for complex valued mixtures

The FastICA algorithm, presented above, is designed for real-valued data, in which case its convergence is shown to be cubic [25]. Independent component analysis for complex-valued data is also considered in the literature, see e.g. [2, 53]. Compared to the case of real valued mixtures, there exists one more indeterminacy of the independent components. Namely, we can always rewrite $x_i = \mathbf{a}_i \mathbf{s} =$

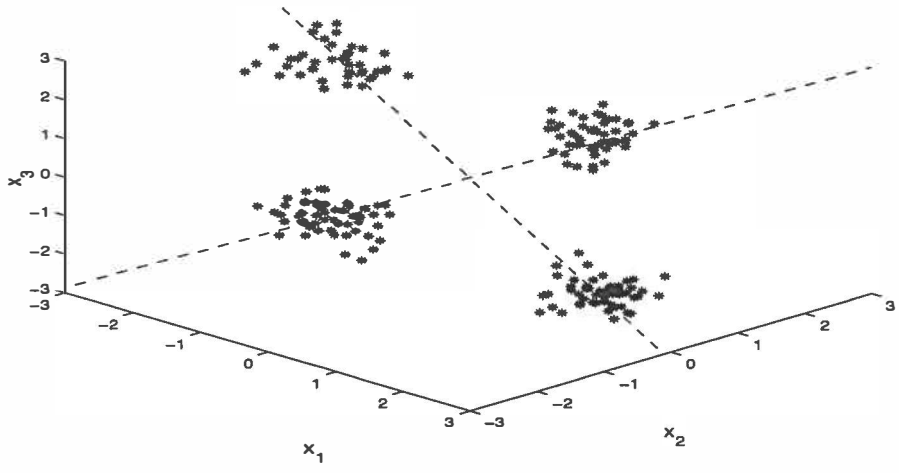

FIGURE 38 Noisy data of two sources observed by three sensors. Dotted lines indicates the directions of two largest variance.

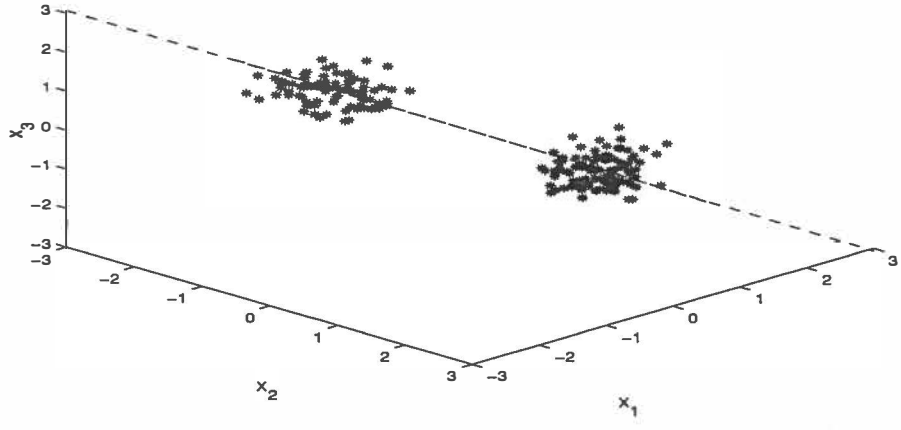

FIGURE 39 The variation of the data in third direction. Dotted line indicates two other directions.

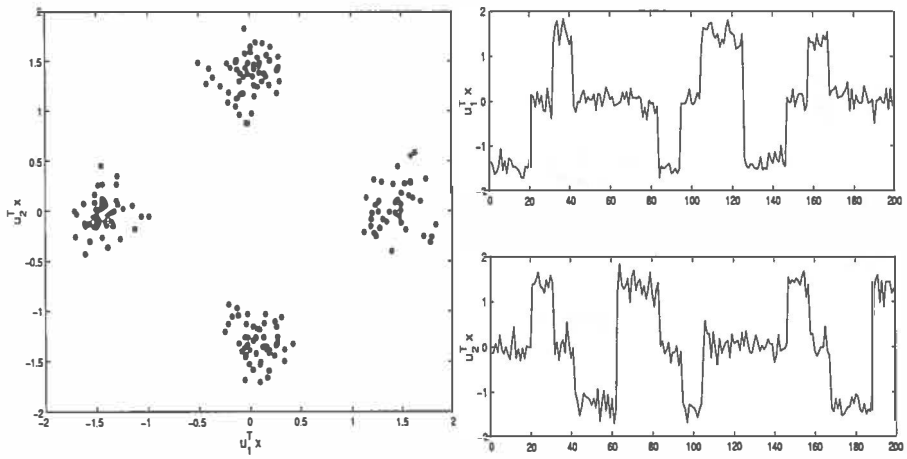

FIGURE 40 The data in PCA subspace (left), and principal components (right).

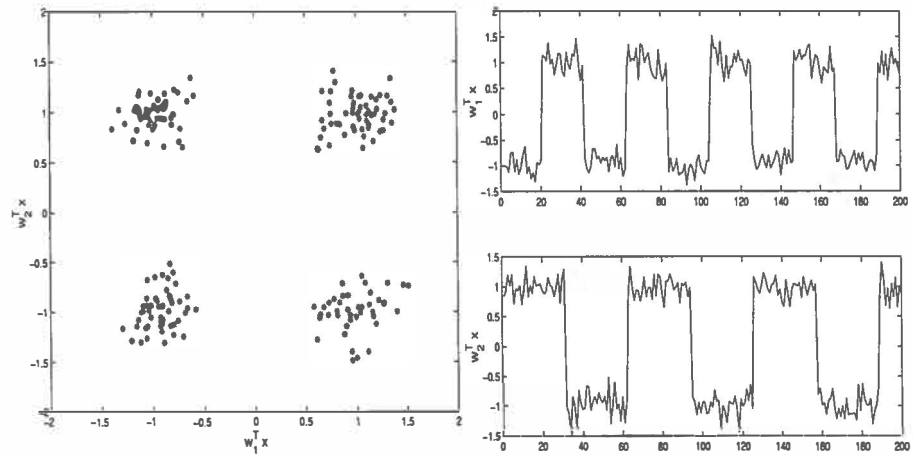

FIGURE 41 The data spanned by ICA basis vectors (left), and independent components (right).

$(e^{j\phi}\mathbf{a}_i)(e^{-j\phi}\mathbf{s})$, where $e^{j\phi}$ is a unit-norm complex scalar. Thus, ICA cannot determine the phases of s_i's.[7]

In this thesis, we apply FastICA for complex valued mixtures, and consider step 2 in the FastICA to be the following:

$$2.\ \text{Let } \mathbf{w}(t) = E\{\mathbf{x}(\mathbf{w}(t-1)^H\mathbf{x})^*|\mathbf{w}(t-1)^H\mathbf{x}|^2\} - \gamma\mathbf{w}(t-1), \tag{143}$$

where $\gamma = 2$ (resp. $\gamma = 3$) for complex valued (resp. real valued) source signals.[8] The update rule in the case $\gamma = 2$ is also considered independently in [6]. However, no convergence proof is yet given for Eq. (143) [28]. In addition, the case $\gamma = 3$ is not considered for complex valued mixtures earlier.

In [6], a class of FastICA algorithms were derived by searching the extrema of $E\{G(|\mathbf{w}^H\mathbf{x}|^2)\}$, where $G : \mathbb{C}^n \rightarrow \mathbb{R}$ is a smooth even function, and $E\{|\mathbf{w}^H\mathbf{x}|^2\} = 1$. Using approximative Newton iterations, the update rule was proposed to be

$$\begin{aligned}\mathbf{w}(t) &= E\{\mathbf{x}(\mathbf{w}(t-1)^H\mathbf{x})^*|\mathbf{w}(t-1)^H\mathbf{x}|^2\} \\ &- E\{g(|\mathbf{w}(t)^H\mathbf{x}|^2) + |\mathbf{w}(t)^H\mathbf{x}|^2 g'(|\mathbf{w}(t)^H\mathbf{x}|^2)\}\mathbf{w}(t),\end{aligned} \tag{144}$$

where $g()$ is the derivative of $G()$, and $g'()$ is the derivative of $g()$. Thus, by choosing $G(y) = \frac{1}{2}y^2$, Eqs. (143) and (144) coincide.

In our case, the derivation of Eq. (143) is based on the analogy with the derivation of FastICA for real valued mixtures in [25]. This is quite a natural way of doing the reasoning, since the same objective function is used, and thus the only extension now is to consider complex instead of real valued mixtures. Therefore, we first only point out some of the core points of the derivation, and the final justification of Eq. (143) is given by the proof of global convergence.

Consider the data Eq. (135), i.e. $\mathbf{x} = \mathbf{A}\mathbf{s}$. In the data model, the sources s_i are assumed to be non-Gaussian, and mutually independent, and the mixing matrix $\mathbf{A}$ to have full column rank. In a complex case, the real and imaginary parts of s_i's are assumed uncorrelated. In addition, the data is assumed to be whitened, which can always be accomplished by PCA [13]. As a consequence, the data to be processed is

$$\mathbf{x} = \mathbf{W}\mathbf{s}, \tag{145}$$

where $\mathbf{W}$ is *orthonormal*. The contrast function to be considered is kurtosis, which can be defined as $J_r(y) = E\{y^4\} - 3(E\{y^2\})^2$ for real valued data, and $J_c(y) = E\{|y|^4\} - 2(E\{|y|^2\})^2$ in complex case [78]. If y is whitened, we may rewrite

[7] Notice that the problems caused by these indeterminacies can be avoided in practise e.g. by differential data modulation in communication, or at least mitigated by a proper initialization of the ICA basis vector when estimating it. This is especially demonstrated later in the numerical experiments.

[8] Notice that the mixing matrix is here always assumed to be complex valued. Hence, the mixture, i.e. the data to be processed, is here always complex valued, even though the source signals might be real valued. QPSK- and BPSK-modulated signals are examples of complex and real valued signals, respectively.

$J_r(y) = E\{y^4\} - 3$, and $J_c(y) = E\{|y|^4\} - 2$. In FastICA for real valued mixtures [25], the iteration of the ICA basis vector $\mathbf{w}$ is performed by

$$\mathbf{w}(t) = E\{\mathbf{x}(\mathbf{w}(t-1)^T\mathbf{x})^3\} - 3\mathbf{w}(t-1). \tag{146}$$

In this updating rule, the first term of the right-hand side is the gradient of $J_r(\mathbf{w}^T\mathbf{x})$ with respect to $\mathbf{w}$, and the second term is due to constraint $\|\mathbf{w}\| = 1$. The meaning of this term is to ensure the fast convergence [25]. Especially, the value -3 in the front of $\mathbf{w}(t-1)$, which is exactly the same constant appearing in the kurtosis J_r, played a key role in guaranteeing the fast convergence. For complex valued mixtures, an algorithm completely analogous to that of Eq. (146) would be

$$\mathbf{w}(t) = E\{\mathbf{x}(\mathbf{w}(t-1)^H\mathbf{x})^*|\mathbf{w}(t-1)^H\mathbf{x}|^2\} - 2\mathbf{w}(t-1), \tag{147}$$

where, as before, now also the first term of the right-hand side is due to the gradient of $J_c(\mathbf{w}^H\mathbf{x})$ with respect to $\mathbf{w}$. The second term is now also justified by the global convergence (see the proof shortly), and the constant value -2 in the front of $\mathbf{w}(t-1)$ also happens to appear in $J_c(y)$.

The proof for global convergence for complex valued sources ($\gamma = 2$):

The proof is analogous to that of [25]. First, a new variable is defined as $\mathbf{z} = \mathbf{W}^H\mathbf{w}$, where $\mathbf{W}$ is the true mixing matrix appearing in Eq. (145). As discussed in the section 4.2.4, ICA is able to estimate the basis vector $\mathbf{w}$ up to a unit norm complex scalar. Hence, the goal is to show that $\mathbf{z}(t) \stackrel{t\to\infty}{\to} [0\ 0\ v\ 0\ 0]^T$, $|v| = 1$, i.e. $\mathbf{w}$ converges to one column of $\mathbf{W}$ with a unit norm complex scalar ambiguity.

For notational convenience, denote $\mathbf{z}^+$ the new value for $\mathbf{z}$. Applying Eq. (143), we thus have

$$\begin{aligned}
\mathbf{z}^+ &= \mathbf{W}^H\mathbf{w}^+ && (148)\\
&= \mathbf{W}^H E\{\mathbf{x}(\mathbf{w}^H\mathbf{x})^*|\mathbf{w}^H\mathbf{x}|^2\} - 2\mathbf{W}^H\mathbf{w} && (149)\\
&= E\{\mathbf{W}^H\mathbf{x}(\mathbf{z}^H\mathbf{W}^H\mathbf{x})^*|\mathbf{z}^H\mathbf{W}^H\mathbf{x}|^2\} - 2\mathbf{z} && (150)\\
&= E\{\mathbf{s}(\mathbf{z}^H\mathbf{s})^*|\mathbf{z}^H\mathbf{s}|^2\} - 2\mathbf{z}. && (151)
\end{aligned}$$

In the third, and fourth equality we have used the facts $\mathbf{w} = \mathbf{W}\mathbf{z}$, and $\mathbf{s} = \mathbf{W}^H\mathbf{x}$, respectively, since $\mathbf{W}$ is orthonormal. To express the last equality in more detail, the following relations are first obtained:

$$\mathbf{z}^H\mathbf{s} = \sum_i z_i^* s_i \tag{152}$$

$$|\mathbf{z}^H\mathbf{s}|^2 = \sum_i |z_i|^2|s_i|^2 + \sum_{i\neq j} z_i^* z_j s_i s_j^* \tag{153}$$

$$(\mathbf{z}^H\mathbf{s})^*|\mathbf{z}^H\mathbf{s}|^2 = \sum_{i,j} z_i|z_j|^2 s_i^*|s_j|^2 + \sum_{h,i\neq j} z_h z_i^* z_j s_h^* s_i s_j^* \tag{154}$$

Therefore, the lth element of $\mathbf{z}^+$ is equal to

$$\begin{aligned} z_l^+ &= E\{s_l(\mathbf{z}^H\mathbf{s})^*|\mathbf{z}^H\mathbf{s}|^2\} - 2z_l && (155)\\ &= z_l|z_l|^2E\{|s_l|^4\} + 2\sum_{i\neq l} z_l|z_i|^2 - 2z_l && (156)\\ &= z_l|z_l|^2E\{|s_l|^4\} + 2z_l(1-|z_l|^2) - 2z_l && (157)\\ &= z_l|z_l|^2J_c(s_l). && (158) \end{aligned}$$

Here the second equality is due to the independence of s_i's, since then for different incides i,j,l,m we have: $E\{|s_i|^2|s_j|^2\} = 1$, and $E\{s_is_j^*|s_j|^2\} = E\{s_i^2(s_j^*)^2\} = E\{s_is_j(s_l^*)^2\} = E\{s_is_j^*|s_l|^2\} = E\{s_i^*s_j^*s_l^2\} = E\{s_is_js_l^*s_m^*\} = 0$. In the third equality, we have used the fact that $\|\mathbf{z}\| = \sum_i |z_i|^2 = 1$. This follows form the fact that $\mathbf{w}$ is normalized to unity after each iteration, and thus $1 = \|\mathbf{w}\| = \|\mathbf{z}\|$, since $\mathbf{W}$ is orthonormal.

The rest of the proof is entirely similar to [25], and therefore only the key steps are now shortly highlighted. First, j is chosen so that $J_c(s_j) \neq 0$, and $z_j(t-1) \neq 0$, so that

$$\frac{|z_i^+|}{|z_j^+|} = \frac{|z_i(t)|\,|J_c(s_i)|}{|z_j(t)|\,|J_c(s_j)|}\left(\frac{|z_i(k-1)|}{|z_j(k-1)|}\right)^3. \qquad (159)$$

is well-defined. This leads to an explicit recursive formula for $\frac{|z_i(t)|}{|z_j(t)|}$:

$$\frac{|z_i(t)|}{|z_j(t)|} = \frac{\sqrt{|J_c(s_i)|}}{\sqrt{|J_c(s_j)|}}\left(\frac{\sqrt{|J_c(s_i)||z_i(0)|}}{\sqrt{|J_c(s_j)||z_j(0)|}}\right)^{3^k}. \qquad (160)$$

For $j = \arg\max_p \sqrt{|J_c(s_p)||z_p(0)|}$ this implies $|z_j| \to 1$, and the other $|z_i| \to 0$, since $\|\mathbf{z}\| = 1$. □

The proof for the real valued sources, i.e. for the case $\gamma = 3$, is somewhat cumbersome. This is because now we also have $E\{s_i^2(s_j^*)^2\} = E\{s_i^2s_j^2\} = 1$ for $i \neq j$, and thus the direct access to the fourth order cumulants does not follow, as was the case in Eq. (158). The results from numerical experiments, however, stand up for $\gamma = 3$ being a correct choice.

4.2.5 ICA for CDMA

In this subsection we discuss the applicability of the CDMA signal model to the ICA scenario. First, recall that the DS-CDMA data have the form of Eq. (22),

$$\mathbf{r}_m = \mathbf{G}\mathbf{a}_m + \mathbf{n}_m. \qquad (161)$$

Without loss of generality, we assume that the processing window of the receiver is 2 symbols. Thus, the data to be processed is $\tilde{\mathbf{r}}_m = [\mathbf{r}_m^T\ \mathbf{r}_{m+1}^T]^T$.

Now consider the time-invariant channel, so that

$$\tilde{\mathbf{r}}_m = \tilde{\mathbf{G}}\tilde{\mathbf{a}}_m + \tilde{\mathbf{n}}_m, \qquad (162)$$

where the matrix $\tilde{\mathbf{G}}$ has dimension $2C \times 3K$, and depends on the spreading codes, and path strengths, while the $3K$-vector $\tilde{\mathbf{a}}_m$ depends only on the symbols. In more detail, $\tilde{\mathbf{G}} = [\tilde{\mathbf{g}}_1\ \tilde{\mathbf{g}}_2\ \tilde{\mathbf{g}}_3 \cdots \tilde{\mathbf{g}}_{3K-2}\ \tilde{\mathbf{g}}_{3K-1}\ \tilde{\mathbf{g}}_{3K}]$,

$$\tilde{\mathbf{g}}_{3k-2} = \sum_{l=1}^{L} a_{kl}[\underline{\mathbf{c}}_{kl}^T\ 0 \cdots 0]^T \tag{163}$$

$$\tilde{\mathbf{g}}_{3k-1} = \sum_{l=1}^{L} a_{kl}\tilde{\mathbf{c}}_{kl}\ , \text{(see Eq. (61) for } \tilde{\mathbf{c}}_{kl}) \tag{164}$$

$$\tilde{\mathbf{g}}_{3k} = \sum_{l=1}^{L} a_{kl}[0 \cdots 0\ \overline{\mathbf{c}}_{kl}^T]^T, \tag{165}$$

and

$$\tilde{\mathbf{a}}_m = [b_{1,m-1}, b_{1,m}, b_{1,m+1}, \cdots, b_{K,m-1}, b_{K,m}, b_{K,m+1}]^T. \tag{166}$$

The observed data $\tilde{\mathbf{r}}_m$ is first whitened. The new data, $\tilde{\mathbf{y}}_m$, is thus

$$\tilde{\mathbf{y}}_m = \tilde{\mathbf{\Lambda}}_s^{-1/2}\tilde{\mathbf{U}}_s^H\tilde{\mathbf{r}}_m \tag{167}$$

$$= \tilde{\mathbf{\Lambda}}_s^{-1/2}\tilde{\mathbf{U}}_s^H\tilde{\mathbf{G}}\tilde{\mathbf{a}}_m + \tilde{\mathbf{\Lambda}}_s^{-1/2}\tilde{\mathbf{U}}_s^H\tilde{\mathbf{n}}_m \tag{168}$$

$$\stackrel{\text{def}}{=} \mathbf{W}\tilde{\mathbf{a}}_m + \mathbf{n}_m^w. \tag{169}$$

where $\tilde{\mathbf{\Lambda}}_s$, and $\tilde{\mathbf{U}}_s$ correspond to $3K$ principal eigenvalues, and -vectors of the autocorrelation matrix $E\{\tilde{\mathbf{r}}_m\tilde{\mathbf{r}}_m^H\}$, respectively. Recall that only $3K$ (instead of $3KL$) eigenvalues are computed, since in the time-invariant channel, the paths are just delayed and scaled copies of each other.

Looking just at the data model Eq. (169), it seems to obey (noisy) ICA model Eq. (135), since $\mathbf{W}$ is unknown, and the elements of $\tilde{\mathbf{a}}_m$ are (roughly) independent. However, the applicability of ICA depends on the nature of the path gains, since in the ICA model, the source process, i.e. $\tilde{\mathbf{a}}_m$ should be non-Gaussian. If this is the case, the estimation of the source ($\tilde{\mathbf{a}}_m$) can be performed given only the observations $\tilde{\mathbf{y}}_m$.

In the time-invariant channel, the source only depends on the symbols, which are non-Gaussian. Thus, ICA arises. The case is different in the time-variant channel, and the data might not obey the ICA model any more. To see this, recall that the contents and dimensions of $\tilde{\mathbf{G}}$ and $\tilde{\mathbf{a}}_m$ are a little bit different if the channel varies in time, see Eqs. (19)-(21). The problem from the ICA point of view is that the contribution of the path gains are now seen in $\tilde{\mathbf{a}}_m$, whose elements might obey Gaussian distribution. This is not acceptable in the ICA model. However, the channel mean is now who plays a crucial role whether ICA ultimately applies or not. Take for example an element $a_{11m}b_{1m}$ from vector $\tilde{\mathbf{a}}_m$. If a_{11m} obeys Gaussian distribution and has zero mean, like Rayleigh distributed fading do, $a_{11m}b_{1m}$ obey the same distribution, and the ICA model does not apply. On the other hand, if a_{11m} has non-zero mean, like Rician distributed fading does, $a_{11m}b_{1m}$ is no more Gaussian, since b_{1m} obeys binomial distribution. In this case, ICA does apply.

4.3 ICA-based blind multiuser detection in timeinvariant channels

The FastICA algorithm has been applied to the CDMA signal separation for the first time in [31], and later on in [70, 71, 33, 75]. In this section, these ideas are refined, and two types of receiver structures, RAKE-ICA and MMSE-ICA, are proposed. The channel is assumed to be time-invariant, or in practice *block fading*, in which case the path gains remain the same during several adjacent symbols.

The basic feature of any ICA method is that it is able to estimate a *set* of independent components, as expressed in Eq. (137), but the order of estimated independent components is somewhat unpredictable. If the method is hierarchic, the sources tend to become separated in the order of decreasing non-Gaussianity (cf. [6]), but this is not, in general, enough to identify each source. A CDMA communication application in mind, it is thus not meaningful to apply the ICA method on its own, since the source signals are well identified by the spreading codes. The utilization of the a prior information becomes thus an important task.

The information about the spreading codes can be utilized directly by adding additional constraints for the ICA iterations, or indirectly by a proper initialization of the ICA iteration. The method in [75] is an example of the former case, where the ICA basis vector was forced to belong to the same space as subspace MMSE filter. In [71, 70], proper initializations by known training symbols or matched filter output, respectively, were considered.

In the following, we consider in more detail two ways of initializing the ICA receiver. The starting point for the receiver development is to look at the noiseless *whitened* data

$$\tilde{\mathbf{y}}_m = \mathbf{W}\tilde{\mathbf{a}}_m, \tag{170}$$

i.e. Eq. (169) without noise. First we notice that the matrix $\mathbf{W}$ is orthonormal. This is due to the uncorrelatedness of the symbols, i.e. $E\{\tilde{\mathbf{a}}_m\tilde{\mathbf{a}}_m^H\} = \mathbf{I}$, because then we have[9] $\mathbf{I} = E\{\tilde{\mathbf{y}}_m\tilde{\mathbf{y}}_m^H\} = E\{\mathbf{W}\tilde{\mathbf{a}}_m\tilde{\mathbf{a}}_m^H\mathbf{W}^H\} = \mathbf{W}\mathbf{W}^H$. The goal hence is to estimate one column of $\mathbf{W}$, say the second column $\mathbf{w}_2$. This is because then by $\mathbf{w}_2$ we can estimate the symbols of the desired user (user $k = 1$): $\mathbf{w}_2^H\tilde{\mathbf{y}}_m = \mathbf{w}_2^H\mathbf{W}\tilde{\mathbf{a}}_m = [0100\cdots0]\tilde{\mathbf{a}}_m = b_{1m}$. Interestingly, from the definition of $\mathbf{W}$ and $\mathbf{G}$ we see that

$$\mathbf{w}_2 = \tilde{\mathbf{\Lambda}}_s^{-\frac{1}{2}}\tilde{\mathbf{U}}_s^H\sum_{l=1}^{L} a_{1l}\tilde{\mathbf{c}}_{1l}, \tag{171}$$

which is exactly the subspace MMSE detector [104] for dispersive channels. Using the terms of source separation, Eq. (171) can be used to *separate* the desired source. It should be noticed, however, that only second order statistics are utilized in Eq. (171). In addition, the subspace parameters, as well as the path gains and delays are always subject to estimation errors, which degrade the separation

[9] Notice that $\mathbf{I} = E\{\tilde{\mathbf{y}}_m\tilde{\mathbf{y}}_m^H\}$, since whitening normalizes component variances [27].

performance of Eq. (171). What is suggested now is that ICA would take the role of the tuning element, and thus to refine Eq. (171) to have better separation performance. This is possible, since the independence of the original sources are not yet utilized in the derivation of Eq. (171). In addition, it is meaningful to apply ICA having Eq. (171) as a starting point, since it already identifies the desired user. This identification is not possible by ICA on its own. The proposed receiver structure, which we label *MMSE-ICA*, contains a subspace MMSE detector, which is continued by ICA iterations.

Alternatively, known or estimated symbols could be used for the initialization of the ICA iteration. This is due to the uncorrelatedness of the symbols, since then we have $E\{\tilde{\mathbf{y}}_m b_{1m}\} = \mathbf{w}_2$, i.e. the subspace MMSE detector again. Since training symbols are not necessarily implemented in all the systems, we prefer the use of the RAKE receiver, or MMSE detector *symbol outputs* to be refined by the means of ICA. The proposed structures are labeled as *RAKE-ICA*, and *MMSEbit-ICA*, respectively.

Since ICA methods cannot determine the sign of the sources,[10] both $\pm\mathbf{w}$ are equally likely to be the ICA solution. This indeterminacy is removed by a comparator element, which chooses the sign according to the RAKE receiver or subspace MMSE detector, respectively. Table 3 summarizes the proposed receiver structures. Especially, FastICA-type iteration Eq. (143) is taken as the ICA counterpart of the proposed schemes.

4.4 Computational considerations

All the proposed blind receiver structures are subspace methods in nature. Therefore, the vectors which span the signal subspace should be estimated. As discussed in section 3.3, this requires computation of order $O(Cm)$, where now $m = K$ (instead of KL) is due to correlated paths.

In ICA, whitening of the data (see Eq. (142)) have computational complexity $O(CK) + O(K^2) = O(CK)$, since $K < C$. This is also the complexity of subspace MMSE detector, when adaptive subspace tracking is used [105]. The additional complexity of the proposed schemes are due to the FastICA iterations, i.e. step 2 in Table 3. The expected value can be estimated by several vector samples. Suppose M samples are used, and form a data matrix $\mathbf{Y} = [\tilde{\mathbf{y}}_1 \cdots \tilde{\mathbf{y}}_M]$. Then the update rule is

$$\mathbf{w}(t) = \frac{1}{M}\mathbf{Y}\tilde{\beta}(t-1)^H - \gamma\mathbf{w}(t-1), \tag{172}$$

where $\tilde{\beta}(t) \stackrel{\text{def}}{=} |\mathbf{w}(t)^H\mathbf{Y}|^2 \odot (\mathbf{w}(t)^H\mathbf{Y})$. Here $|\cdot|^2$ is taken elementwise, and $\odot$ stands for elementwise multiplication. Now, $\mathbf{w}^H\mathbf{Y}$ needs KM multiplications and summations, and is thus of order $O(KM)$. Consequently, $\tilde{\beta}(t)$ is of order $O(KM) + O(M)$, where the last term is due to the elementwise multiplications. Thus, the

[10] The source s_i is as independent from the others as $-s_i$.

TABLE 3 ICA-assisted blind multiuser receiver structures.

Let k be the desired user, $\gamma = 2, 3$ for complex and real valued symbols, respectively, and $\tilde{\mathbf{y}}_m$ the whitened data. Then the iterative algorithms for blind multiuser detection are

1. Initialize $\mathbf{w}(0) = \frac{\mathbf{w}_k}{\|\mathbf{w}_k\|}$, where
   (a) MMSE-ICA: $\mathbf{w}_k = \tilde{\mathbf{\Lambda}}_s^{-1/2} \tilde{\mathbf{U}}_s^H \sum_{l=1}^{L} a_{kl} \tilde{\mathbf{c}}_{kl}$.
   (b) RAKE-ICA: $\mathbf{w}_k = E\{\tilde{\mathbf{y}}_m \hat{b}_{km}^{RAKE}\}$.
   (c) MMSEbit-ICA: $\mathbf{w}_k = E\{\tilde{\mathbf{y}}_m \hat{b}_{km}^{MMSE}\}$.

   Let $t = 1$.
2. Update $\mathbf{w}(t) = E\{\tilde{\mathbf{y}}_m (\mathbf{w}(t-1)^H \tilde{\mathbf{y}}_m)^* | \mathbf{w}(t-1)^H \tilde{\mathbf{y}}_m|^2\} - \gamma \mathbf{w}(t-1)$.
3. Divide $\mathbf{w}(t)$ by its norm.
4. If $|\mathbf{w}(t)^H \mathbf{w}(t-1)|$ is not close enough to 1, let $t = t + 1$, and go back to step 2.
5. Output the vector $\mathbf{w} = \epsilon \mathbf{w}(t)$, where $\epsilon = \text{sign}(Re(\mathbf{w}(0)^H \mathbf{w}(t)))$

final complexity of one iteration is of order $O(KM)$. Putting all together, the computational complexity of any proposed scheme is of order $O(CK) + O(KM)$ per one iteration of subspace tracking and FastICA.

4.5 Numerical experiments

Since there does not exist a useful analytical performance measure for the iterative detectors (cf. [35]), numerical simulations are given instead. We compared the methods in the downlink environment with time-invariant (i.e. fixed) multipath channel. The methods for symbol estimation were: RAKE, RAKE-ICA, subspace MMSE detector, MMSE-ICA, and MMSEbit-ICA. In some experiments the exact MMSE detector was also used as an optimal linear detector. Exact MMSE assumes the codes of the interfering user to be known. In one simulation, a block of $M = 100, ..., 500$ symbols (of randomly chosen user) was estimated with randomly generated complex path gains, time delays, and noise realization. Path delays were randomly chosen from $\{0, 1, \ldots, C-1\}$, and complex path strengths obeyed zero mean normal distribution. All the measured quantities are averaged

over 10000 simulations. No coding was considered, and thus the results are expressed in raw bit- and block-error-rates (BER and BLER, respectively).

Simulation setups are classified primarily to the cases of low and high inter-path-interference (IPI), which is a limiting factor for the performance of the traditional RAKE receiver [40]. Strong IPI was generated by using a small code length (e.g. $C = 8$), and multipath channel. In the case of low IPI, the length of the code sequence was taken bigger (e.g. $C = 31$).

Setup A: low IPI, and varying SNR

The system included $K = 20$ users, and the channel included three fixed multipaths ($L = 3$). The delays and the path gains were assumed to be known. All the interfering users were assigned with 5 dB stronger power. Hence, the interference power is 17.8 dB. Gold codes of length $C = 31$ were used, and Signal-to-Noise Ratio (SNR) in the chip-matched filter output was -10 to 20 dB. The size of the data block was $M = 500$ BPSK data symbols. In Table 3, $\gamma = 3$ was used.

Figure 42 shows the achieved bit-error-rates for the methods as a function of average SNR. The performance of RAKE is quite moderate due to the near-far situation. Consequently, RAKE-ICA is able to improve RAKE only marginally. Subspace MMSE detector suffers from interference floor with higher SNR's. One reason for this is the estimation inaccuracy of the signal subspace. Even though MMSE-ICA uses the same estimate for the signal subspace, it is able to exploit the statistical independence of the source signal, and seems to follow quite closely the exact MMSE. Figure 43 shows the corresponding block-error-rates for the methods. Recall, that the block is correctly estimated, if *all* the symbols in a block are estimated correctly. It is seen that RAKE-ICA actually improves the performance of RAKE quite remarkably in BLER, even though the overall BER is not improved that much. This brings out the characteristic nature of an ICA method: if it fails, it fails totally. This is illustrated in Figure 44, from which it is seen that (with SNR of 0 dB) the most probable numbers for correctly estimated symbols (out of $M = 500$) are around 270 and 500, where the estimated cumulative distribution function increases the most. Fast convergence of FastICA is seen in Figure 45. With higher SNR's, only less than 20 iterations are needed. The criterion for stopping the iteration was: $|\mathbf{w}(k)^H \mathbf{w}(k-1)| > 1 - 10^{-5}$.

Setup B: low IPI, and varying delay estimation errors

The setup was otherwise the same as the previous one, but now the SNR was set to 5 dB. In addition, the delay estimation was assumed to be inaccurate by letting the error of the estimated delay to obey zero mean normal distribution, whose variance was varied from 0 to 0.01 chips. Figures 46 and 47 shows the achieved BER's and BLER's, respectively, for the methods as a function of the delay error variance. As expected, RAKE was more robust against delay mismatch than subspace MMSE detector. With delay error variances less than 0.006 chips, FastICA was always able to improve the performance both in BER and BLER.

The improvement was quite significant especially in BLER: RAKE-ICA achieved the raw BLER of 10^{-1} yet with the delay error variance of 0.01, and MMSE-ICA achieved even the BLER of 10^{-2} approximately with the delay error variance of 0.0025. The most significant improvements, however, was achieved by MMSEbit-ICA, which was able retain its performance, regardless of the timing inaccuracies (up to 0.01 in variance). One reason for this is that the binary structure of the signals was taken into account in the symbol decisions of the subspace MMSE detector. Among all the methods, only MMSEbit-ICA could offer the BLER of 10^{-2} in the whole dynamic range of the setup.

Setup C: strong IPI, and varying SNR and system load

The system now included $K = 1, \ldots, 8$ users, and the channel included two fixed multipaths ($L = 2$). The delays and the path gains were assumed to be known. All the users were assigned with the same power. Walsh codes of length $C = 8$ were used, and Signal-to-Noise Ratio (SNR) in the chip-matched filter output was -10 to 20 dB. The size of the data block was $M = 100$ QPSK data symbols. In Eq. (143), $\gamma = 2$ was used.

The achieved BER-curves are seen in the Figures 48-49 for subspace MMSE detector, and MMSE-ICA, respectively. Both methods achieved the BER of 10^{-2} with at most $K = 6$ users, but MMSE-ICA needed generally $1 - 5$ dB higher SNR. On the other hand, with higher SNR, and system loads up to $K = 4$ users, MMSE-ICA reached better performance (at most $2 * 10^{-4}$) than subspace MMSE detector (at most $1.5 * 10^{-3}$). The corresponding BLER-curves are seen in Figures 52-53. Now, MMSE-ICA achieved the BLER's of 10^{-1} and 10^{-2} with $K = 6$ and $K = 3$ users, respectively, whereas the numbers for subspace MMSE detector were $K = 3$ and $K = 2$, respectively. In addition, with $K = 3$ MMSE-ICA achieved the BLER of 10^{-1} with approximately 10 dB lower SNR.

The performance of RAKE is seen in Figures 50 and 54. The effect of IPI is seen immediately in the single-user case, where even the BER-level of $2 * 10^{-3}$ was not reached. Moreover, with SNR of 20 dB at most, the BLER of 10^{-1} was achieved only in the single-user case. RAKE-ICA, on the other hand, reached the single-user BER and BLER of RAKE with $K = 4$ and $K = 5$ users, respectively. If the BER of 10^{-2} is taken as a target, RAKE and RAKE-ICA can support $K = 4$ and $K = 5$ users, respectively. However, with few users ($K = 1, 2, 3$), RAKE can achieve the target BER with $0 - 3$ dB lower SNR than RAKE-ICA. In BLER comparison, RAKE-ICA reached the target 10^{-1} (in single-user case) with 12 dB lower SNR than RAKE. In addition, only RAKE-ICA could satisfy the BLER of 10^{-2}, which was the case for example with $K = 3$ users at the SNR of 17 dB.

Setup D: strong IPI, and varying channel estimation errors

The setup was otherwise the same as the previous one, but now SNR was set to 10 dB. In addition, the channel estimation was assumed to be inaccurate by letting the relative error of the absolute value of the estimated path gain to obey

zero mean normal distribution, whose variance was varied from 0 to 0.02. Figures 56-59 shows the achieved BER's, and Figures 60-63 the corresponding BLER's.

From Figures 56 and 57 it is seen that ICA iterations are able to improve the BER of subspace MMSE with the system loads up to $K = 4$ users, when the channel is inaccurately estimated. No BER improvement occur with the higher system loads. On the other hand, the BLER performance is always improved, as can be seen from Figures 60 and 61. If the raw BLER of 10^{-1} is taken as a target, subspace MMSE detector and MMSE-ICA can support 2 and 5 users, respectively, with approximately the same relative error variance of 0.013. The difference between MMSE-ICA and MMSEbit-ICA was minor. RAKE is robust against channel mismatch both in BER and BLER, as can be seen from Figure 58 and 62, respectively. Also, the symbol estimates of RAKE seems to be good enough, since the ICA iterations always improved the performance, as can be seen from the corresponding Figures 59 and 63, respectively, of RAKE-ICA. Quite remarkably, RAKE was not able to satisfy the BLER of 10^{-1} at all, whereas RAKE-ICA did with system loads up to $K = 5$ users.

Setup E: the effect of multiple access interference

This setup was to demonstrate the near-far resistance of the methods. The system included $K = 3$ users in $L = 2$ fixed path channel. The MAI per user was varied from -10 to 20 dB. $C = 8$ Walsh codes, and QPSK-modulation were used, and SNR was set to 20 dB. The performance in BER and BLER are seen in the Figures 64 and 65, respectively.

RAKE is not near-far resistant, which is seen as increasing BER with increasing MAI. This naturally also causes some performance drop for RAKE-ICA. However, if the raw BER of 10^{-2} is taken as a target, RAKE-ICA gives, in this setup, an improvement of approximately 3.5 dB compared to RAKE. More remarkably, the raw BLER of 10^{-1} was achieved with 22 dB higher MAI per user, and the raw BLER of 10^{-2} was achieved only by RAKE-ICA with MAI's up to 2 dB per interfering user. It is also interesting to compare RAKE-ICA and subspace MMSE detector. In this case, RAKE-ICA gives better BLER performance up to MAI of 10 dB, and is also able to offer raw BLER of 10^{-2}, unlike subspace MMSE detector.

The case of MMSE-ICA is much clearer, since its near-far resistance is seen as nearly the same performance, regardless of the level of MAI. Quite remarkably, the BLER performance is really close to the optimal MMSE detector.

Setup F: the effect of model order mismatch

In this setup, the effect of model order mismatch was simulated. The system included $K = 3$ users of equal power in a $L = 2$ fixed path channel. Hence, the true model order was $3K = 9$, while it was varied from $3, \ldots, 16$ in the simulations. $C = 8$ Walsh codes were used. The window size of two symbol was used, and thus the dimension of the data vector was equal to $2C = 16$. This is also the maximum

dimension of the signal subspace. SNR was set to 20 dB, and QPSK-modulation was used.

The results in BER are seen in Figure 66. RAKE does not need the model order, and hence its performance remains at the same level. On the other hand, subspace MMSE is sensitive to the selection of the model order. The ICA-parts of both RAKE-ICA and MMSE-ICA needs the estimate for the model order. Both RAKE-ICA and MMSE-ICA seems still to improve the performance of RAKE, and subspace MMSE detector, respectively, even with overestimated model order. Moreover, with highly overestimated model order, RAKE-ICA outperforms even the subspace MMSE detector. On the other hand, both RAKE-ICA and MMSE-ICA usually worsen the performance of RAKE, and the subspace MMSE detector, respectively, in the case of underestimated model order. However, what is quite remarkable, is that MMSE-ICA is not affected that much by the slight or even high model order overestimation. This observation suggests rather to choose a "pessimistic" than "optimistic" value for the model order estimate.

The BLER-curves are much clearer, as can be seen from Figure 67. Especially, the sensitivity of the subspace MMSE detector is clearly seen: both under- and overestimation of the model order, even if being slight, may degrade the BLER-performance even below RAKE. Only RAKE-ICA and MMSE-ICA are able to respect the raw BLER of 10^{-2}. This requires, in this setup, that the model order is not underestimated, but may be even quite heavily overestimated.

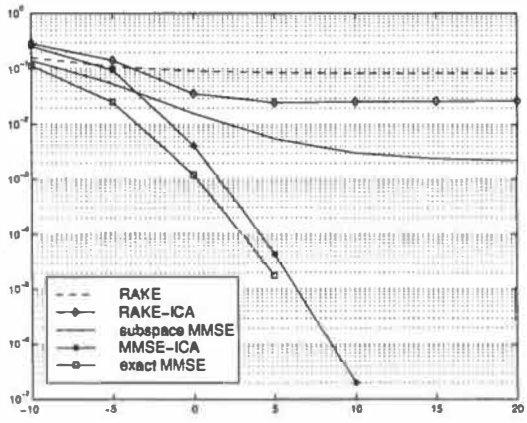

FIGURE 42 Bit-error-rate as a function of SNR $(-10, \ldots, 20)$. The system includes $K = 20$ users, and the average MAI is 5 dB per interfering user.

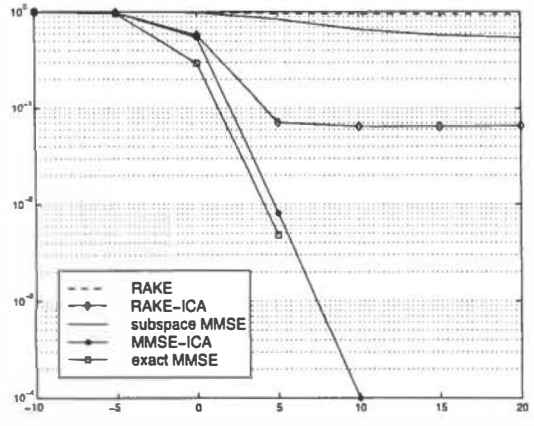

FIGURE 43 Block-error-rate as a function of SNR $(-10, \ldots, 20)$. The system includes $K = 20$ users, and the average MAI is 5 dB per interfering user.

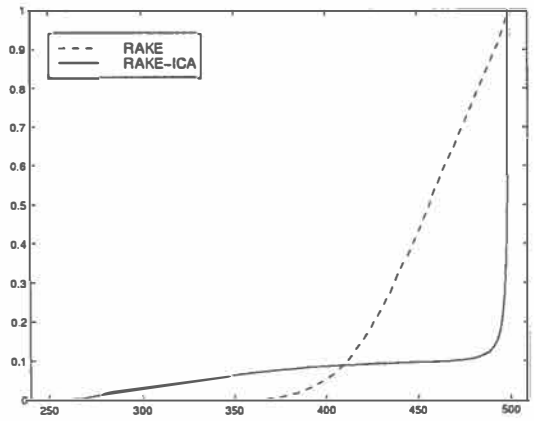

FIGURE 44 Estimated cumulative distribution function for RAKE and RAKE-ICA as a function of correctly estimated symbols (out of $M = 500$). The system includes $K = 20$ users. The average MAI is 5 dB per interfering user, and the average SNR is 0 dB.

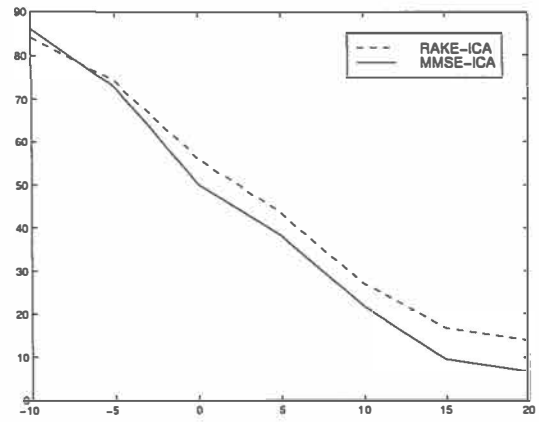

FIGURE 45 Number of iterations as a function of SNR $(-10, \ldots, 20)$. The system includes $K = 20$ users, and the average MAI is 5 dB per interfering user.

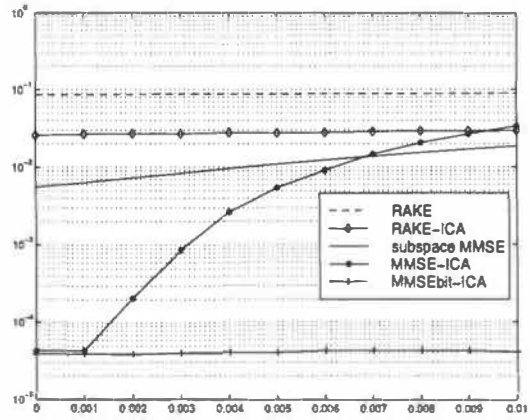

FIGURE 46 Bit-error-rate as a function of the variance of the delay estimation error $(0, \ldots, 0.01)$. The system includes $K = 20$ users, and the average MAI is 5 dB per interfering user.

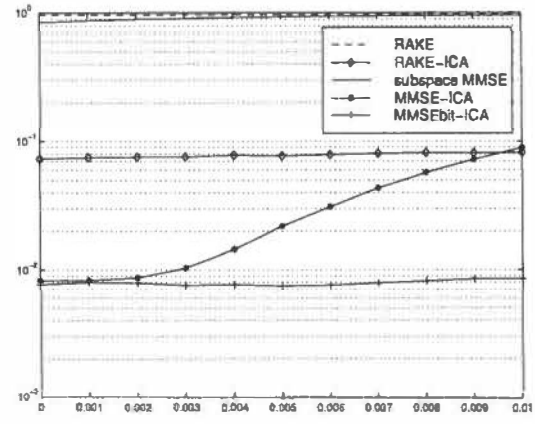

FIGURE 47 Block-error-rate as a function of the variance of the delay estimation error $(0, \ldots, 0.01)$. The system includes $K = 20$ users, and the average MAI is 5 dB per interfering user.

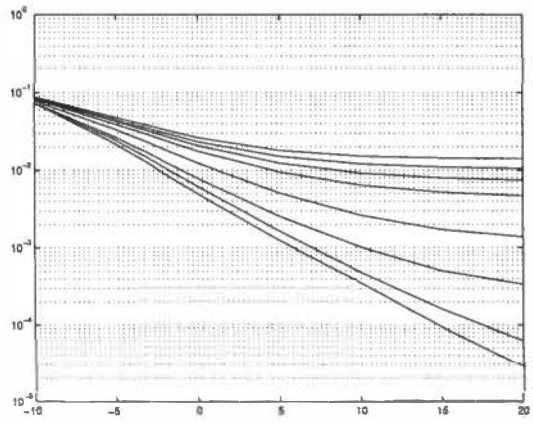

FIGURE 48 Bit-error-rate as a function of the average SNR $(-10, \ldots, 20)$, and the number of users ($K = 1$ (lowermost), $\ldots, 8$ (uppermost)) for subspace MMSE detector.

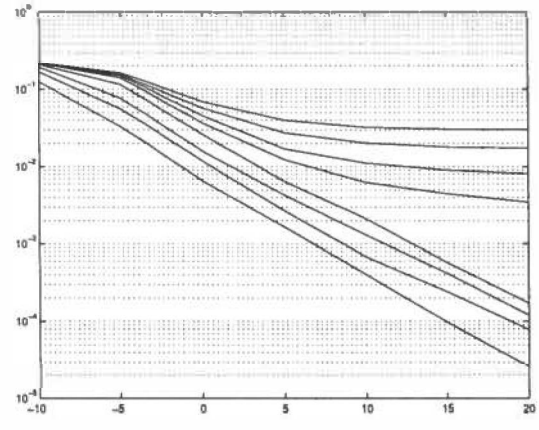

FIGURE 49 Bit-error-rate as a function of the average SNR $(-10, \ldots, 20)$, and the number of users ($K = 1$ (lowermost), $\ldots, 8$ (uppermost)) for MMSE-ICA.

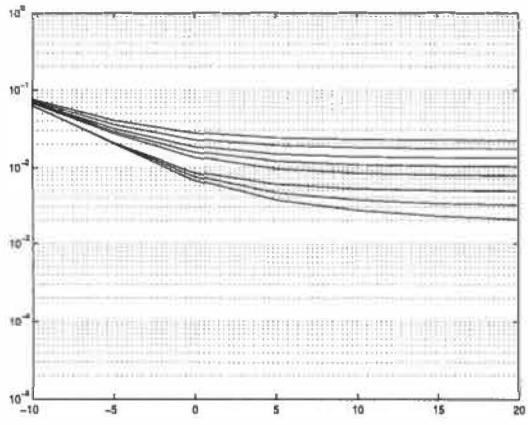

FIGURE 50 Bit-error-rate as a function of the average SNR $(-10, \ldots, 20)$, and the number of users ($K = 1$ (lowermost), $\ldots, 8$ (uppermost)) for RAKE.

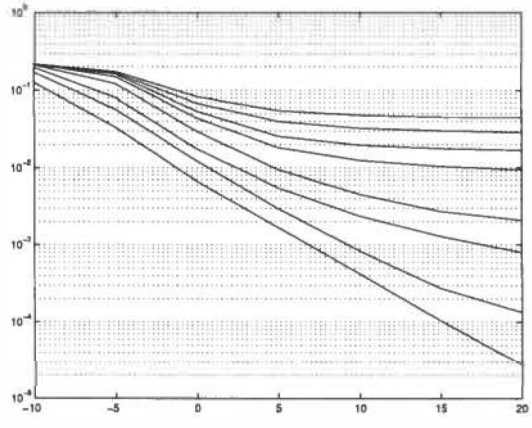

FIGURE 51 Bit-error-rate as a function of the average SNR $(-10, \ldots, 20)$, and the number of users ($K = 1$ (lowermost), $\ldots, 8$ (uppermost)) for RAKE-ICA.

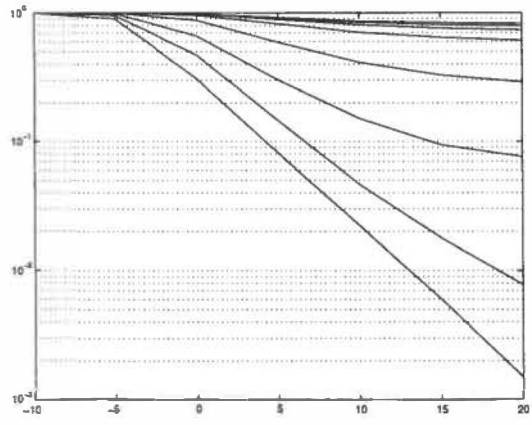

FIGURE 52 Block-error-rate as a function of the average SNR $(-10, \ldots, 20)$, and the number of users ($K = 1$ (lowermost), $\ldots, 8$ (uppermost)) for subspace MMSE detector.

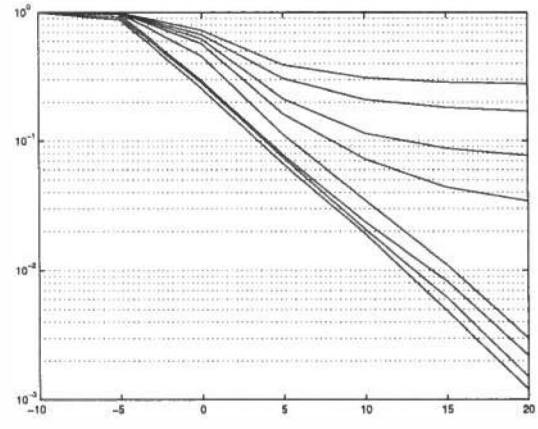

FIGURE 53 Block-error-rate as a function of the average SNR $(-10, \ldots, 20)$, and the number of users ($K = 1$ (lowermost), $\ldots, 8$ (uppermost)) for MMSE-ICA.

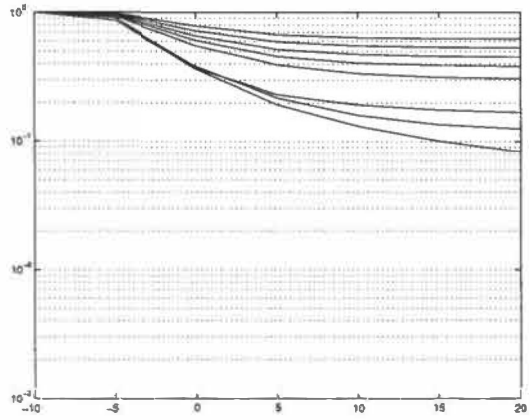

FIGURE 54 Block-error-rate as a function of the average SNR $(-10, \ldots, 20)$, and the number of users ($K = 1$ (lowermost), $\ldots, 8$ (uppermost)) for RAKE.

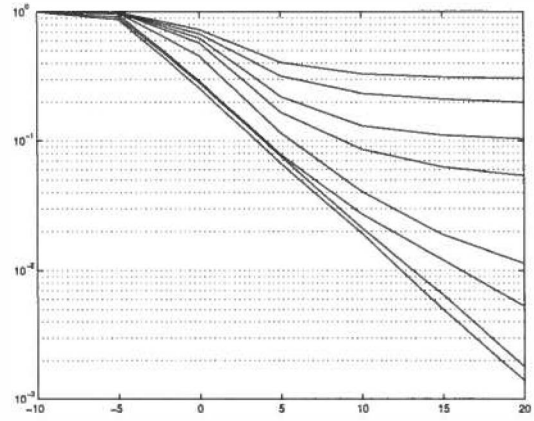

FIGURE 55 Block-error-rate as a function of the average SNR $(-10, \ldots, 20)$, and the number of users ($K = 1$ (lowermost), $\ldots, 8$ (uppermost)) for RAKE-ICA.

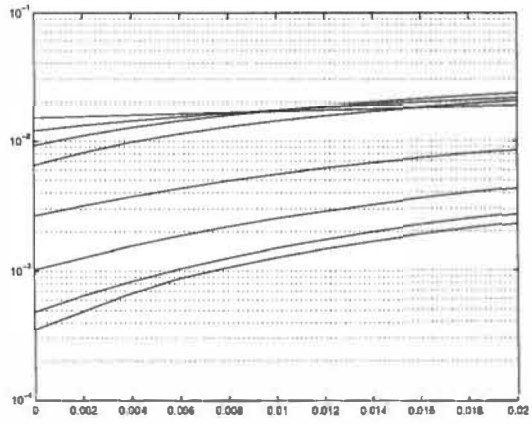

FIGURE 56 Bit-error-rate as a function of relative path gain error variance $(0, \ldots, 0.02)$, and the number of users ($K = 1$ (lowermost), $\ldots, 8$ (uppermost)) for subspace MMSE detector.

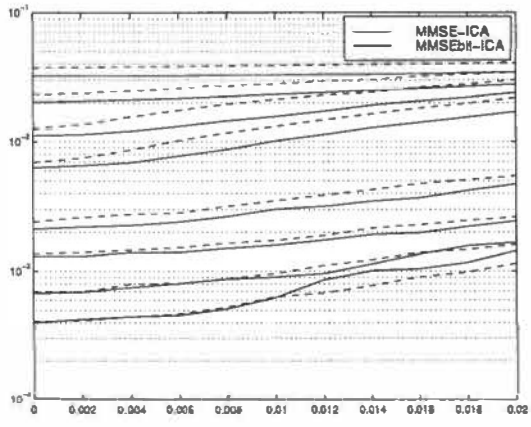

FIGURE 57 Bit-error-rate as a function of relative path gain error variance $(0, \ldots, 0.02)$, and the number of users ($K = 1$ (lowermost), $\ldots, 8$ (uppermost)) for MMSE-ICA detector.

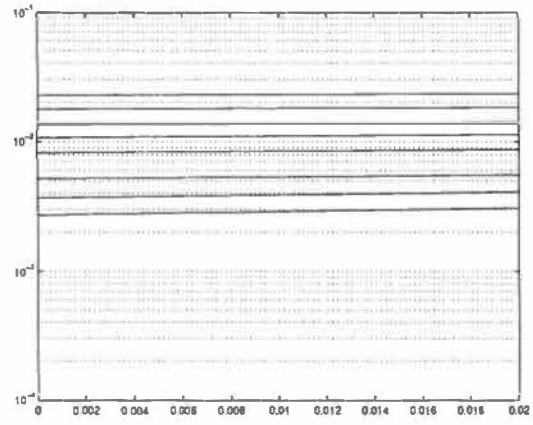

FIGURE 58 Bit-error-rate as a function of relative path gain error variance $(0, \ldots, 0.02)$, and the number of users ($K = 1$ (lowermost), $\ldots, 8$ (uppermost)) for RAKE receiver.

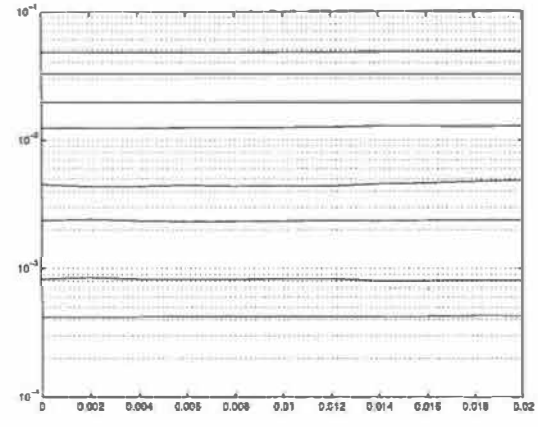

FIGURE 59 Bit-error-rate as a function of relative path gain error variance $(0, \ldots, 0.02)$, and the number of users ($K = 1$ (lowermost), $\ldots, 8$ (uppermost)) for RAKE-ICA.

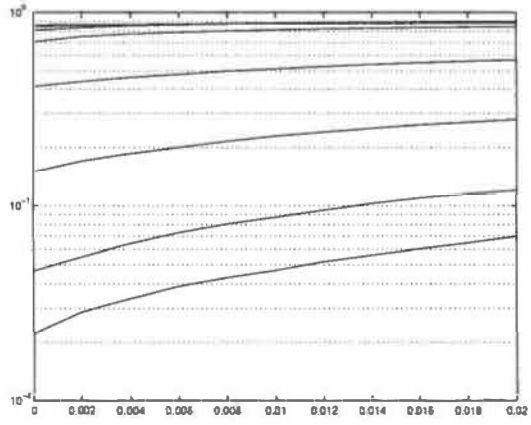

FIGURE 60 Block-error-rate as a function of relative path gain error variance $(0, \ldots, 0.02)$, and the number of users ($K = 1$ (lowermost), $\ldots, 8$ (uppermost)) for subspace MMSE detector.

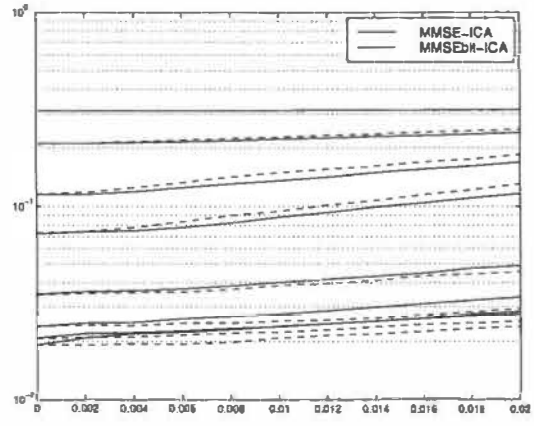

FIGURE 61 Block-error-rate as a function of relative path gain error variance $(0, \ldots, 0.02)$, and the number of users ($K = 1$ (lowermost), $\ldots, 8$ (uppermost)) for MMSE-ICA.

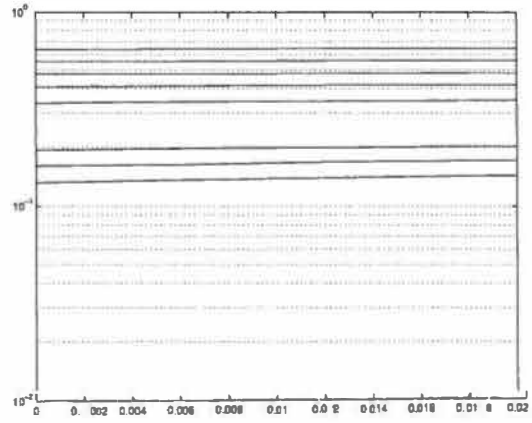

FIGURE 62 Block-error-rate as a function of relative path gain error variance $(0, \ldots, 0.02)$, and the number of users ($K = 1$ (lowermost), $\ldots, 8$ (uppermost)) for RAKE receiver.

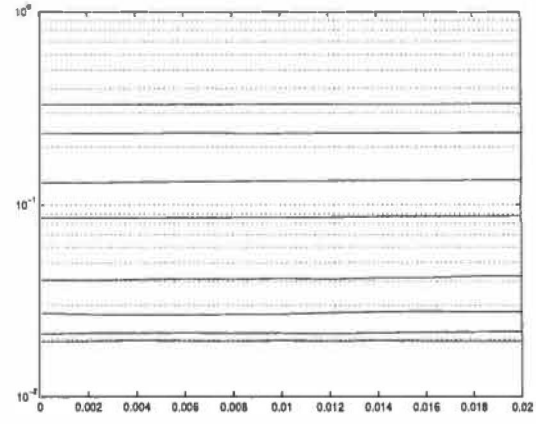

FIGURE 63 Block-error-rate as a function of relative path gain error variance $(0, \ldots, 0.02)$, and the number of users ($K = 1$ (lowermost), $\ldots, 8$ (uppermost)) for RAKE-ICA.

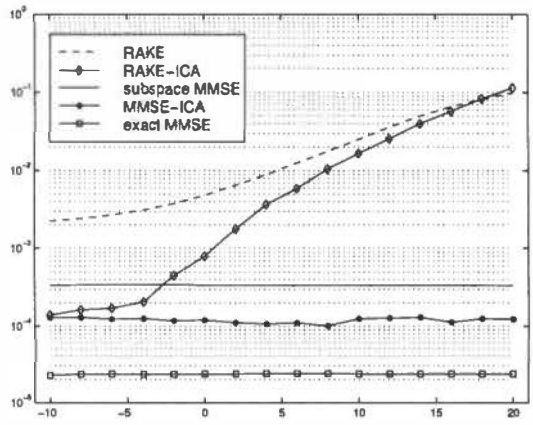

FIGURE 64 Bit-error-rate as a function of multiple access interference per user $(-10, \ldots, 20$ dB). The system includes $K = 3$ users, and the average SNR is 20 dB.

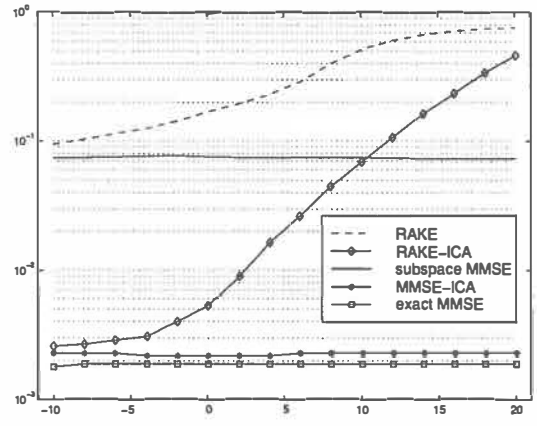

FIGURE 65 Block-error-rate as a function of multiple access interference per user $(-10, \ldots, 20$ dB). The system includes $K = 3$ users, and the average SNR is 20 dB.

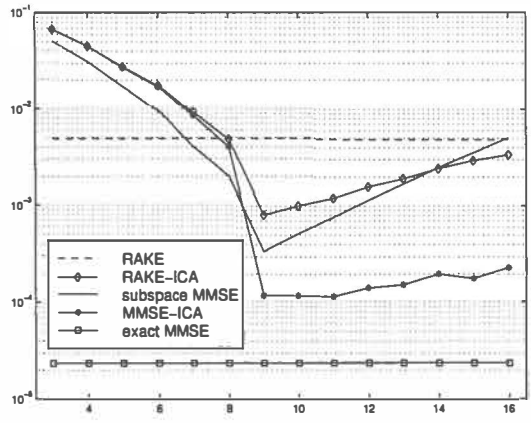

FIGURE 66 Bit-error-rate as a function of the model order estimate $(3, \ldots, 16)$, when the true model order is 9. The system includes $K = 3$ users, and the average SNR is 20 dB.

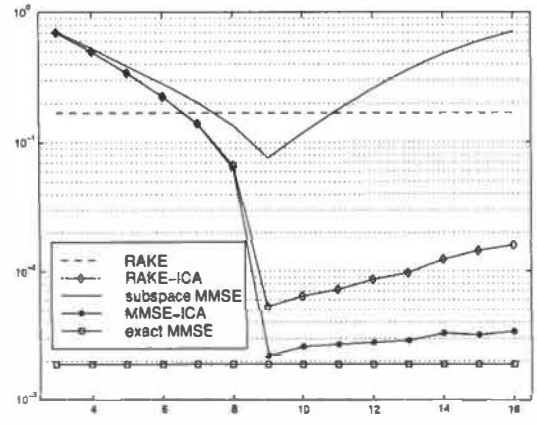

FIGURE 67 Block-error-rate as a function of the model order estimate $(3, \ldots, 16)$, when the true model order is 9. The system includes $K = 3$ users, and the average SNR is 20 dB.

4.6 Summary

In this chapter we have considered blind multiuser detection by the means of independent component analysis. Modifications of FastICA [25] with complex valued data were proposed, and the proof for global convergence was given in the case of complex valued source signals. The main observations made in the chapter were as follows:

- ICA offers a near-far resistant estimator for the symbols in a DS-CDMA system.
- In ICA, no knowledge of the channel nor spreading code is needed.

In practice, however, the spreading code should be utilized to identify each user. In addition, the phase of the channel is needed, unless the data are differentially modulated. The a-prior information about the channel and code timing was proposed to be utilized indirectly by using that information in the initialization of ICA iterations, and in the final decision of the ICA filter. Three types of symbol estimation schemes was proposed, labeled as RAKE-ICA, MMSE-ICA, and MMSEbit-ICA, whose characteristics were as follows:

- RAKE-ICA, and MMSEbit-ICA use the RAKE and subspace MMSE detector symbol estimates, respectively, to the initialization of ICA iterations.
- MMSE-ICA uses directly the subspace MMSE detector for ICA initialization.
- in any ICA-assisted scheme above, the ICA part has a role of "tuning" element, attached to an existing method.

The reasons for taking ICA as an additional element, were the following:

- RAKE is not near-far resistant, but its symbol estimates can be good enough for ICA initialization.
- even if the powers of the signals are the same, additional multiple access interference can be mitigated by ICA, thus improving the performance of RAKE.
- in the presence of timing and channel estimation errors, the performance of subspace MMSE detector gets worse. This drop in performance can be mitigated by ICA.
- in time-invariant channel, ICA can mitigate the performance loss caused by the fact that only a limited number of paths are taken into account in RAKE and subspace MMSE detector.
- the independence of the source signals of different users can be exploited.

5 CONCLUSIONS

In this thesis we studied code timing acquisition and blind multiuser detection in direct-sequence code-division multiple access communication system.

Chapter 1 contained the introductory part, where we began with basic concepts of multiple access, and spread spectrum communication, and discussed the problems in wireless access and CDMA.

In Chapter 2, the DS-CDMA signal model was introduced, as well as its discrete-time vector representation, which was used in the remaining part of the thesis.

Chapter 3 was dedicated to the code timing acquisition. First, some of the benchmark methods were reviewed. Then a class of methods based on differential correlation was proposed. Numerical simulations were used to measure the performance in probability of acquisition, where either the strongest or just any multipath component was acquired. Mean acquisition time analysis was carried out semi-analytically.

In Chapter 4, symbol estimation was considered. We first discussed the earlier work done in the area, and continued with the description of independent component analysis (ICA). One of the benchmark methods for ICA, FastICA [25], was taken into deeper consideration. Two variants of FastICA were proposed for complex valued data, and the proof for global convergence was given in the case of complex valued source signals. The suitability of ICA for CDMA was verified, and ICA-based methods for blind multiuser detection was proposed. Performance of these iterative methods was measured by bit- and block-error-rates, which were concluded from the numerical simulations.

The main contributions of the thesis were those collected in the sections 3.6 and 4.6, which can be highlighted shortly as follows:

- A concept of differential correlation in code acquisition was treated, and methods with analytical reasoning were proposed.
- The performance of the proposed methods were assessed numerically by the probability of acquisition, and semi-analytically by the mean acquisition

time analysis.

- Compared to conventional acquisition, traditional MUSIC, and CMOE method, performance gains were noticed possible to be achieved in near-far scenario, in highly loaded systems, and in fading multipath channel.
- A concept of independent component analysis was considered as a solution for the blind multiuser detection problem in CDMA.
- Two FastICA-type methods were proposed for linear BSS/ICA problem, and a rigorous convergence proof was given in the case of complex valued sources.
- ICA-assisted blind multiuser detectors were proposed, whose performance was assessed numerically by bit- and block-error-rates.
- Compared to the conventional RAKE receiver, and subspace MMSE detector, performance gains were noticed possible to be achieved in near-far scenario, in the presence of chip timing errors, in the presence of channel estimation errors, with moderate system loads and SNR, and in the presence of model order mismatch.

BIBLIOGRAPHY

[1] S.-I. Amari and S. Cichocki, "Adaptive Blind Signal Processing - Neural Network Approaches", *Proc. IEEE*, vol. 86, pp. 2026-2048, October, 1998.

[2] A.D. Back, and A.C. Tsoi, "Blind deconvolution of signals using a complex recurrent network", *Neural Networks for Signal Processing 4, Proc. 1994 IEEE Workshop*, J. Vlontzos, J. Hwang, and E. Wilson (eds), IEEE Press, pp. 565-574, 1999.

[3] A.N. Barbosa, and S.L. Miller, "Adaptive Detection of DS/CDMA Signals in Fading Channels", *IEEE Transactions on Communications*, vol. 46, no. 1, pp. 115-124, January 1998.

[4] S. Bensley and B. Aazhang, "Subspace-Based Channel Estimation for Code Division Multiple Access Communication Systems". *IEEE Transactions on Communications*, vol. 44, no. 8, pp. 1009-1020, August 1996.

[5] S. Bensley and B. Aazhang, "Maximum-Likelihood Synchronization of a Single User for Code-Division Multiple-Access Communication Systems". *IEEE Transactions on Communications*, vol. 46, no. 3, pp. 392-399, March 1998. (Initially in *Proc. Inform. Sciences Systems*, 1994, under the same title.)

[6] E. Bingham, and Hyvärinen, "A Fast Fixed-point Algorithm For Independent Component Analysis of Complex Valued Signals", to appear in *International Journal of Neural Systems*.

[7] Bluetooth Specification, Version 1.0 B, at "http://www.bluetooth.com/"

[8] J.-F. Cardoso, "Blind signal separation: statistical principles", *Proc. IEEE*, October 1998.

[9] J.-F. Cardoso, Ch. Jutten, and Ph. Loubaton (eds.), *Proc. First International Workshop on Independent Component Analysis and Signal Separation* (ICA'99), Aussois, France, January 11-15, 1999.

[10] A.B. Carlson, *Communication Systems - An Introduction to Signals and Noise in Electrical Communication*, third edition, McGraw-Hill, 1986.

[11] L.-C. Chu, and U. Mitra, "Performance Analysis of an Improved MMSE Multiuser Receiver for Mismatched Delay Channels", *IEEE Transactions on Communications*, vol. 46, no. 10, pp. 1369-1380, October 1998.

[12] C.-D. Chung, "Differentially Coherent Detection Technique for Direct-Sequence Code Acquisition in a Rayleigh Fading Channel", *IEEE Transactions on Communications*, vol. 43, no. 2/3/4, pp. 1116-1126, February/March/April 1995.

[13] P. Comon, "Independent Component Analysis - a New Concept?," *Signal Processing*, vol. 36, pp. 287-314, 1994.

[14] N. Delfosse and P. Loubaton, "Adaptive blind separation of independent sources: a deflation approach", *Signal Processing*, vol. 45, pp. 59-83, 1995.

[15] M.G. El-Tarhuni, and A.U.H. Sheikh, "Code Acquisition of DS/SS Signals in Fading Channels Using an LMS Adaptive Filter", *IEEE Communications Letters*, vol. 2, no. 4, pp. 85-88, April 1998.

[16] T.J. Endres, B.D.O. Anderson, C.R. Johnson, Jr., and M. Green, "On the robustness of the fractionally-spaced constant modulus criterion to channel order undermodeling: Part I", *Proc. IEEE Signal Processing Workshop on Signal Processing Advances in Wireless Communications*, Paris, France, pp. 37-40, 16-18 April, 1997.

[17] U. Fawer and B. Aazhang, "A Multiuser Receiver for Code Division Multiple Access Communications over Multipath Channels," *IEEE Transactions on Communications*, vol. 43, no. 2/3/4, pp. 1556-1565, February/March/April 1995.

[18] R. De Gaudenzi, F. Giannetti, and M. Luise, "Design of a Low-Complexity Adaptive Interference-Mitigating Detector for DS/SS Receivers in CDMA Radio Networks", *IEEE Transactions on Communications*, vol. 46, no. 1, pp. 125-134, January 1998.

[19] K.S.Gilhousen et al.,"On the Capacity of a Cellular CDMA System", *IEEE Transactions on Vehicular Technology*, vol. 40, no. 2, May 1991, pp. 303-312.

[20] S.G. Glisic, T.J. Poutanen, W.W. Wu, G.V. Petrovic, and Z. Stefanovic, "New PN Code Acquisition Scheme for CDMA Networks with Low Signal-to-Noise Ratios", *IEEE Transactions on Communications*, vol. 47, no. 2, pp. 300-310, February 1999.

[21] D.N. Godard, "Self-recovering equalization and carrier tracking in two-dimensional data communication systems", *IEEE Transactions on Communications*, vol. 28, no. 11, pp. 1867-1875, November 1980.

[22] G.H.Golub, and C.F. Van Loan, *Matrix Computations*, Baltimore, The Johns Hopkins Press, 1983.

[23] M.L. Honig, U. Madhow, and S. Verdu, "Blind Adaptive Multiused Detection", *IEEE Transactions on Information Theory*, vol. 41, no. 4, pp. 944-960, July 1995.

[24] K. Hooli, M. Latva-Aho, and M. Juntti, "Multiple Access Interference Suppression with Linear Chip Equalizers in WCDMA Downlink Receivers", *Proc. 1999 IEEE Global Telecommunications Conference*, Rio de Janeiro, Brazil, December 5-9, 1999, pp. 467-471.

[25] A. Hyvärinen and E. Oja, "A Fast Fixed-Point Algorithm for Independent Component Analysis," *Neural Computation*, 9:1483-1492, 1997.

[26] A. Hyvärinen, "Noisy Independent Component Analysis by Gaussian Moments", *Proc. International Workshop on Independent Component Analysis and Signal Separation*, Aussois, France, January 11-15, 1999, pp. 473-478.

[27] A. Hyvärinen, "Survey on Independent Component Analysis", *Neural Computing Systems*, 2:94-128, 1999.

[28] A. Hyvärinen, personal communication.

[29] C.R. Johnson, Jr., P. Schniter, T.J. Endres, J.D. Behm, D.R. Brown, and R.A. Casas, "Blind Equalization Using the Constant Modulus Criterion: A Review", *Proc. IEEE*, October 1998.

[30] J. Joutsensalo, "Semi-Blind Source Parameter Separation," in W. Gerstner *et al.* (Eds.) *Artificial Neural Networks-ICANN'97*, Springer Lecture Notes in Computer Science 1327, pp. 577-582, 1997.

[31] J. Joutsensalo and T. Ristaniemi, "Learning Algorithms for Blind Multi-User Detection in CDMA Downlink", *Proc. 9th IEEE International Symposium on Personal, Indoor, and Mobile Radio Communications*, Boston MA, USA, September 1998, pp. 1040-1044.

[32] J. Joutsensalo and T. Ristaniemi, "Single-User Synchronization in Fading Channel", in *Proc. IEEE Signal Processing Workshop on Signal Processing Advances in Wireless Communications*, Annapolis, Maryland, USA, May 9-12, 1999, pp. 133-137.

[33] J. Joutsensalo and T. Ristaniemi, "Blind Multi-User Detection by Fast Fixed Point Algorithm without Prior Knowledge of Symbol-Level Timing", *Proc. IEEE Signal Processing Workshop on Higher Order Statistics*, Ceasarea, Israel, June 1999, pp. 305-308.

[34] J. Joutsensalo and T. Ristaniemi "Differentially Coherent Initial Timing Acquisition in CDMA System", *Proc. 50th IEEE Vehicular Technology Conference*, Amsterdam, The Netherlands, September 19-22, 1999, pp. 708-712.

[35] M.J. Juntti, B. Aazhang, and J.O. Lilleberg, "Iterative Implementation of Linear Multiuser Detection for Dynamic Asynchronous CDMA Systems", *IEEE Transactions on Communications*, vol. 46, no. 4, pp. 503-508, April 1998.

[36] C. Jutten and J. Herault, "Blind Separation of Sources, Part I: An Adaptive Algorithm Based on Neuromimetic Architecture," *Signal Processing*, vol. 24, no. 1, pp. 1-10, July 1991.

[37] J. Karhunen, "Optimization Criteria and Nonlinear PCA Neural Networks", *Proc. IEEE Int. Conf. on Neural Networks*, Orlando, July 1994, pp. 1241-1246.

[38] S. Kay, *Modern Spectral Estimation: Theory and Applications*, Prentice-Hall, 1988.

[39] P. Komulainen, and M.J. Heikkilä, "Adaptive Channel Equalization Based on Chip Separation for CDMA Downlink", *Proc. 11th IEEE International Symposium on Personal, Indoor, and Mobile Radio Communications*, Osaka, Japan, September 12-15, 1999, pp. 1114-1118.

[40] M. Latva-Aho, "Advanced Receivers for Wideband CDMA Systems", Doctoral Thesis, Acta. Univ. Ouluensis, C 125, September 1998.

[41] M. Latva-Aho, J. Lilleberg, J. Iinatti, and M. Juntti, "CDMA Downlink Code Acquisition Performance in Frequency-Selective Fading Channels", *Proc. 10th IEEE International Symposium on Personal, Indoor, and Mobile Radio Communications*, Boston, USA, September 8-11, 1998, pp. 1476-1480.

[42] W.Y.C. Lee, "Mobile Cellular Communications", *McGraw Hill*, New York, 1989.

[43] R. Lidl, and H. Niederreiter, "Finite Fields", in G.-C. Rota (ed.) *Encyclopedia of Mathematics and Its Applications*, vol. 20, Addison-Wesley Publ. Co., 1983.

[44] Z.-S. Liu, J. Li, and S.L. Miller, "An Efficient Code-Timing Estimator for Receiver Diversity DS-CDMA Systems", *IEEE Transactions on Communications*, vol. 46, no. 6, pp. 826-835, June 1998.

[45] R. Lupas, S. Verdu, "Near-Far Resistance of Multiuser Detectors in Asynchronous Channels", *IEEE Transactions on Communications*, vol. 38, no. 4, pp. 496-508, April 1990.

[46] U. Madhow, and M.L. Honig, "MMSE Interference Suppression for Direct-Sequence Spread-Spectrum CDMA", *IEEE Transactions on Communications*, vol. 42, no. 12, pp. 3178-3188, December 1994.

[47] U. Madhow, "Blind Adaptive Interference Suppression for the Near-Far Resistant Acquisition and Demodulation of Direct-Sequence CDMA Signals," *IEEE Transactions on Signal Processing*, vol. 45, no. 1, pp. 124-136, January 1997.

[48] U. Madhow, "MMSE Interference Suppression for Timing Acquisition and Demodulation in Direct-Sequence CDMA System", *IEEE Transactions on Communications*, vol. 46, no. 8, pp. 1065-1075, August 1998.

[49] U. Madhow, "Blind Adaptive Interference Suppression for Direct-Sequence CDMA", *Proc. IEEE*, pp. 2049-2069, October 1998.

[50] U. Madhow and M.L. Honig, "On the Average Near-Far Resistance for MMSE Detection of Direct-Sequence CDMA Signals with Random Spreading", *IEEE Transactions on Information Theory*, accepted for publication.

[51] J. Miguez, and L. Castedo, "A Linearly Constrained Constant Modulus Approach to Blind Adaptive Multiuser Interference Suppression", *IEEE Communications Letters*, vol. 2, no. 8, pp. 217-219, August 1998.

[52] S. Miller, "An Adaptive Direct-Sequence Code-Division Multiple-Access Receiver for Multiuser Interference Rejection", *IEEE Transactions on Communications*, vol. 43, no. 2/3/4, pp. 1746-1755, February/March/April 1995.

[53] E. Moreau, and O. Macchi, "Complex Self-Adaptive Algorithms for Source Separation Based on High Order Contrasts", *Proc. VII European Signal Processing Conference*, vol. 2, pp. 1157-1160, Edinburgh, Scotland, September 1994.

[54] S. Moshavi, "Multi-user detection for DS-CDMA communications", *IEEE Commununications Magazine*, vol. 34, no. 10, pp. 124-137, October 1996.

[55] A. Nandi (ed.), "Blind Estimation Using Higher-Order Statistics", Kluwer, 1999.

[56] E. Oja, "A simplified neuron model as a principal component analyzer", *J. Math. Biol.*, vol. 15, pp. 267-273, 1982.

[57] E. Oja, "Neural networks, principal components, and subspaces", *Int. J. Neural Systems*, vol. 1, pp. 61-68, 1989.

[58] E. Oja, "Principal components, minor components, and linear neural networks", *Neural Networks*, vol. 5, 927-935, 1992.

[59] F. Ovesjö, E. Dahlman, T. Ojanperä, A. Toskala, and A. Klein, "FRAMES multiple access mode 2 - wideband CDMA", *Proc. IEEE International Symposium on Personal, Indoor, and Mobile Radio Communications*, Helsinki, Finland, pp. 42-46, 1997.

[60] T. Ojanperä, and R. Prasad, *Wideband CDMA for Third Generation Systems*, Artech House, 1998.

[61] S. Parkvall, *Near-Far Resistant DS-CDMA Systems: Parameter Estimation and Data Detection*. Ph.D. Thesis, Royal Institute of Technology, October 1996.

[62] S. Parkvall, E.G. Strm, L.B. Milstein, and B.E. Ottersten, "Asynchronous Near-Far Resistant DS-CDMA Receivers Without A Priori Synchronization", *IEEE Transactions on Communications*, vol. 47, no. 1, pp. 78-88, January 1999.

[63] J.D. Parsons, *The Mobile Radio Propagation Channel*, Pentech Press, London, 1992.

[64] R.L. Pickholtz, D.L. Schilling, and L.B. Milstein, "Theory of Spread-Sprectum Communications - A Tutorial", *IEEE Transactions on Communications*, vol. 30, no. 5, pp. 855-884, May 1982.

[65] A. Polydoros and C. Weber, "A unified approach to serial search spread-spectrum code acquisition - part I: General Theory", *IEEE Transactions on Communications*, vol. 32, no. 5, pp. 542-549, 1984.

[66] A. Polydoros and C. Weber, "A unified approach to serial search spread-spectrum code acquisition - part II: A matched filter receiver", *IEEE Transactions on Communications*, vol. 32, no. 5, pp. 550-560, 1984.

[67] R. Price, and P.E. Green, "A Communication Technique for Multipath Channels", *Proc. IRE*, vol. 46, pp. 555-570, March 1958.

[68] J.G. Proakis, *Digital Communications*, third edition, McGraw-Hill, 1995.

[69] R.R. Rick, and L.B. Milstein, "Optimal Decision Strategies for Acquisition of Spread-Sprectum Signals in Frequency-Selective Fading Channels", *IEEE Transactions on Communications*, vol. 46, no. 5, pp. 686-694, May 1998.

[70] T. Ristaniemi, and J. Joutsensalo, "Novel Scheme for Blind Symbol Separation in CDMA Downlink", *Proc. 32th Asilomar Conference on Signals, Systems, and Computers*, Monterey, U.S.A, November 1-4, 1998, pp. 1853-1857.

[71] T. Ristaniemi, and J. Joutsensalo, "On the Performance of Blind Source Separation in CDMA Downlink", *Proc. First International Workshop on Independent Component Analysis and Signal Separation*, (ICA'99), Aussois, France, January 11-15, 1999, pp. 437-442.

[72] T. Ristaniemi and J. Joutsensalo, "Iterative Algorithms for Blind Interference Suppression in CDMA", *Proc. IEEE 2nd Workshop on Signal Processing Advances in Wireless Communications*, Annapolis MD, USA, May 1999, pp. 203-206.

[73] T. Ristaniemi and J. Joutsensalo, "Nonlinear Algorithm for Blind Interference Cancellation", *Proc. IEEE Signal Processing Workshop on Higher Order Statistics*, Ceasarea, Israel, June 1999, pp.43-47.

[74] T. Ristaniemi, "Accurate Pilot Assisted PN Code Acquisition", *Proc. 50th IEEE Vehicular Technology Conference*, Amsterdam, The Netherlands, September 19-22, 1999, pp. 723-727.

[75] T. Ristaniemi and J. Joutsensalo, "Independent Component Analysis with Code Information Utilization in DS-CDMA Signal Separation", *Proc. IEEE Global Telecommunication Conference* (GLOBECOM'99), Rio de Janeiro, Brazil, December 5-9. vol. 1a, pp. 320-324.

[76] C. Sankaran, and A. Ephremides, "Solving a Class of Optimum Multiuser Detection Problems with Polynomial Complexity", *IEEE Transactions on Information Theory*, September 1998.

[77] D.V. Sarwate, "Acquisition of Direct-Sequence Spread-Sprectum Signals", in *Wireless Communications - TDMA versus CDMA*, S.G. Glisic and P.A. Leppänen (eds.), Kluwer Academic Publishers, 1997.

[78] Seber, G. A. F., *Multivariate observations*, New York Wiley, 1984.

[79] R. Schmidt, "Multiple Emitter Location and Signal Parameter Estimation", *Proc. RADC Spectral Estimation Workshop*, Rome, NY, 1979, pp. 243-258.

[80] R. Schmidt, "Multiple Emitter Location and Signal Parameter Estimation", *IEEE Transactions on Antennas, and Propagation*, AP-34, pp. 276-290, March 1986.

[81] R. Steele, *Mobile Radio Communications*, Pentech Press, London, 1992

[82] E. Ström, S. Parkvall, S. Miller, and B. Ottersten, "Propagation Delay Estimation in Asynchronous Direct-Sequence Code Division Multiple Access Systems", *IEEE Transactions on Communications*, vol. 44, pp. 84-93, January 1996.

[83] S. Talwar, M. Viberg, and A. Paulraj, "Blind estimation of multiple co-channel digital signals arriving at an antenna array", *Proc. 27th Asilomar Conf. on Signals, Systems, and Computers*, Pacific Grove, CA, USA, 1993.

[84] S. Talwar, M. Viberg, and A. Paulraj, "Blind estimation of multiple co-channel digital signals using an antenna array", *IEEE Signal Processing Letters*, vol. 1, no. 2, pp. 29-31, February 1994.

[85] S. Talwar, and A. Paulraj, "Performance Analysis of Blind Digital Signal Copy Algorithms", *Proc. IEEE Military Communications Conference*, pp. 123-128, 1994

[86] S. Talwar, M. Viberg, and A. Paulraj, "Blind Separation of Synchronous Co-Channel Digital Signals Using an Antenna Array. Part I. Algorithms", *IEEE Transactions on Signal Processing*, vol. 44, no. 5, pp. 1184-1197, May 1996.

[87] S. Talwar, and A. Paulraj, "Blind Separation of Synchronous Co-Channel Digital Signals Using an Antenna Array. Part II. Performance Analysis", *IEEE Transactions on Signal Processing*, March 1997.

[88] TIA/EIA-95-B, *Mobile Station - Base Station Compatibility Standard for Dual-Mode Wideband Spread Sprectum Systems*, Telecommunications Industry Association, Washington, D.C.

[89] J.R. Treichler and B.G. Agee, "A new approach to multipath correction of constant modulus signals", *IEEE Transactions on Acoustics, Speech, and Signal Processing*, vol. 31, no. 2, pp. 459-472, April 1983.

[90] J.R. Treichler and M.G. Larimore, "New processing techniques based on constant modulus algorithm", *IEEE Transactions on Acoustics, Speech, and Signal Processing*, vol. 33, no. 2, pp. 420-431, April 1985.

[91] M.K. Tsatsanis, "Inverse Filtering Criteria for CDMA System", *IEEE Transactions on Signal Processing*, vol. 45, no. 1, pp. 102-112, January 1997.

[92] S. Ulukus, and R.D. Yates, "Optimum Multiuser Detection Is Tractable for Synchronous CDMA Systems Using M-Sequences", *IEEE Communications Letters*, vol. 2, no. 4, pp. 89-91, April 1998.

[93] M. Varanasi, and B. Aazhang, "Multistage Detection in Asynchronous Code-Division Multiple-Access Communications", *IEEE Transactions on Communications*, vol. 38, no. 4, pp. 509-519, April 1990.

[94] M. Varanasi, and B. Aazhang, "Near-Optimum Detection in Synchronous Code-Division Multiple-Access Systems", *IEEE Transactions on Communications*, vol. 39, no. 5, pp. 725-736, May 1991.

[95] A.J. van der Veen and A. Paulraj, "An Analytical Constant Modulus Algorithm", *IEEE Transactions on Signal Processing*, vol. 44, no. 5, pp. 1136-1155, May 1996.

[96] A.J. van der Veen and J. Tol, "Separation of Zero/Constant Modulus Signals", *Proc. IEEE International Conference on Acoustics, Speech, and Signal Processing*, Munich, Germany, pp. 3445-3448, April 21-24, 1997.

[97] A.J. van der Veen, "Analytical Method for Blind Binary Signal Separation", *IEEE Transactions on Signal Processing*, vol. 45, no. 4, pp. 1078-1082, April 1997.

[98] S. Verdú, "Minimum Probability of Error for Asynchronous Gaussian Multiple-Access Channels", *IEEE Transactions on Information Theory*, vol. 32, no. 1, pp. 85-96, January 1986.

[99] S. Verdú, "Optimum Multiuser Asymptotic Efficiency," *IEEE Transactions on Communications*, vol. COM-34, no. 9, pp. 890-897, September 1986.

[100] S. Verdú, "Multiuser detection", in *Advances in Statistical Signal Processing*, vol. 2, pp. 369-409, JAI Press Inc., Greenwich, CT, 1993.

[101] S. Verdú, "Demodulation in the Presence of Multiuser Interference: Progress and Misconceptions", in D. Docampo, A. Figueiras, and F. Perez (editors) *Intelligent Methods in Signal Processing and Communications*, Chapter 2, pp. 15-46. Birkhauser, Boston, 1997.

[102] S. Verdú, *Multiuser Detection*, Cambridge University Press, 1998.

[103] A. Viterbi, *CDMA - Principles of spread spectrum communications*, Addison-Wesley, 1995.

[104] X. Wang and H.V. Poor, "Blind Equalization and Multiuser Detection in Dispersive CDMA Channels", *IEEE Transactions on Communications*, vol. 46, no. 1, pp. 91-103, January 1998.

[105] X. Wang and H.V. Poor, "Blind Multiuser Detection: A Subspace Approach," *IEEE Transactions on Information Theory*, vol. 44, no. 2, pp. 677-690, March 1998.

[106] X. Wang and H.V. Poor, "Adaptive Joint Multiuser Detection and Channel Estimation in Multipath Fading CDMA Channels," *Wireless Networks*, 4, (1998), pp. 453-470.

[107] M. Wax and T. Kailath, "Detection of Signals by Information Theoretic Criteria", *IEEE Transactions on Acoustics, Speech, and Signal Processing*, vol. 33, no. 2, pp. 387-392, April 1985.

[108] B. Yang, "Projection approximation subspace tracking", *IEEE Transactions on Signal Processing*, vol. 44, no. 1, pp. 95-107, January 1995.

[109] B. Yang, "An extensions of the PASTd algorithm to both rank and subspace tracking", *IEEE Signal Processing Letters*, vol. 2, no. 9, pp. 179-182, September 1995.

[110] M.H. Zarrabizadeh and E.S. Sousa, "A Differentially Coherent PN Code Acquisition Receiver for CDMA Systems", *IEEE Transactions on Communications*, vol. 45, no. 11, pp. 1456-1465, November 1997.

[111] H.H. Zeng, L. Tong, and R.C. Johnson, Jr., "Relationship Between the Constant Modulus and Wiener Receivers", *IEEE Transactions on Information Theory*, vol. 44, no. 4, pp. 1523-1538, July 1998.

[112] D. Zheng, J. Li, S.L. Miller, and E.G. Ström, "An efficient code-timing estimator for DS-CDMA signals", *IEEE Transactions on Signal Processing*, vol. 45, no. 1, pp. 82-89, January 1997.

APPENDIX 1: LIST OF ABBREVIATIONS

ACQ	acquisition
ADC-MF	accurate DC-MF
ADC-MUSIC	accurate DC-MUSIC
AIC	Akaike information criteria
AWGN	additive white gaussian noise
BPSK	binary phase shift keying
BER	bit-error-rate
BLER	block-error-rate
BSS	blind source separation
CDMA	code division multiple access
CM	constant modulus
CMA	constant modulus algorithm
CMOE	constrained minimum output energy
CRB	Cramer-Rao lower bound
DC-MF	differential correlations based MF
DC-MUSIC	differential correlations based
DD	decorrelating detector
DS	direct sequence
FA	finite alphabet
FDD	frequency division dupplex
FDMA	frequency division multiple access
FH	frequency hopping
IC	independent component
ICA	independent component analysis
IPI	inter-path interference
ISI	inter-symbol interference
IS-95	Interim Standard 95
LMS	linear mean squares
MAI	multiple access interference
MF	matched filter
MDL	minimum description length
MLSD	maximum likelihood sequence detector
MLM	maximum likelihood method
MMSE	minimum mean-square error
MUD	multi-user detection
MUSIC	multiple signal classification
PASTd	projection approximation subspace tracking with deflation
PCA	principal component analysis
PLL	phase-lock loop
PN	pseudo-noise
QPSK	quaternary phase shift keying

RMS	recursive least squares
RMSE	root-mean-square error
SIR	signal-to-interference ratio
SNR	signal-to-noise ratio
SUD	single user detector
SVD	singular value decomposition
SS	spread spectrum
TDMA	time division multiple access
UMTS	universal mobile telephone system
US	uncorrelated scatterer
WCDMA	wideband CDMA
WDC-MF	whitened DC-MF
WSS	wide-sense stationary

APPENDIX 2: DERIVATION OF EQ. (78).

First, from Eq. (19) we have

$$\mathbf{GA}(\tau) = [\underline{\mathbf{c}}_{11}, \overline{\mathbf{c}}_{11}, \ldots, \underline{\mathbf{c}}_{1L}, \overline{\mathbf{c}}_{1L}, \ldots, \underline{\mathbf{c}}_{KL}, \overline{\mathbf{c}}_{KL}] \left[\begin{array}{ccc|c} \mu_1^2\bar{\alpha}_1(\tau)\mathbf{1} & & \mathbf{0} & \\ & \ddots & & \mathbf{0} \\ \mathbf{0} & & \mu_L^2\bar{\alpha}_L(\tau)\mathbf{1} & \\ \hline & \mathbf{0} & & \mathbf{0} \end{array}\right] \tag{173}$$

$$= [\mu_1^2\bar{\alpha}_1(\tau)(\underline{\mathbf{c}}_{11} + \overline{\mathbf{c}}_{11}) \cdots \mu_L^2\bar{\alpha}_L(\tau)(\underline{\mathbf{c}}_{1L} + \overline{\mathbf{c}}_{1L})\, 0 \cdots 0] \tag{174}$$

$$= [\mu_1^2\bar{\alpha}_1(\tau)\mathbf{c}_{11} \cdots \mu_L^2\bar{\alpha}_L(\tau)\mathbf{c}_{1L}\, 0 \cdots 0], \tag{175}$$

where the second equation follows from $\mathbf{1} = \begin{bmatrix} 1 & 1 \\ 1 & 1 \end{bmatrix}$, and the third is due to definition $\mathbf{c}_{1l} = \underline{\mathbf{c}}_{1l} + \overline{\mathbf{c}}_{1l}$. Therefore we have

$$\mathbf{GA}(\tau)\mathbf{G}^T = \sum_{l=1}^{L} \mu_l^2\bar{\alpha}_l(\tau)(\mathbf{c}_{1l}\underline{\mathbf{c}}_{1l}^T + \mathbf{c}_{1l}\overline{\mathbf{c}}_{1l}^T), \tag{176}$$

from which (78) immediately follows.

APPENDIX 3: DERIVATION OF EQS. (89) AND (90).

Recall from section 3.3, that

$$\mathbf{R}(\tau) = \bar{\alpha}(\tau)\mathbf{c}_{11}\mathbf{c}_{11}^T, \text{ and} \tag{177}$$

$$\mathbf{c}_{11} = (1-\delta)\mathbf{s}_1(d) + \delta\mathbf{s}_1(d+1). \quad (178)$$

Thus, we first may write

$$\begin{aligned}\mathbf{c}_{11}\mathbf{c}_{11}^T &= (1-\delta)^2\mathbf{s}_1(d)\mathbf{s}_1(d)^T + \delta^2\mathbf{s}_1(d+1)\mathbf{s}_1(d+1)^T \\ &+ \delta(1-\delta)\mathbf{s}_1(d)\mathbf{s}_1(d+1)^T + \delta(1-\delta)\mathbf{s}_1(d+1)\mathbf{s}_1(d)^T. \quad (179)\end{aligned}$$

With definition $\eta_i = \mathbf{s}_1(d)^T\mathbf{s}_1(d+i)$, we have

$$\begin{aligned}\mathbf{s}_1(d)^T\mathbf{R}(\tau)\mathbf{s}_1(d) &= \bar{\alpha}(\tau)[1-\delta)^2\eta_0^2 + \delta^2\eta_1^2 + \delta(1-\delta)\eta_0\eta_1 + \delta(1-\delta)\eta_1\eta_0] \\ &= \bar{\alpha}(\tau)[(1-\delta)\eta_0 + \delta\eta_1]^2, \quad (180)\end{aligned}$$

from which Eq. (89) follows. The derivation of Eq. (90) is entirely similar and is omitted.

APPENDIX 4: DERIVATION OF EQ. (91).

To shorten notations, define

$$A = \mathbf{s}_1(d)^T\mathbf{R}(\tau)\mathbf{s}_1(d)\text{ , and} \quad (181)$$

$$B = \mathbf{s}_1(d+1)^T\mathbf{R}(\tau)\mathbf{s}_1(d+1). \quad (182)$$

Taking squareroots on both sides of Eqs. (89) and (90), we have

$$\pm\sqrt{A} = \sqrt{\bar{\alpha}(\tau)}[(1-\delta)\eta_0 + \delta\eta_1] \quad (183)$$

$$\pm\sqrt{B} = \sqrt{\bar{\alpha}(\tau)}[(1-\delta)\eta_1 + \delta\eta_0], \quad (184)$$

which is a system of equations with two unknowns, δ, and $\sqrt{\bar{\alpha}(\tau)}$. Dividing Eq. (183) by Eq. (184) we obtain

$$\pm\sqrt{\frac{A}{B}} = \frac{(1-\delta)\eta_0 + \delta\eta_1}{(1-\delta)\eta_1 + \delta\eta_0}. \quad (185)$$

By simple algebraic manipulations it leads to

$$\delta[\pm\sqrt{\frac{A}{B}}\eta_0 \mp \sqrt{\frac{A}{B}}\eta_1 + \eta_0 - \eta_1] = \eta_0 \mp \sqrt{\frac{A}{B}}\eta_1, \quad (186)$$

from which Eq. (91) is obtained by denoting $P(d) = \sqrt{\frac{A}{B}}$.

YHTEENVETO (FINNISH SUMMARY)

Tässä työssä tutkitaan signaalinkäsittelyä CDMA-tietoliikennejärjestelmissä. Huomio kiinnitetään erityisesti alasuunnan tiedonsiirtoon (esim. tukiasemalta liikkuvalle käyttäjälle), jolloin signaalin vastaanottajalla on sekä vähäinen tietämys järjestelmän parametreista että rajallinen signaalinkäsittelykapasiteetti. Työssä esitetään algoritmeja sekä viiveiden että symbolien estimointiin.

Signaalin etenemispolkujen viiveiden estimointi, jota kutsutaan myös koodisynkronoinniksi, on välttämätön edellytys tavanomaisille vastaanottimille. Kun viiveet on estimoitu, voidaan estimoida myös kanava ja lopuksi itse lähetetyt symbolit. Työssä esitetään differentiaaliseen korrelaatioon perustuvia algoritmeja viiveen estimointiin. Ne pystyvät käyttämään hyväkseen muuttuvan kanavan aikakorrelaation, toisin kuin tavanomaiset menetelmät. Toivotut ominaisuudet, kuten alhainen laskennallinen kompleksisuus ja kyky suodattaa pois voimakkaita häiritseviä signaaleja saavutetaan. Numeeriset esimerkit todentavat algoritmien kilpailukyvyn olemassaoleviin menetelmiin verrattuna.

Symbolien estimointiin esitetään käytettäväksi tilastollista menetelmää nimeltä *riippumattomien komponenttien analyysi*, ICA, joka erottelee vastaanotetusta sekoituksesta halutun signaalin sokeasti. Termi "sokea" viittaa siihen, että käytössä ei ole muuta etukäteistietoa kuin oletus signaalien riippumattomuudesta. Työssä esitetään algoritmeja sokeaan monen käyttäjän ilmaisuun, jossa ICA on liitetty joko tavanomaiseen tai MMSE-pohjaiseen vastaanottimeen. ICA:n suurin hyöty CDMA:ssa on se, että sen avulla saadaan aikaan lähi-kaukoresistantti estimaattori, joka ei eksplisiittisesti riipu viiveen eikä kanavan estimointivirheistä, jotka saattavat heikentää tavanomaisten ja muiden lähi-kaukoresistanttien vastaanottimien suorituskykyä. Lisäksi signaalien riippumattomuus voidaan hyödyntää.